Single cell approaches to study the interaction between normal and transformed cells in epithelial monolayers

a dissertation submitted for the degree of

Doctor of Philosophy
(Ph.D.)

Department of Cell and Developmental Biology

University College of London (UCL)

Author

Anna Bove

Supervisors: Prof. Guillaume Charras
Dr. Alan Lowe

I, Anna Bove, confirm that the work presented in this report is my own. Where information has been derived from other sources, I confirm that this has been indicated in the report

Acknowledgment

First and fore most, I would like to thank my supervisors Guillaume and Alan, for the support and motivation you gave me since the day you accepted me in your lab. In particular, I would like to thank Guillaume for being such an efficient reader of all sort of boring documents I provided throughout the years and Alan for his patience with my poor coding skills. Working with you has always been challenging and never boring. Thanks for teaching me that negative results and failure are part of the game and are important in the personal and professional formation of a scientist.

A special thanks goes to Shiladitya, for joining the "competition" team and for his great comments and contribution to the Thursday meetings.

Thanks to all the people I collaborated with: Susana and Pedro, Helen, Julien and Oliver. You have been an incredible help.

I am extremely thankful to the members of my PhD jury, Catherine Hogan and Ricardo Henriques for having accepted to evaluate my work.

My deep thank goes to all the members of my team. You always ensured a great atmosphere in the lab and made these years pass very quickly. Richard, you are the essence of LCN; thanks for being always keen on solving all possible issues, from microscopes failure to liquid nitrogen shortage. Nargess, thanks for supporting and sustaining me all the time I needed you. Ana, thank you for being my best example of scientific "German" integrity, IT support, Friday night entertainer, personal trainer and sweet singer of "FELICITA". Manasuccia, it was always nice to discuss science, cell division, both Indian and European gossip with you over a coffee break. Julia, thanks for being a source of positive energy and for all of the encouraging smiles and chocolate temptations you provided me. Daniel, thanks for being my competition m8y, an "anchor" during the stormy times of publication; you rock! Thanks to JoJo, my enthusiastic LN2 colleague, a genuine and everlasting source of criticism and "polemic". Thanks to Malti and Amina, for literally being on my side (of the bench) during the past 4 years. I

think that I shared with you the best moments of my PhD. Finally, thanks to Windie and Jasmine, the new generation of PhD students and the future of the lab, and the nice and precious people who joined recently, Kazu and Pierre.

A special thanks goes to the members of the "Lowe lab": Roxie, Hugo, Kwasi and Tom. Your company made that dark and humid basement a nice place to work and discuss "deep learning", listening to the typical rock music selection of Hugo.

A big thank goes to the former members of the lab: Andrew, Majid, Tommasaccio, Jess. Jess, you have been my partner in crime many times; I still hear the echo of your voice all the times I am not able to pronounce some difficult English word. Tommy, sharing depressing moments in the depression place with you made them less depressing!

Thanks also to my soul mate,"mu" Flavia, for being my happy island, dancing, drinking and life companion. Thanks to my craziest friend Andrea "the gipsy" for assisting me in his very own and special way. Thanks to my idealist, old friend Piccolomo, for the many discussions on life, idealism, literature,"futuro incerto" and afternoon wondering around on the beautiful landscape of our Murgia. And thanks to Simona, Irma Normanno and my sweet and beautiful giuggiolotto Luigi, for making this cold London place a little warm Bari during our winter "panzerottate".

My strongest thank goes to my family, that always supported and fed me with massive parcels containing taralli, wine and all sort of Apulian delicatessen. You stick with me and love me in such an unconditioned way. You know all my fears and anxiety, and help me fighting against them everyday. You are my everything.

Finally, thanks to Giuseppe, who has been with me since the beginning of this journey. Thanks for being always critical on the quality of my images (and for working your magic on them many times) and for bearing with me in this madness.

Abstract

Cell competition is a quality control mechanism through which tissues eliminate unfit cells. Cell competition can result from short-range biochemical signals or long-range mechanical cues. However, little is known about how cell-scale interactions give rise to population shifts in tissues, due to the lack of experimental and computational tools to efficiently characterise interactions at the single-cell level.

In the work presented in this thesis, I address these challenges by combining long-term automated microscopy with deep learning image analysis to decipher how single-cell behaviour determines tissue make-up during competition. Using a novel high-throughput analysis pipeline, I show that competitive interactions between MDCK wild-type cells and cells depleted of the polarity protein scribble are governed by differential sensitivity to local density and the cell-type of each cell's neighbours. I find that local density has a dramatic effect on the rate of division and apoptosis under competitive conditions. Strikingly, such analysis reveals that proliferation of the winner cells is up-regulated in neighbourhoods mostly populated by loser cells.

These data suggest that tissue-scale population shifts are strongly affected by cellular-scale tissue organisation. I present a quantitative mathematical model that demonstrates the effect of neighbour cell-type dependence of apoptosis and division in determining the fitness of competing cell lines.

Impact Statement

Our research will provide new understanding of how cell fate is determined by local interactions within heterogeneous cell populations.
By controlling geometrical confinement using micropatterning techniques and nutrient supply using microfluidics, it will be possible to determine how these interactions are influenced by microenvironmental conditions, something with broad relevance to developmental and stem cell biology in addition to cancer.
Our experiments will provide insight into the temporal evolution of tumour genetic composition both during growth and in response to therapeutic treatment.
Computational models calibrated using our experiments will allow understanding of cancer cell interaction based on a rigorous game theoretical framework.
From a clinical standpoint, our experiment and simulation pipeline will allow exploration of how antioncogenic drugs affect a heterogeneous tumour, and allow for multi-drug therapy design.

Contents

List of Figures

List of Tables

List of videos

Movie 1: Automated tracking of cell division events. Small region of a representative time-lapse movie containing a pure population of H2b-GFP MDCK wt cells (white). The time-lapse movie was acquired by wide-field epifluorescence using 20x magnification. Timings are indicated in the top left corner in hours and minutes. Cell trajectories are represented as comet tails and are coloured by unique identifier (ID). The unique cell ID is shown in green text adjacent to the cell centre. Following division events, the parent ID is shown in parentheses following the unique cell ID.

Movie 2: Automated tracking of a pure population of MDCK wild type cells. Representative time-lapse movie containing a pure population of H2b-GFP MDCK wt cells (white). The time-lapse movie corresponds to one field of view (1600 x 1200 pixels, 530μm x 400μm) acquired by wide-field epifluorescence using 20x magnification. Cell trajectories are represented as comet tails and are coloured by unique identifier.

Movie 3: Automated tracking of cells in competition. Representative time-lapse movie containing H2b-GFP MDCK wt (green) and H2b-RFP $scribble_{kd}$ (magenta) cells mixed in an initial 90:10 ratio. The time-lapse movie corresponds to one field of view (1600 x 1200 pixels, 530μm x 400μm) acquired by wide-field epifluorescence using 20x magnification. Timings are indicated in the top left corner in hours and minutes. Cell trajectories are represented as comet tails and are coloured according to the cell type ($MDCK_{WT}$- green and $scribble_{kd}$ - magenta).

Movie 4: Combined (transmission at the top, m-RFP at the bottom) stack representative of a time-lapse movie containing a pure population of H2b-RFP $scribble_{kd}$ cells induced with doxycycline (tet+). The time-lapse movie corresponds to one field of view (1600 x 1200 pixels, 530μm x 400μm) acquired by wide-field epifluorescence using 20x magnification. Scale bar represents 25 μm.

Movie 5: Combined (transmission at the top, m-cherry at the bottom)stack

representative of a time-lapse movie containing a pure population of H2b-RFP *scribble*$_{kd}$ cells (tet-). The time-lapse movie corresponds to one field of view (1600 x 1200 pixels, 530μm x 400μm) acquired by wide-field epifluorescence using 20x magnification. Scale bar represents 25 μm.

Movie 6: Time-lapse movie of competition experiment where H2b-GFP MDCK wt cells and induced H2b-RFP *scribble*$_{kd}$ cells (tet+) were mixed in 50:50 relative proportions. The time-lapse movie corresponds to one field of view (1600 x 1200 pixels, 530μm x 400μm) acquired by wide-field epifluorescence using 20x magnification. Scale bar represents 25 μm.

Movie 7: Time-lapse movie of competition experiment where H2b-GFP MDCK wt cells and induced H2b-RFP *scribble*$_{kd}$ cells (tet+) were mixed in 10:90 relative proportions. The time-lapse movie corresponds to one field of view (1600 x 1200 pixels, 530μm x 400μm) acquired by wide-field epifluorescence using 20x magnification. Scale bar represents 25 μm.

All movies are stored in the following open-access repository:

https://doi.org/10.6084/m9.figshare.c.4073576.v1 (figshare.)

1 Introduction

1.1 Introduction and study concept

Most adult human cancers originate from the transformation of a single cell within a healthy epithelial cell sheet. Following this event, several rounds of mutation and selection are believed to take place giving rise to tumour progenitors Moreno (2008). The cellular make up of cancerous tumours is highly heterogeneous and continuously evolving Sottoriva et al. (2013),Vogelstein et al. (2013), Navin et al. (2011). Indeed, as the tumour grows from a single cell lesion to a detectable aggregate of $>10^9$ cells, individual cells progressively acquire more mutations leading to the emergence of genetically distinct cell lineages. Over time, the tumour genetic make up becomes spatially heterogeneous with distinct spatial domains dominated by distinct cancerous cell lineages. Some mutations confer a competitive advantage (or disadvantage) to the lineage that only becomes apparent when it interacts with other tumour lineages. Boundaries between domains, where cells from one lineage interact with those from another lineage, are prime regions for inter-lineage interaction. Understanding these interactions is key to understanding the evolution of tumours and their response to therapeutic treatments.

Detecting a pre tumour lesion when the number of mutant cells in the tissue is on the order of hundreds to thousands is a challenging task (Figure 1.1). Furthermore, it has recently been shown that clonal expansion of transformed cells can be balanced by the apoptotic elimination of normal cells, thus allowing mutant cells to proliferate without any detectable morphological aberration. Hence, it appears that transformed cells compete with their non-transformed or less transformed neighbours during the initial stages of tumour growth and the establishment of metastases. How transformed cells interact with their neighbours is poorly understood, despite a better understanding of the early stages of cancer progression, and such knowledge would be extremely useful for developing effective screening strategies as well as new treatments. Little is known about how single cell-level interactions give rise to the global evolution of tumour make-up because we lack the experimental, computational and analytical tools to efficiently characterise interactions between different cancer cell lineages at

the level of single cells. Therefore, the work described in this thesis was aimed at developing techniques for characterising the relationships between epithelial cancer cell lineages at the single-cell level, to understand how cellular interactions can lead to shifts in the make-up of tissues.

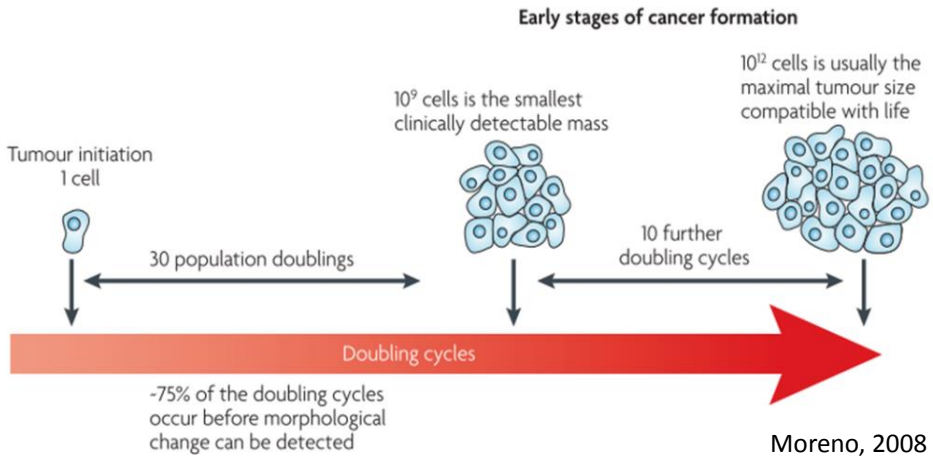

Figure 1.1: The numbers of cancer The numbers of cancer: 75% of doubling cycles occur before any change is detectable. Early stages are phenotypically silent, because expansion of transformed cells is balanced by the apoptotic elimination of wild type cells, thus allowing mutant cells to proliferate without any detectable morphological aberration. Hence, transformed cells compete with their non-transformed or less transformed neighbours during the initial stages of tumour growth and the establishment of metastases. The image is from Moreno (2008).

1.2 Tumour cell heterogeneity: origins and implications

Neoplasias are highly heterogeneous. Four types of genetic heterogeneity are relevant to tumourigenesis (Figure 1.2): (i) intra-tumoural (heterogeneity among the cells of one tumour), (ii) inter-metastatic (heterogeneity among different

metastatic lesions), (iii) intra-metastatic (heterogeneity among the cells of an individual metastasis) and (iv) inter-patient (heterogeneity among the tumours of different patients). Here the term heterogeneity refers to the presence of cellular differences within a tumour, due to lineage difference, arising from both genetic and epigenetic processes. Particularly, (i) is important to understand cancer evolution and to design specific treatments. Indeed, from this heterogeneity, (ii) arises. The founder of a metastasis is a cell that has escaped from the primary tumour, which proliferated. Founder cells of each metastasis, in theory, derive from distinct areas of the primary tumour; therefore, they might present distinctive generic alterations. The inter-metastatic heterogeneity has a huge clinical relevance Vogelstein et al. (2013). Considering that a typical patient on a clinical trial usually displays multiple detectable metastatic lesions, if each one of such lesions derives from a cell with very different genetic background, then chemotherapeutic cures would be nearly impossible to achieve.

Cellular sub populations were isolated from cancers of every major histological type and organ site and from both experimental and human cancers. Moreover, intra tumour heterogeneity was found in tumours induced by a variety of carcinogen factors (chemical, physical, or viral agents) Heppner (1984). The origin of such heterogeneity has extensively been debated and investigated over the years Sottoriva et al. (2013), Fidler (2016). Two major theories were formulated in order to explain intra-tumour diversity: the cancer stem cell hypothesis and the clonal evolution model Campbell and Polyak (2007). The cancer stem cell hypothesis suggests that, at early stages, a tumour is initiated by a small set of cells with stem cell-like features (self-renewal and differentiation abilities). Such cells are thought to drive both initiation and progression of the neoplasia and, through their differentiation, to generate the various cell types within the tumour, thus explaining the intra tumour heterogeneity (Figure 1.3 a). Evidence supporting the existence of such cells was first found in 1994 when it was shown that a small population of cells from human acute myeloid leukemia expressing some cell surface markers associated with normal hematopoietic stem cells could initiate leukemia in immuno-deficient mouse Lapidot et al. (1994). Since then, further studies have reported the existence of stem cells in many tumour types such as lung, brain, skin, prostate, and colon Fang et al. (2005), Singh et al. (2003). The cancer stem cell model has been validated via transplantation assays, which test the tumorigenic potential of isolated cells in highly immuno-compromised mice. Nevertheless, it has been argued that there may be cancer cells that might be able to contribute to growth and progression of cancer, but that fail to exhibit this potential after transplantation due to the xenogenic immune response.

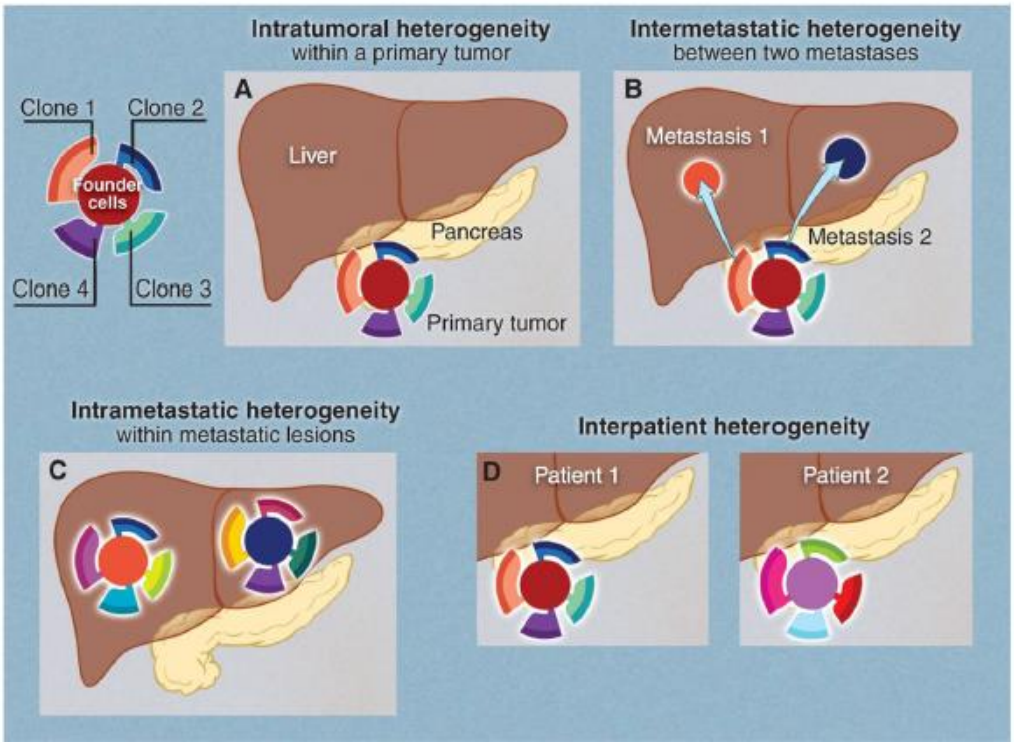

Figure 1.2: Types of tumour diversity Four types of tumour heterogeneity. Clonal heterogeneity arises from mutations that occurred during initiation of primary tumour. At the top left, a primary tumour is illustrated by cells with a large fraction of the total mutations (founder cells in red) from which coloured sub-clones are derived. Differently coloured regions in the sub-clones represent stages of evolution within a sub-clone. (A) Intra-tumoural: heterogeneity among the cells of the primary tumour. (B) Inter-metastatic: heterogeneity among different metastatic lesions in the same patient. (C) Intra-metastatic: heterogeneity among the cells of each metastasis develops as the metastases grow. (D) Inter-patient: heterogeneity among the tumours of different patients. Image from Vogelstein et al. (2013).

Conversely, the clonal evolution model hypothesizes that a tumour is initiated by a cell undergoing several rounds of mutations conferring competitive advantage, and its progression is driven by natural selection (Figure 1.3 b). According to this idea, the tumour progenitor can be a random single cell that, following multiple mutations, gained a selective growth advantage over adjacent normal cells. Then, genetic instability and uncontrolled proliferation are thought to give rise to the generation of cells with additional mutations and hence new characteristics. Therefore, in this model, heterogeneity is caused by the emergence

of new hereditary traits in pre malignant and tumour cells. The clonal evolution theory accounts for various traits of tumours, as the above mentioned genomic instability, which was identified as an "enabling feature" of cancer itself Hanahan and Weinberg (2011). Various studies have reported mutational heterogeneity such as diploid and aneuploid clones within a tumour, and different allelic losses in cells from the same tumour. In 2006, Maley and co-workers showed for the first time a direct relationship between clonal diversity in pre malignant lesions and progression to cancer Michor and Polyak (2010), finding that high degrees of clonal diversity correlate with increased risk of malignancy. Patterns of mutation compatible with the clonal model were also found in breast carcinomas Campbell and Polyak (2007). The two theories rely on very different assumptions, but they are not mutually exclusive and can be reconciled (Figure 1.4 a). A third theory on the growth and development of tumours has been suggested in recent years: the "Big Bang" model, Sottoriva et al. (2015). This last model was validated on samples of colorectal carcinomas and large adenomas and predicts that, after initiation, a tumour grows as a single expansion of numerous heterogeneous sub-clones. After initiation, subsequent replication errors are supposed to generate multiple "private" alterations, accumulating in addition to the "public" alterations which are present in the progenitor cells. Such private mutations, although being non-dominant, will persist and spread across the lesion if generated during the early stages of expansion. Conversely, late-arising alterations will only be found in small regions of the tumour (Figure 1.4, b). Despite the debate on the origin of such heterogeneity, the clinical importance of intra tumour diversity is universally acknowledged. Firstly, it affects prognosis by interfering with the molecular classification of tumours into clinically relevant subtypes. Biopsy samples taken from a patient might not be representative of the whole cancerous lesion. How many biopsies does a typical surgeon collect? The heterogeneity signifies that if this number is low, they might not identify the malignant populations. Furthermore, each clone deriving from a defined combination of mutations might display different sensitivity to therapy. Anti-oncogenic therapies may affect one cancer cell lineage more than others and recent work, performed by modelling spatial growth and genetic evolution, revealed this can lead to rapid change in tumour composition selecting for the more malignant lineages Waclaw et al. (2015). Hence, the specific therapeutic strategy of choice depends on identity and make up of the resistant cell populations. A better knowledge of the composition of tumours or pre malignant lesions at early stages (during diagnosis) will play a crucial role for improving both the prognosis and set up of therapeutic treatment of patients.

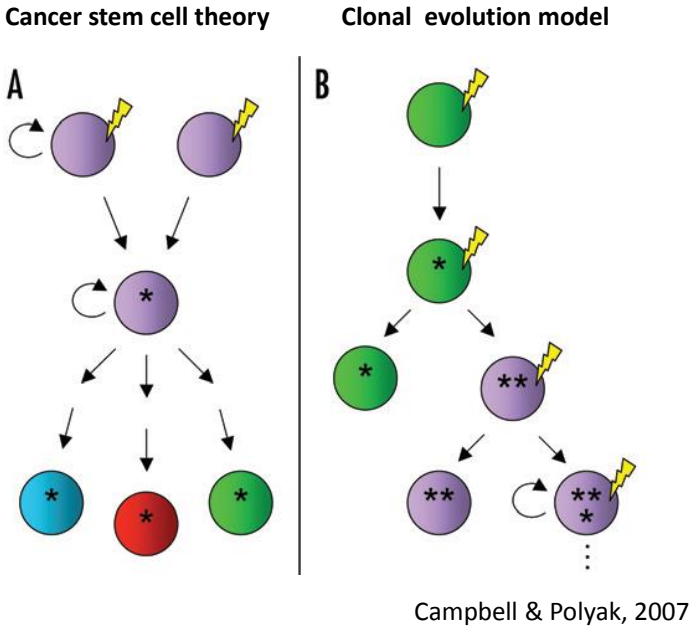

Figure 1.3: The origin of heterogeneity (a) The stem cell theory of cancer identifies a small subset of cells having self renewal and differentiation abilities, as being responsible for intra-heterogeneity. (b) The clonal evolution theory of cancer. Any cell can undergo transformation and acquire additional mutations, giving rise to new lineages of tumour cells. In this cartoon, circles represent cells (with purple indicating stem or progenitor properties), lightning bolts represent mutagenesis, and stars represent mutations. The first star in each circle indicates the multiple mutations needed to convert a normal cell into a cancer cell. The image is from Campbell and Polyak (2007).

1.2.1 Tumour cell plasticity: role of cellular interactions and micro-environmental conditions

In addition to being genetically diverse, cancerous tumours present spatially confined heterogeneous micro-environments with gradients in nutrient availability and oxygenation (Figure 1.5). The tumour environment is, indeed, composed of heterogeneous populations of neoplastic cells growing in a complex cellular array of normal host cells, tumour-derived and/or entrained mesenchymal cells and inflammatory cells (tumour-associated stroma) in a highly dynamic physical and biochemical environment Joyce and Pollard (2009). Tumours are, indeed,

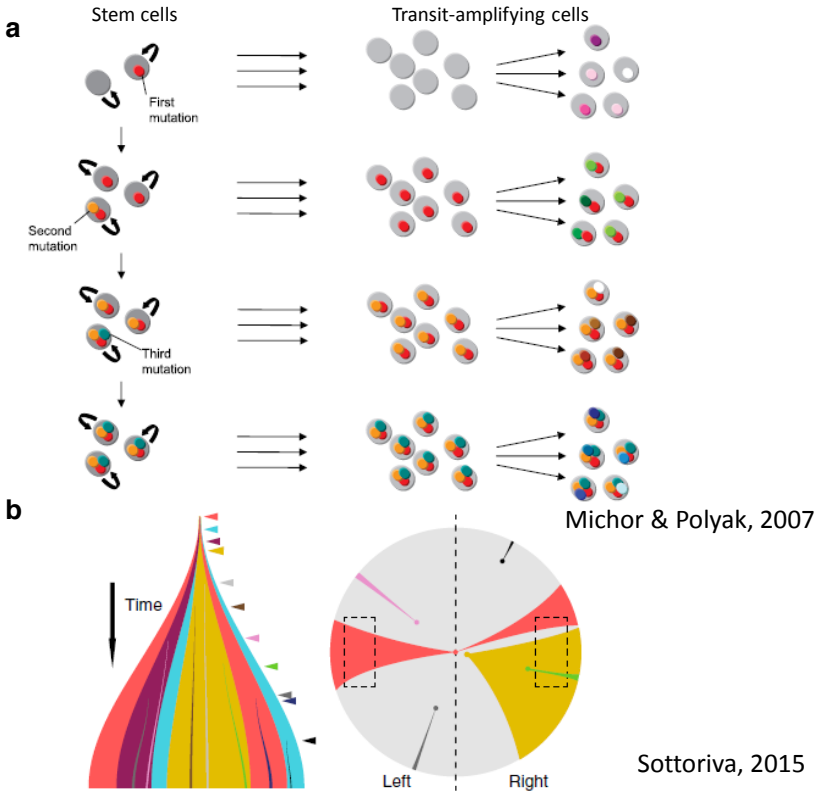

Figure 1.4: Emergence and types of tumour diversity (a) Intra tumour heterogeneity can result from both the differentiation of cancer stem cells (parallel horizontal arrows) and the accumulation of mutations in cancer stem cells (vertical arrows) and transit-amplifying cells (diverging arrows). Image adapted from Michor and Polyak (2010). (b) Left: The Big bang model of tumour growth suggests that, after initiation, tumour undergoes a single expansion, made up of numerous intermixed sub-clones. Alterations in the initiating cell will be present in all tumour cells (clonal). New alterations will continuously be generated as a result of replication errors (coloured arrow heads). The earliest mutations will be pervasive, whereas later alterations will be localized in progressively smaller sub-populations. Right: Diagram illustrating how early private alterations (yellow or red) are pervasive within the tumour, so that they can scatter and spread in distant regions during expansion (red). Alterations arising at later stages are limited to small regions (black, pink, gray). Image from Sottoriva et al. (2015).

characterised by a fast growing irregular network of blood vessels, which are more poorly organized than in normal tissues. Such inefficient network organization causes poor delivery of nutrients and oxygen and inefficient clearance of metabolic breakdown products from the tumour. As a result, the chemical environment is characterised by regions of hypoxia, where cells activate glycolitic metabolism,

thus increasing the concentration of acid by-products (Figure 1.5).
Early studies using spontaneously arising tumours in syngenic mice demonstrated that the number of cells needed to transplant a tumour varies according to the location of transplantation and their environment. Particularly, such landmark studies showed that transplantation efficiency was increased when lethally irradiated cells were injected along with the viable tumour cells (Revesz effect) Klímek (1962). More recent work demonstrated the increased efficacy of transplantation in orthotopic sites when cell suspensions containing putative cancer stem cells are mixed with Matrigel prior implantation Hill (2006), indicating a role for the growth factors contained in such membrane-like substance to support proliferation of cancer cells. Indeed, over the years more experimental evidence has been presented supporting the idea that interaction and stimulation from the micro-environment determines the transplantation efficiency together with the spread and growth of tumour lineages. For instance, it was shown that cross-talk mediated by nitric oxide signalling between stem cells and endothelial cells present in the perivascular niche is involved in the progression of gliomagenesis Charles et al. (2010). Recent work on fixed samples also suggested that micro-environmental conditions affect the outcome of interaction between cell lineages Garvey et al. (2016). Such evidence led to consider the role of cancer cell plasticity in determining tumour heterogeneity. An alternative hypothesis to the cancer stem cell model was formulated, stating that tumour cells retain degrees of stemness and that these are variably expressed depending on the environment to which the cells are exposed Hill (2006). In addition to this, several reports have demonstrated the ability of cancer cells to recruit other cell types and induce their differentiation in order to promote tumour growth and metastasis progression. For instance, it was shown that cancer cells are able to convert stromal fibroblasts to a cancer-associated fibroblast (CAF) phenotype. Such CAFs were responsible, in an *in vivo* model of breast cancer, for the remodelling of the extra cellular matrix, thus enabling cancer cell invasion and promotion of metastasis Avgustinova et al. (2016). Thus, understanding how cancer cell lineages interact in realistic micro-environments or under stress is crucial for designing anti-cancer therapies. Traditionally, the biology of solid tumours has been governed by the study of genetic and epigenetic alterations that transformed cells undergo during the course of multi-step tumour pathogenesis. However, in recent years, the idea that the micro-environment is an important determinant of tumour behaviour has gained increasing popularity Mcallister and Weinberg (2014).

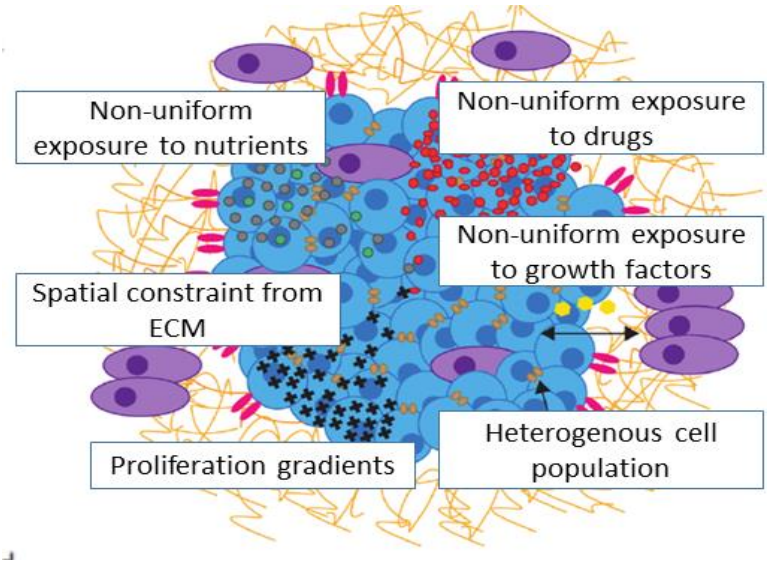

Figure 1.5: The tumour micro-environment. In the past, cancer biology was focussed on genetic mutations that normal cells acquire in the carcinogenesis process. This approach is important but limited, as it does not consider the interaction with other cell types present in the environment, like stromal cancer associated fibroblasts (CAFs) or immune system (IS) cells that have been shown to play a role in collaborating to the proliferation and spreading of malignant phenotype. New approaches for studying cancer are focused on heterotypic signalling between the diverse cell types within a tumour. Also, together with complexity in their cellular composition, solid tumours are characterised by a dynamic and variable chemical environment. Indeed, they are supported by an irregular vascular network, and this gives rise to poor delivery of nutrients and oxygen as well as an inefficient clearance of metabolic breakdown products from the tumour.

1.3 Cell competition: definition of classical and super competition

Cell competition was originally observed by Gines Morata and Pedro Ripoll Morata and Ripoll (1975) during research studies in *Drosophila melanogaster* epithelia. While studying a class of mutants called Minutes (M) carrying a loss of function for protein components of ribosomes, they discovered that homozy-

gous individuals were not viable, whereas heterozygotes (M/+) were still viable, although they displayed a decreased growth rate. Interestingly, when Minute heterozygous cells were in genetic mosaics, confronted to wild-type cells, (M/+) were eliminated by apoptosis and replaced by wild-type cells. The eliminated M/+ cells were referred to as "losers" while wild-type cells were termed "winners" as they outcompeted the M/+ cells. The following empirical rules of cell competition were deduced from the first landmark studies: (i) the viability of a cell and its representation in the final tissue are context dependent, (ii) less competitive cells are eliminated (iii), cell competition does not alter total tissue size, so competition is phenotypically silent. This happens because the expansion of "winners" is balanced by elimination of "losers" through apoptosis. No change in overall tissue size and morphology can be detected after competitive interactions have occurred (Figure 1.6 a).

Further studies revealed that many other genes regulating cell growth and proliferation play a role in cell competition Tamori and Deng (2011),Simpson and Morata (1981),Oliver et al. (2004). For instance, it was found that mutant mouse embryonic stem cells heterozygous at the Bst locus, which encodes for a riboprotein, did not contribute to chimaeras after transplantation into blastocysts of a wild type animal. Nevertheless, in reverse transplantation experiments, wild type cells contributed disproportionately throughout the animal. This additional evidence led to consider changes in ribosomal activity as a trigger of cell competition in mice Oliver et al. (2004). Such results led the field to think, at first, that the competitive status of a cell (i.e. winner or loser) was linked to its relative growth rate. Therefore, cell competition was thought to work as an intrinsic homeostatic control mechanism, maximising tissue fitness by destroying suboptimal cells.

Cell competition attracted further interest after the discovery of super competitors (Figure 1.6 b): cells that, upon acquisition of an advantageous mutation, are able to eliminate cells of normal fitness, even if they are vastly outnumbered Merino et al. (2015), Moreno et al. (2004). The first example of super competitors was found in *Drosophila melanogaster* mosaics that juxtaposed cells with different expression levels of dMyc, a conserved transcription factor regulating multiple downstream targets involved in proliferation and apoptosis de la Cova, Claire and Johnston (2010). Clones of cells expressing hypomorph dMyc (which reduces but does not completely eliminate the function of dMyc) in mutant flies were viable when surrounded by similar cells, but were eliminated in the proximity of wild type cells. This confirmed the existence of a mechanism able to eliminate suboptimal cells (cells with lower levels of Myc) in a developing tissue. Interestingly, wild type cells themselves were eliminated when surrounded by cells over-expressing the myc gene (3 x Myc cells), which were therefore considered

super competitors. When small clones of cells over expressing dMyc were found in a wild type background, they over-proliferated, as expected. However, in addition to this enhanced growth rate, it was shown that cells over expressing dMyc were able to induce apoptosis in wild type neighbours Cova et al. (2004),Moreno et al. (2004). Such induction of cell death was not only due to the increased proliferation of the dMyc over expressing cells. Indeed, it was shown that cells over-expressing cyclin E over-proliferated but were not able to induce apoptosis in neighbouring wild type clones Cova et al. (2004). The induction of cell death by dMyc over expressing cells caused the tissue to retains its original size, while becoming dominated by dMyc over expressing cells. Interestingly, this scenario is reminiscent of field cancerisation Rubin (2011), a theory of cancer development where a mutation in a single cell allows the mutant cells to progressively colonise a tissue (Figure 1.6 b).

1.3.1 Characterisation of cell competition

The first evidence of the existence of competitive interactions between normal and transformed cells was shown in *Drosophila melanogaster* imaginal disc epithelia, as mentioned in the previous paragraph. Epithelial monolayers in the imaginal discs of Drosophila are ideal *in vivo* models to examine the interaction between transformed and normal cells. The clonal techniques available in Drosophila, by using genetic tools and inducible site-specific recombination events, enable researchers to induce mosaic expression of a target genetic mutation. Hence, such techniques made possible the creation of epithelial monolayers where mutant cells are surrounded by wild type cells. Specific genes or RNAi constructs can be targeted in cells within these patches. Using such genetic tools, researchers demonstrated that transformed cells showed distinct cell responses when surrounded by wild type cells compared to when the whole tissue is populated by transformed cells. For instance, the context-dependent viability of Minute and Myc mutants was demonstrated by following over time the size and number of cells in each patch carrying the target mutation. In this way, it was discovered that wild type cells in a Minute heterozygous background expanded to cover larger areas of the adult wing than Minute cells, while Minute cells were eliminated by apoptosis from a wild type tissue. The effect of apoptosis on colony size and dimensions is relatively easy to test, by expression of dominant negative forms of important pro-apoptotic proteins (as c-Jun N-terminal kinases, JNK) or, on the contrary, by site-specific induction of cell death (via expression of Hid, a generic apoptosis inducer). Overall, these techniques allowed to test for cell-autonomous or non cell-autonomous behaviour and, as a consequence, *Drosophila melanogaster* became a very important model system to identify signalling pathways, features

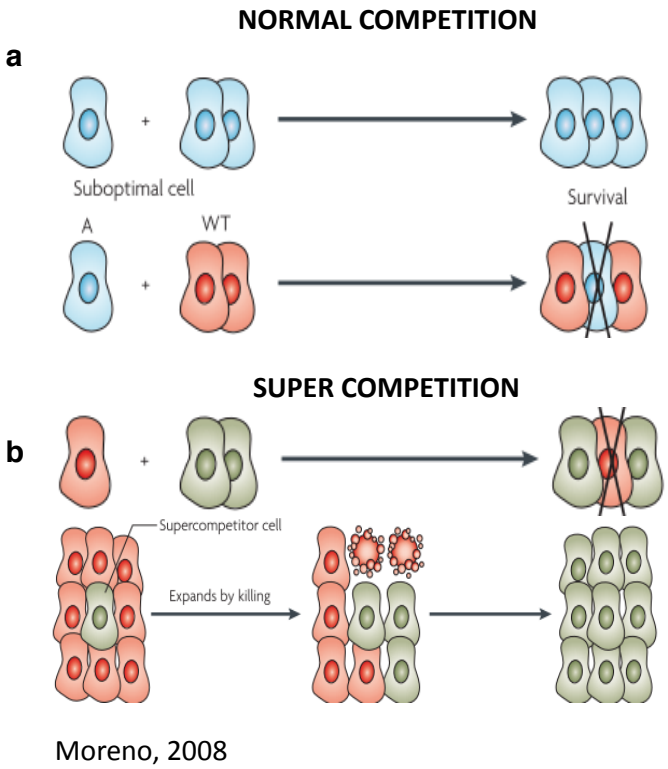

Figure 1.6: Cell competition as a context dependent phenomenon a) Top: A clone of mutant cells is viable in a homotypic environment. Bottom: when mutant cells are cultured in a heterotypic environment, they are eliminated by healthier wild type cells (WT). b) Top: Competition between mutant cells with increased cell fitness (super competitors in grey), inducing apoptosis in surrounding wild type cells. Bottom: Super competition contributes to cancer progression before morphological changes are detectable, creating field cancerization. Image from Moreno (2008).

and rules of cell competition processes.
The study of cell competition *in vitro* has mostly been performed by using stable cell lines where expression of an shRNA or constitutively active mutants of oncogenes can be induced by addition of tetracycline Hogan et al. (2009), Kajita et al. (2010), Norman et al. (2011), as I describe in section 1.6.3. By mixing in pre-determined ratios such inducible lines with the wild type lineage, it is possible to produce mosaic tissues where transformed cells are surrounded by normal neighbours. Importantly, such system allows to control the time of the induction of the mutant lines. A typical strategy is to let the monolayer grow and let the neighbouring cells establish mature intercellular junctions before induc-

ing the transforming mutation. Then, a common approach is to use time-lapse imaging to follow the fate of mutant cells confronted to wild type neighbours. Such a protocol has the advantage of enabling to monitor cells over a long time period (several days) rather than examining just a few fixed time points. It also allows observation of live cells in real time, from which analysis of cell shape, morphology and cell death can be performed. Indeed, researchers demonstrated the occurrence of competition in mammalian cell culture systems by showing that transformed cells have a higher rate of cell death when in contact with normal neighbours than when surrounded by similar neighbours. After having assessed this, many groups oriented their subsequent analysis to the characterisation of the mechanism by which loser cells are removed from the epithelium. By means of immuno-fluorescence, confocal imaging and post-processing analysis of time-lapse data, the interface between winner and loser cells and the morphology of inter-cellular interactions were studied. For instance, the analysis of the elimination of v-Src or RasV12 cells from MDCK monolayers demonstrated the existence of common features in this process (Figure 1.8). In both cases, it was found that the interaction with normal cells was important to determine the fate of loser cells. Morphological studies revealed that, prior to elimination, transformed cells undergo cell shape changes and increase their height due to different organization of the actin-myosin cytoskeleton Hogan et al. (2009),Kajita et al. (2010). From the molecular characterisation of cellular interactions, many aspects of cell competition were discovered as, for instance, the downstream activation of MAPK kinases signalling pathways. These reports also suggest the importance of understanding the molecular mechanisms by which cells belonging to different lineages recognise each other and indicate a potential role for physical properties of cells, based on the observation that transformed cells (RasV12 or v-Src) have altered physical properties (i.e. membrane elasticity) compared to normal cells. A few years later, the importance of the morphology of winner-loser interface during cell competition was demonstrated by Levayer and colleagues, Levayer et al. (2015). They developed a new approach to investigate the interactions between winner and loser cells, focusing on the analysis of adhesion and tension generated at the interfaces of competing cell types in Drosophila epithelia. They demonstrated that elimination of losers is proportional to the area shared with winners and that mixing between the two cell types is crucial for such elimination to happen. By measuring via laser nano-ablation the tension generated at homotypic and heterotypic junctions, they showed that winner-loser and loser-loser contacts were more stable (had lower tension) than winner-winner interfaces. Such difference in tension reflected differences in F-actin levels between loser and winner junctions.

To date, most studies have quantified competition at the tissue scale, concentrating on increases in cell death and reporting these for the whole tissue. However, a tissue scale description of outcome obscures key characteristics of how competition takes place at the single cell level. Little is known bout how single cell events can lead to population-wide change to give rise to field cancerisation, for lack of a good experimental system. Importantly, while apoptosis of loser cells was thoroughly investigated, the role of cell division has been, so far, overlooked.

1.4 Molecular mechanism of cell competition

1.4.1 The ligand capture model

More than a quarter of a century after the initial discovery of cell competition, the mechanisms of this phenomenon have not been completely explained at the molecular level. Cell competition reminiscent phenomena have been reported to occur across different species and in many tissues, each situation having peculiarities and differences that makes the identification of a universal mechanism challenging Amoyel and Bach (2014). Two alternative models were suggested in the first instance: the ligand capture model, which involves a passive fight for a survival factor, and the "fitness fingerprint" model, where cells communicate with each other to compare their fitness status and, according to this interaction, activate specific competitive outcomes (Figure 1.7 a).
The first hypothesis suggested the existence of a Darwinian-like competition among cells for limiting amounts of survival-promoting factors, resulting in removal of less fit cells. Such theory was initially formulated on the basis of studies performed by the Moreno lab, while they were looking at the level of the morphogen Decapentaplegic (Dpp) in Drosophila imaginal discs Moreno et al. (2002) ,Moreno et al. (2004). Dpp is a member of the transforming growth factor (TGFβ) family and is known to play a crucial role in determining correct cell patterning, survival, and growth in flies Burke and Basler (1996). Moreno and co-workers were able to show, using the Minute and the dMyc models of cell competition, that markers of diminished Dpp signalling were observed in both losers of Minute- and dMyc-induced competition Moreno et al. (2002),Moreno et al. (2004),Tyler et al. (2007). Moreover, it was demonstrated that losers having reduced dMyc expression could be rescued by increasing the expression of positive regulators of Dpp signal transduction Moreno et al. (2004). Such evidence led them to propose that cells compete for Dpp through efficient capture of the ligand via receptor-mediated endocytosis. This would explain why Minute and dMyc mutant cells with weaker ribosomal activity are outcompeted by wild type cells:

they are less efficient at Dpp uptake and/ or Dpp-dependent signal transduction. However, other reports contradict this model Cova et al. (2004). For instance, cells depleted in the Dpp receptor Thickveins (Tkv) were out-competed by wild type cells; nevertheless, these cells thrive when confronted to a Minute background Burke and Basler (1996). This evidence showed that tkv mutant cells can survive when competing against less fit cells, independently of their lack of Dpp signalling. Therefore, as the ligand capture model failed in explaining all aspects of cell competition, an alternative model was introduced, focussed on the importance of relative fitness of cells for understanding the competition phenomenon.

1.4.2 The comparative fitness model

The "comparative fitness" theory states that cells are able to: (i) recognise differences with neighbouring cells, (ii) acquire either a winner or loser status, according to the outcome of fitness comparison, (iii) eliminate cells with losers status if they have a winner status. This theory is based on the definition of fitness as a parameter that cells are able to measure and compare with one another. To date, cell and developmental biologist involved in characterisation of cell competition have not agreed on a definition of fitness that could be universally applied to all competition scenarios. At first, when Minute and dMyc competition studies were published, fitness was thought to refer to proliferation and growth rate Simpson and Morata (1981). Subsequent work demonstrated that this was not necessarily the case, by revealing that competition could be triggered by mutations that do not affect biogenesis and proliferation Rodrigues et al. (2012). Accordingly, it was demonstrated that not all the growth regulators (i.e. PI3K, insulin signalling, cyclin D and cyclin-dependent kinase 4) can induce cell competition Cova et al. (2004),Vincent et al. (2011).

Further studies performed by Rhiner and colleagues identified a putative signalling code by which *Drosophila melanogaster* cells compare their fitness status by using different isoforms of a transmembrane protein, Flower (Figure 1.7 b), Rhiner et al. (2010). Using microarray techniques, Rhiner identified several genes specifically activated in cells with low levels of dMyc expression relative to their neighbours. They found a transcript that was present only in outcompeted cells, which they called Flower (Fwe). Fwe has three splice variants: Fwe^{ubi}, expressed in all of the cells within the imaginal disc, Fwe^{LoseA} and Fwe^{LoseB} which are only expressed by outcompeted cells. The Fwe^{LoseA} and Fwe^{LoseB} were also found in out-competed scribble, tkv-/- and Minute cells. Such evidence suggested that this was not a specific feature of dMyc induced cell competition. Moreover, Fwe^{LoseA} and Fwe^{LoseB} were expressed by all of the cells in the outcompeted clone, not only in those in contact with wild type neighbours. This suggested

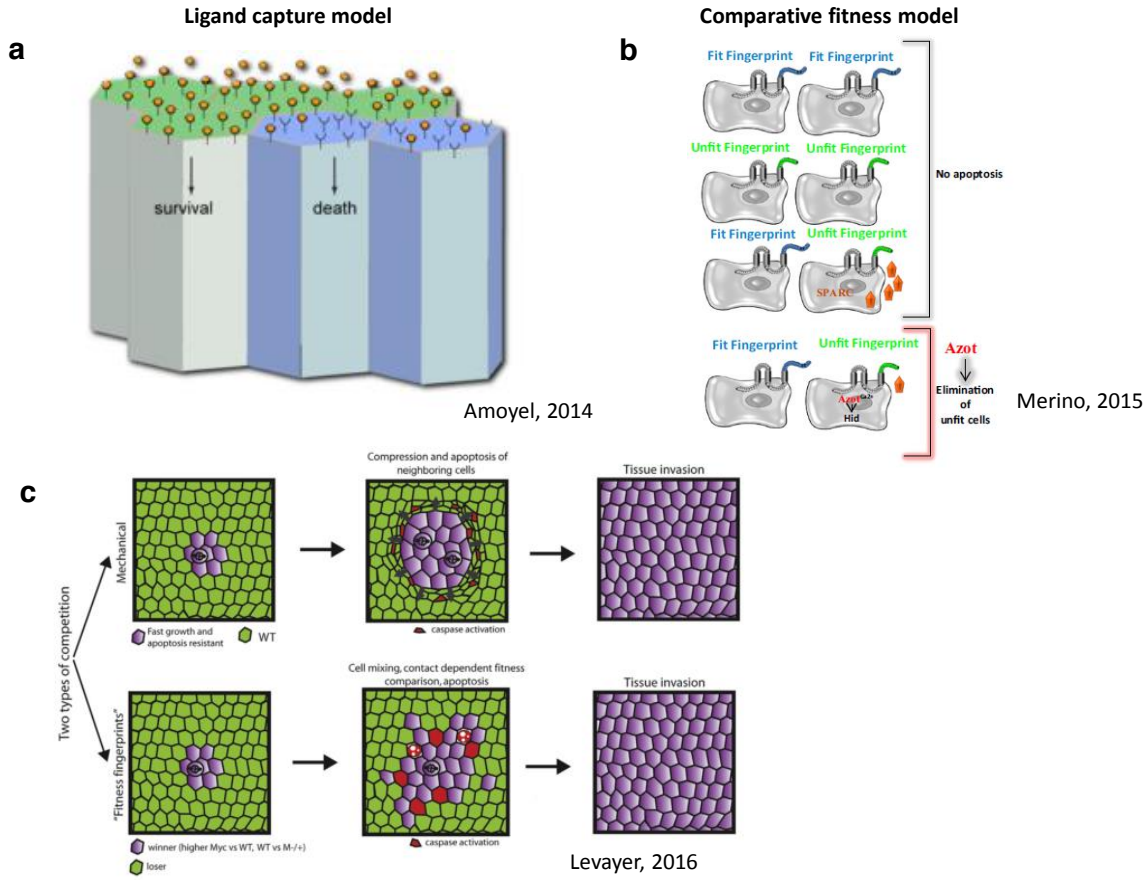

Figure 1.7: Proposed mechanisms of cell competition. a) In the ligand capture model, winners cells (green) are more efficient in the capture of a survival- promoting factor (orange circles). As an effect of such a Darwinian-like competition, cell death of losers cells (blue) occurs, because of the lack of sufficient survival signal. Competition is, therefore, independent on cellular interactions. Image is adapted from Amoyel and Bach (2014). In contrast, in the comparative fitness model (b), cell competition arises from interactions and direct comparison of cellular fitness among neighbour cells through specific fitness markers (Fwe^{Lose}, dSparc, Azot). The cartoon shows four different scenarios: for instance, cells expressing Fwe^{Lose} but that are either surrounded by cells with equal or higher levels of Fwe^{Lose} or that express high levels of dSparc are not eliminated by the tissue. Cells with higher relative levels of Fwe^{Lose} and not enough dSparc are eliminated, following expression of the gene azot. Image is taken from Merino et al. (2015). (c) Schematic showing the "fitness fingerprint" competition, as opposed to the "mechanical competition". The former is based on a contact-dependent fitness comparison enhanced by mixing between competing lineages; the latter is dominated by long range mechanical cues, occurring when a clonal population with faster growth and resistant to apoptosis induces crowding in the neighbouring cells and activates apoptosis. Image from Levayer et al. (2015).

that expression of the Fwe^{LoseA} and Fwe^{LoseB} was not induced by interaction with wild type cells Rhiner et al. (2010). It was shown that the expression of Fwe^{Lose} isoforms at the cell membrane of a cell does not imply that the cell will be eliminated. Indeed, for elimination to happen, the neighbours of a target cell need to have lower Fwe^{Lose} isoforms expression: if neighbouring cells have similar levels of Lose isoforms, no apoptosis is observed Merino et al. (2015), Rhiner et al. (2010). Furthermore, a secreted protein called dSparc, which acts in an opposite pathway to the Fwe^{Lose} isoforms, was discovered Portela et al. (2010). Similarly to Fwe^{Lose}, dSparc expression increased upon cell competition and functional analysis showed that it acted upstream of apoptosis of loser cells. Indeed, Portela and collaborators hypothesised that dSparc functions to delay apoptosis of loser cells, by demonstrating that transcriptional activation of dSparc provides transient protection from apoptosis to loser cells, pushing them to a sort of intermediate state (Figure 1.7 b).

1.4.3 Mechanical competition

Finally, recent experimental evidence suggested the existence of a different mode for cell competition, named mechanical competition, where mechanical stress and cell density within the tissue are the major determinants of the competition outcome (Figure 1.7 c). Levayer and co-workers Levayer et al. (2016) formulated this model while studying delamination occurring in the mid-line of *Drosophila melanogaster* notum epithelia. They found that apoptosis and delamination in this region was non cell-autonomous, but influenced by local tissue properties. Therefore, they tested the hypothesis that mechanical stress affected cell delamination non cell-autonomously by inducing ectopic local increases in cell density. Ras signalling is known to increase proliferation and block apoptosis Kurada and White (1998); therefore they induced rapid growth and survival through clonal expression of an active allele of the oncogene Ras. By doing this, they showed that activation of the Ras oncogene in isolated clones was sufficient to compress the neighbouring tissue and eliminate wild type cells up to several cell diameters away from the clones Levayer et al. (2016). Notably, these apoptosis/delaminations were not driven by fitness-dependent competition as they were not strictly contact dependent and no expression of the fitness markers Fwe^{Lose} or dSparc was detected in the loser cells. Therefore, a new model of super competition that acts independently of cell recognition and fitness comparison was postulated. Such model proposed that this type of competition was triggered only by mechanical stress due to the comparison of population having different growth rate. Interestingly, Levayer and colleagues also argued that dMyc induced super competition is unlikely to be driven by crowding induced death, as strong

over-expression of dMyc is known to increase apoptosis within the clone. In addition to this, dMyc over-expressing clones undergo cell intercalation and cell mixing with the surrounding wild type tissue Levayer et al. (2015). Therefore no major deformations in the neighbouring tissue were observed, suggesting that the mechanical stress is dissipated. While competition was initially thought to take place only at the interface between cell lineages, the discovery of mechanical competition revealed that this is not necessarily the case and that extrusion may take place several cell diameters away from this interface.

1.5 Cell competition in cancer evolution

Over the years, scientific reports have linked cell competition to the carcinogenesis process. In its original definition (Figure 1.6 a), cell competition was interpreted as a sort of defence mechanism, whose aim was to maximise tissue fitness and organ function by eliminating suboptimal cells Moreno et al. (2004). Indeed, several groups showed selective apoptosis of transformed cells Hogan et al. (2009), Kajita et al. (2010) or cells where the expression of important tumour suppressor genes was knocked-down Brumby and Richardson (2003),Tamori et al. (2010), Tamori and Deng (2011) when such mutated cells were confronted with wild type neighbours. In 2009, Hogan and co-workers demonstrated that upon expression of constitutively active oncogenic Ras (RasV12), 80% of transformed MDCK cells were eliminated by wild type neighbours, via apical extrusion (Figure 1.8) Hogan et al. (2009). No extrusion was observed when transformed cells were cultured in pure populations. It is important to mention that Ras GTPase is a key regulator of multiple cellular processes, such as cell growth and proliferation, cell survival, actin cytoskeletal reorganization, and cell polarity Vigil et al., 2010. Therefore, when mutated to a constitutively active form, Ras is a very dangerous oncogene, representing an early event in almost 33% of all human cancers Karnoub and Weinberg (2008). Similar results were obtained when Rous sarcoma virus Src gene expression was induced in both MDCK cells (Figure 1.8) and *Zebrafish* systems Kajita et al. (2010). V-Src was the first retro-viral oncogene to be identified Hunter and Sefton (1980); it encodes for a tyrosine kinase which can phosporylate multiple proteins on tyrosine residues. Src regulates the activity of a variety of cellular processes and functions (the actin cytoskeleton, cell adhesions, cell proliferation).

The possible role of cell competition as an intrinsic homeostatic system through which normal cells sense and remove pre cancerous cells was confirmed by further studies performed on a class of polarity genes: scribble (Scrib), lethal-giant larvae (Lgl), and discs large (Dlg). These genes are required for establishment and

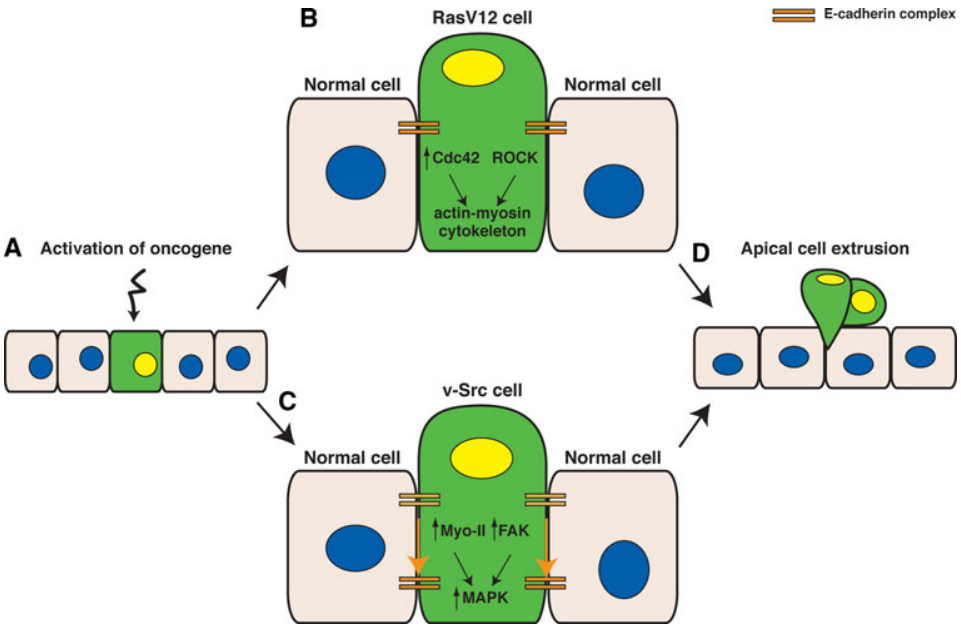

Figure 1.8: Mechanism of apical extrusion of transformed cells from normal epithelial monolayers. a) Activation of an oncogene (RasV12 or v-Src) in a single epithelial cell (green) within a monolayer of normal cells. b-c) Interaction with normal neighbours cause the transformed cell to modulate its shape, signalling, and behaviour, suggesting that transformed and normal cells recognize differences between them. The process of apical extrusion of transformed epithelial cells from normal monolayers requires specific common features: (i) the interaction with normal cells, (ii) myosin II-dependent increase in cell height and cell shape of the transformed cells and (iii) activation of MAPK signaling pathways. d) Oncogene-transformed cells are apically extruded from normal epithelial monolayers. Image from Hogan et al. (2011).

maintenance of apico-basal polarity in epithelial tissues of both flies and mammals. Therefore mutants epithelia have structural defects (polarity mismatches) and their cells were termed as structurally defective cells (SDCs). Moreover, the *Drosophila melanogaster* Scrib, Lgl, and Dlg were shown to negatively regulate cell proliferation and were therefore classified as tumour suppressor genes Bilder (2004). A similar role was described for scribble and Lgl in mammals; it was demonstrated that loss of scribble induces disruption of three dimensional architecture of

mammary epithelial cells and inhibits apoptosis Zhan et al. (2011). In mice, knock-out of the mammalian homologue of Lgl leads to hyper-proliferation and loss of cell polarity in neuroepithelial cells Klezovitch et al. (2004). Cells mutant for any of these three genes are viable, show a faster proliferation, and a higher growth rate that will eventually lead to overgrowth when in a homotypic environment. However, when mutant clones are confronted with wild type cells, they are eliminated in a context specific way, which is a typical hallmark of cell competition Bilder (2004). Interestingly, in this type of competition, the losers are the faster proliferating population, in contrast to Myc and Minute-induced competition where the opposite is observed. Hence, in the context of SDC cells, competition works as a defence mechanism which preserves tissue homeostasis against the proliferation of cells showing a tumourigenic potential (Figure 1.9 a).

The involvement of tumour suppressor pathways in cell competition was demonstrated in mammals by using mouse models Bondar, Tanya (2010). By injecting bone marrow from low dose irradiated (IR) and untreated mice into lethally irradiated recipient mice, Bondar and co-workers found that the hematopoietic stem and progenitor cells (HSPCs) from untreated mice outcompeted those from irradiated mice. These results are consistent with the concept of cell competition as a mechanism that selects for the least damaged cells. Using an elegant technique, Bondar and colleagues produced genetic mosaic mice models where they could alter p53 gene expression. By performing experiments in this model, they showed that cells with lower p53 activity are somehow able to outcompete cells with higher p53 activity, following irradiation. In contrast to what found in cell competition occurring in *Drosophila melanogaster* epithelia, in the hematopoietic system apoptosis was not required for the p53+/- cells to dominate. Bondar and collaborators reported, instead, a senescence-like phenotype in outcompeted HSPCs, with increased expression of senescence markers p16INK4a and Ezh2 Bondar, Tanya (2010). In this situation, winner cells displace other stem cells (losers) from their niche, causing their differentiation. As a result, loser cells do not contribute to the stem cell pool. The IR stress induced p53-mediated cell competition showed, therefore, some distinct aspects from the competition features described in *Drosophila melanogaster* studies Moreno et al. (2004). For instance, in the p53 competition, loser cells are outcompeted only after IR stress is induced. Nevertheless, this phenomenon is reminiscent of cell competition and indicates the first evidence of p53 involvement in this process. Moreover, since it targets long-lived HSPCs, where mutations are believed to accumulate during oncogenesis, it may be a key player in early stages of cancer development.

The discovery that the proto-oncogene Myc was able to induce super competition led to the hypothesis that cell competition could be related to cancer, but in an

opposite way to what I discussed so far. Indeed, in the case of super competition, transformed cells are able to expand by killing surrounding wild type tissue by apoptosis, leading to the proliferation of oncogene activated phenotypes. In flies, only two related pathways were identified that can transform cells into super competitors Ziosi et al. (2010): the Myc and the Hippo (Hpo) -Yorkie (Yki) Zhao et al. (2011) pathways (Figure 1.9 b). The highly conserved Hpo signaling pathway is important in the regulation of organ size, preventing hyperplastic disease by restricting the activity of the transcriptional cofactor Yki. Further studies reported that, upon over expression of Yki or down regulation of Hpo, apoptosis of wild type neighbours was specifically observed in the presence of transformed cells Chen et al. (2012). In contrast to dMyc induced super competition, which I discussed in the previous paragraph, when Yki was over- expressed the tissue size (i.e. *Drosophila melanogaster* eyes) was not preserved; rather it expanded abnormally. Later, it was shown that dMyc is a transcriptional target of Yki and that dMyc upregulation is a common feature of Hpo pathway mutant cells Ziosi et al. (2010). In addition to this, Ziosi and co-workers demonstrated that some of the effects of Yki are mediated by Myc. For instance, the protein biosynthesis and cellular growth due to dMyc over expression is responsible for promoting the clonal expansion of Hpo pathway mutant cells. Nevertheless, Yki has additional effects besides activating dMyc, as demonstrated by the fact that Hpo pathway mutants do not undergo spontaneous apoptosis as dMyc expressing cells do. Hence, it appears that the two genes cooperate, with the Hpo pathway mutant cells being able to use high levels of dMyc to proliferate rapidly. Furthermore, it was discovered that when Yki over expressing cells were found in a dMyc over expressing background, their clonal expansion was reduced. Importantly, YAP (the Yki ortholog in humans) deregulation was reported in various types of human cancers M. (2009). The cooperation of dMyc and Yki in super competition helped elucidate the dual role that cell competition might play in cancer. Indeed, it appears that cell competition could either restrict or promote tumour progression; the determinant in each situation will be the output of the genetic interactions occurring with adjacent cells.

1.6 The scribble complex and its function in epithelia

Scribble was first identified in 2000 as a mutant that disrupted epithelial morphogenesis in *Drosophila melanogaster* embryos (Figure 1.10 c). Drosophila scribble is a large scaffold protein (1,756 amino-acids) containing 16 amino terminal leucine rich repeats (LRR), two LAP specific domains and four (PDZ) domains located

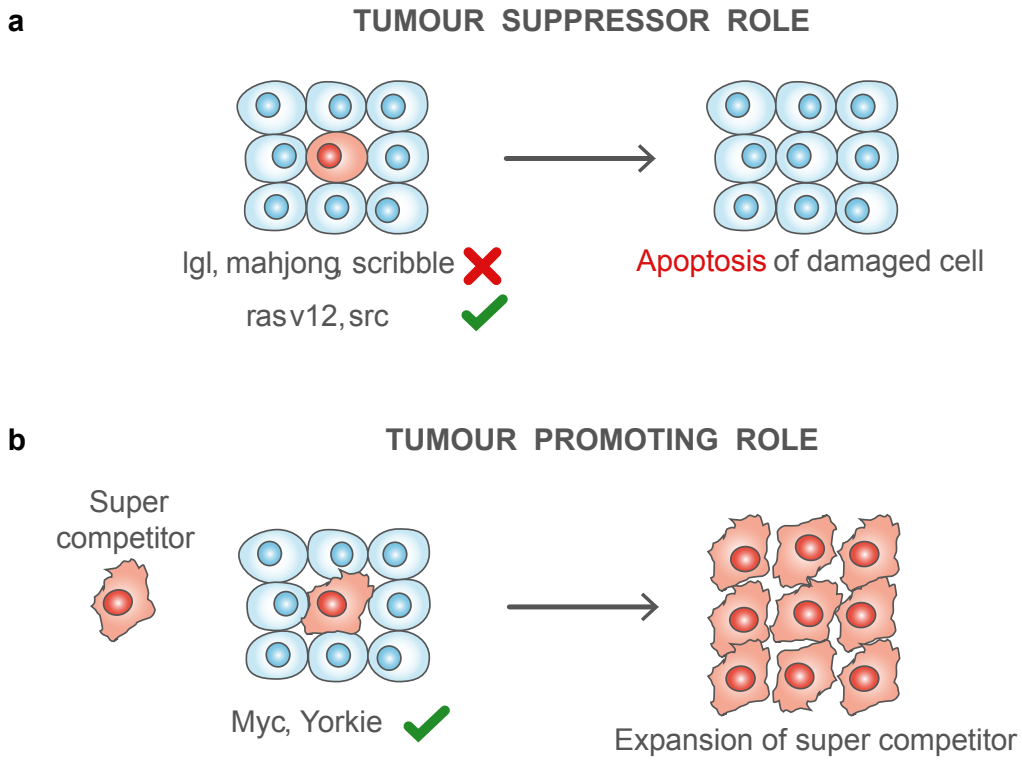

Figure 1.9: Cell competition and its role in cancer evolution a) Tumour suppressor (lgl, dgl, scribble) inactivation or activation of oncogenes (Ras V12, vSRC) lead to the elimination of pre-cancerous cells by cell competition mechanisms. Thus, in this scenario, cell competition acts as a defence mechanism. b) supercompetition phenomena can transform cells into supercompetitors, which are able to induce apoptosis in surrounding wild type cells. Super competition, therefore, promotes field cancerization and the expansion of the mutated phenotype in the tissue.

towards the carboxyl terminus of the protein (Figure 1.10 b) Bilder and Perrimon (2000). In *Drosophila melanogaster*, scribble protein localised to the septate junction (analogous to the tight junction in vertebrates), at the interface between the apical and the basolateral cell membranes (Figure 1.10 a). The LRR repeats are responsible for the specific plasma membrane localization, both in mammalian cells and in *Drosophila melanogaster* Navarro et al. (2005). Indeed, it was shown that substitution of a single amino-acid in the LRR sequence caused cytoplasmic scribble localization, thus inactivating the function of the protein Navarro et al. (2005). The PDZ domains were shown to play an important role for mediating interactions with other proteins Nagasaka et al. (2010), but were not required

for rescuing the polarity defects in scribble mutants. Scribble structure has been highly conserved during evolution, so that proteins from *Caenorhabditis elegans, Drosophila melanogaster* and mammals share common domains. Indeed, in 2003, a mammalian homologue of scribble (hScrib) was found Dow et al. (2003). Human scribble is slightly shorter (1630 amino-acids) than its *Drosophila melanogaster* homologue, with whom it shares 37% total amino acid sequence, with higher homology at the highly conserved LRR and PDZ regions (Figure 1.10 b) Dow et al. (2003). Interestingly, expression of GFP-hScrib in *Drosophila melanogaster* scribble mutant clones rescues the mutant phenotype (Figure 1.10 d), demonstrating the functional conservation of the proteins Dow et al. (2003).

Together with the lethal giant larvae homologue (Lgl) and the disc-large homologue (Dlg), scribble forms a complex known to determine baso-lateral membrane identity and regulate the expansion of the apical domain Bilder and Perrimon (2000). A major function of this complex is to restrict the Par complex to its apical localisation Humbert et al. (2008). The establishment and maintenance of polarity in epithelial cells is, indeed, strictly determined by three complexes (Figure 1.10 a): the Crumbs complex which localises to the apical membrane, the Par complex which localises to the sub-apical region, and the Scribble complex. In mammalian epithelial cells, the Scribble complex is found at the basolateral membrane whereas it is at the septate junction in flies. Likewise, the Par complex has a slightly different localisation in mammalian and *Drosophila melanogaster* epithelial cells. In the former, it is found at the tight junction, whereas in the latter it is localised apical to the septate junction. In spite of these differences, the molecules and interactions between these complexes are highly conserved between species Humbert et al. (2008).

Mutants for Scrib, Lgl and Dgl genes were identified by their similar neoplastic phenotype, characterised by aberrant growth of larval tissues. Deletion in any one of the components of the scribble complex caused larvae to develop normally until their lgl, dgl and scrib maternal supplies run out. Hence, their epithelial imaginal discs lose their polarised architecture. As a result, epithelial cells fail to differentiate and over proliferate, giving rise to a multi-layered amorphous mass Bilder (2004). The larvae cannot proceed to pupal development and eventually die as giant overgrown larvae. For this reason, the three genes (Scrib, Lgl, Dgl) were labelled as Drosophila neoplastic tumour suppressor genes.

In mammalian cells, the contribution of scribble to the regulation of apical-basal polarity and epithelial morphogenesis is less clear. No major disruption in apico-basal polarity in mammalian epithelial cells lacking scribble was observed when culturing cells in standard *in vitro* culture. Similarly, when culturing MCF-10A or

MDCK cells in 3D, either using Matrigel or type I collagen gels, the formation of 3D cysts with the correct polarity was observed, although there was a significant suppression of apoptosis, which is required for the proper formation of the acini structure Dow et al. (2003).

1.6.1 Scribble and its role in regulating cell proliferation

Cross-talk between polarity complexes and signalling pathways regulating tissue growth has been shown both in *Drosophila melanogaster* and mammalian cells. Further work in *Drosophila melanogaster* showed that scribble mutant cells proliferate aberrantly Brumby and Richardson (2003) in addition to failing in differentiation. Indeed, scribble was identified in a screen for suppressors of a cyclin E hypomorph mutation in *Drosophila melanogaster* eye imaginal discs, suggesting that it regulates entry into S phase (Figure 1.10 a). In the developing eye, Lgl and Scrib mutant clones also show abnormal expression of CycE, together with a higher number of cells in S phases than control Brumby and Richardson (2003). The role of scribble in the control of CycE expression was also demonstrated by a study of genes required for basolateral junction signalling in the follicular epithelial cells of the Drosophila ovary Zhao et al. (2008). According to this study, loss of scribble (and Lgl, Dgl) produced ectopic expression of CycE, followed by early S phases and mitoses. Therefore, in Drosophila epithelial cells, Scrib, Dlg and Lgl appear to negatively regulate proliferation by controlling cell cycle progression.
Experimental evidence suggests that scribble also regulates cell proliferation in mammalian cell lines, although the mechanism by which this regulation occurs is less well characterized. For instance, it was shown that over-expression of hScrib in various cell lines, either epithelial (MDCK, HeLa) or fibroblastic (NIH3T3) inhibited cell proliferation by arresting the cell cycle in G1 phase and blocking their progression through S phase. Conversely, knock-down of scribble in Caco-2 epithelial cells resulted in an increased number of cells in S phase Nagasaka et al. (2006). Altogether, these results suggested a role for scribble in controlling entry into S phase, thus regulating proliferation Nagasaka et al. (2006). Recently, it was shown that hScrib can directly regulate the extracellular signal-regulated kinase (ERK) Nagasaka et al. (2010). Indeed, this study reported that loss of hScrib caused elevated phospho-ERK levels and nuclear translocation in human keratinocytes. Despite these results, no evidence of scribble knock-down causing abnormal or overgrown phenotypes similar to the Drosophila giant larvae has been reported in mammalians models (reviewed by Humbert et al. (2008)).

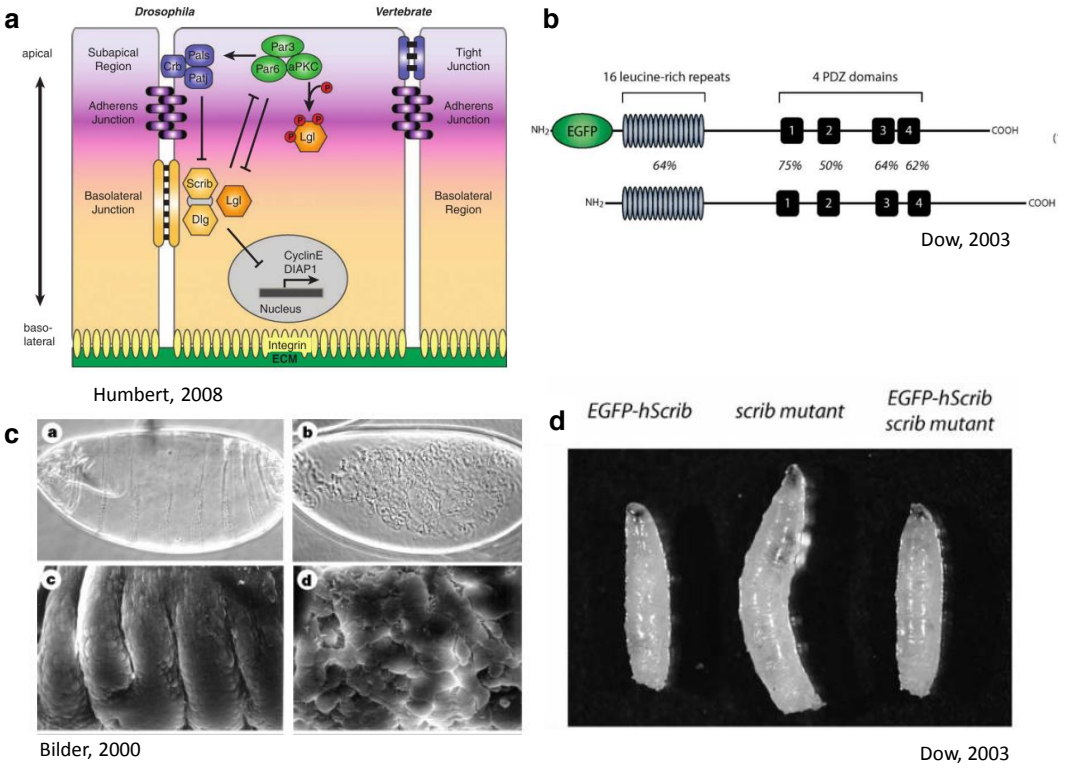

Figure 1.10: The scribble complex is a key regulator of apico-basal polarity. (a) Three modules are responsible for the polarization of epithelial cells: the Crumbs complex, the Par complex, and the Scribble polarity module. The localization of polarity complexes is essential to their function. Antagonistic interactions regulate the activity and localization of such complexes. Polarity proteins have been shown to be at the centre of signalling pathways. The Scribble polarity complex works as a tumour-suppressor by inhibiting the expression of either Cyclin E, a crucial cell cycle regulator, or DIAP1, an apoptosis inhibitor. Image from Humbert et al. (2008). (b) Schematic representation of EGFP-hScrib fusion protein with reference to dScrib. Similarly to its Drosophila homologue, hScrib contains 16 LRRs and four PDZ domains. Image from Dow et al. (2003). (c) Scrib mutations cause disorganization of epithelia. Top: Wild-type cuticle (left), Cuticle from scribble mutant embryo (right). Bottom: SEM image of wild type embryo showing an organised integrated epithelium structure (Left) scribble mutant embryo SEM picture showing a disorganised structure, with poor cellular adhesion. Image from Bilder and Perrimon (2000). (d) hScrib is a functional homologue of the Drosophila tumour suppressor scribble, as it is able to rescue the giant larvae phenotype induced by scribble inactivating mutations. Image from Dow et al. (2003).

1.6.2 Scribble in human cancer and cancer models

Scribble, together with the other proteins of the Scribble complex, Dlg and Lgl, has been linked to the development of tumours, not only in *Drosophila melanogaster* but also in mammalians models (reviewed in Humbert et al. (2008)). As described in the previous section, mutations in *Drosophila* Scrib, Dlg and Lgl produced neoplastic tumours in epithelial tissues, characterised by apico-basal cell polarity mismatches and loss of proliferation control. Mutants with loss of function or depletion of scribble displayed disrupted apico-basal polarity, and some cooperation with oncogenic signals to promote tumour cell migration, invasion, and survival. Low expression or loss of function of scribble protein is frequently observed in advanced tumours (Table 1.11), where the epithelial cytoarchitecture is normally disrupted Martin-Belmonte and Perez-Moreno (2012). Furthermore, recent evidence has shown that reduction in the expression or mislocalization of scribble has an inhibitory effect on apoptosis but also enhances transformation through the proto-oncoprotein Myc in 3D cultures of human epithelial cells Zhan et al. (2011). Similar effects have been shown in human breast tumours and transgenic mouse mammary tumours caused by scribble down-regulation or mislocalization, which resulted in block of apoptosis and enhancement of carcinogenesis. By using a murine cancer model, it was shown that cells over expressing Myc, which had also undergone scribble knock-down, produced detectable tumours quicker than Myc mutants alone when injected into mammary fat pads of mice Zhan et al. (2011).

The most direct link between the scribble protein and tumour initiation was indicated in the property of this protein of being targeted by oncoviral proteins (reviewed by Thomas et al. (2005)). Human scribble was isolated in a screen for proteins targeted for ubiquitin-mediated degradation by the High-Risk Papillomavirus E6 (HPV E6) oncoprotein. Therefore, it appeared that binding and ubiquitination of scribble from E6 oncoprotein would result in its proteosomal degradation, the decreasing level of scribble correlating with increasing malignancy in cervical cancers Nakagawa and Huibregtse (2000). Indeed, over expression of scribble was shown to inhibit transformation of mice epithelial cells by HPV E6/7 proteins Nakagawa and Huibregtse (2000). Notably, Human papillomavirus (HPV) infections are associated with over 90% of cervical cancers. Other proteins containing a PDZ domain (therefore other polarity proteins) were shown to be targeted for degradation by the human papilloma virus (HPV) oncoproteins, E6 and E7 Nakagawa and Huibregtse (2000), thus complicating the identification of the specific contribution of loss of scribble in HPV infected tumours Thomas et al. (2005). However, it was demonstrated that over-expression of scribble in cell culture suppresses colony formation in cells that contain the E7 oncoprotein

and oncogenic RasV12 Nakagawa and Huibregtse (2000), suggesting that loss of scribble is important for HPV driven tumour initiation.

Although these data suggested a model where scribble acts as an evolutionary-conserved tumour suppressor, its role in human cancer, *in vivo*, is more debated. In contrast to the scientific evidence reporting that scribble expression is lost during human carcinogenesis, other studies have shown that scribble levels increase and that the protein is improperly localised in certain human tumours *in vivo* Vaira et al. (2011). A comparative study conducted on samples of cancers of the colon, liver, prostate, uterus, thyroid, lung, bladder, breast, ovary, and stomach tissues found strong scribble immunoreactivity in all cases, except for the thyroid Vaira et al. (2011). For instance, scribble activity was ubiquitously high and often found in the cytosol of cells from tumour tissues representing various breast cancer types, regardless of the hormonal receptor. These data are supported by reports that found the chromosomal region corresponding to the scribble locus (8q24.3) amplified in a wide range of cancer cell lines, as well as breast and ovarian tumours SangWun Kim, JaeWook Kim, Young Tae Kim,* Jae Hoon Kim, Sunghoon Kim, Bo Sung Yoon and Kim (2007),Naylor et al. (2005). Experiments performed by transfecting anti-scribble siRNA in lung cancer models demonstrated that such depletion strongly affected cell migration and limited cell invasion. Notably, the samples examined were independent of oncogenic signalling or viral (HPV) transformation. It is important to mention that experimental evidence, first collected in *Drosophila melanogaster* and later extended to mammalian cells, demonstrated that scribble works as a general regulator of directional cell motility, mostly via the assembly of multiprotein complexes and the activation of small GTPase signalling at the leading edge of migrating cells (reviewed Humbert et al. (2008)). Hence, in this alternative model, scribble is proposed to promote carcinogenesis by enhancing aberrant cell motility and invasion, thus partially contributing to a type of epithelial-mesenchymal transition. Another study of scribble in human cancer shows that scribble expression in tumours is very heterogeneous, with very low levels of the protein in some regions but strong expression in others Zhan et al. (2011). Furthermore, in the regions where scribble expression was maintained, the tumour-associated scribble exhibited a diffuse cytoplasmic reactivity, suggesting that the protein could be mutated. Future investigations should address whether scribble mutations are common events in human cancers, and if they are the cause of scribble delocalization into the cytosol.

***SCRIB* complex**			
SCRIB (scribble)	Mislocalized or downregulated	High-grade HPV-positive cervical squamous intraepithelial lesions and invasive cervical carcinoma samples	Correlates with invasiveness
	Mislocalized or downregulated	Neoplastic colon mucosa	Loss of tissue architecture
	Mislocalized or downregulated	Human breast cancer tissue samples	Loss of three-dimensional cell polarity and inhibition of apoptosis
DLG1 (DLG)	Mislocalized or downregulated	High-grade uterine cervical neoplasm samples	Role in cytokinesis, viral trafficking and metastasis pathways
	Mislocalized or downregulated	Neoplastic colon mucosa samples	Loss of tissue architecture
LLGL1 (LGL1)	Downregulated	Tissue samples from breast, prostate, lung and ovarian tumours	Disruption of cell polarity and tissue architecture, uncontrolled proliferation and growth of neoplastic lesions
	Downregulated	Colon cancer cell lines and colon cancer primary tissue samples	Associated with advanced stage and lymph node metastases
	Aberrantly spliced mRNA and the expression of truncated protein	Hepatocellular carcinoma cell line and primary tissues	Associated with poor differentiation and large tumour size
	Mislocalized or downregulated	Samples of human gastric epithelial dysplasia and adenocarcinoma	Disruption of tissue morphology

Figure 1.11: Alterations of the scribble complex in epithelial transformation and human cancer. Low expression, loss of function and mislocalization of scribble and the other polarity proteins belonging to the scribble complex are frequently observed in advanced human tumours Martin-Belmonte and Perez-Moreno (2012).

1.6.3 Scribble and cell competition

Together with Minute and Myc, cell competition triggered by Scrib suppression is one of the best characterised examples in literature. The phenomenon was initially observed in *Dropophila melanogaster* by Brumby and colleagues. They reported apoptosis in clones of scribble depleted cells when induced in wild type background, as opposed to the giant larva phenotype observed when the tissue was homogeneously depleted of scribble Brumby and Richardson (2003). These studies were performed in the *Drosophila* eye disc, which is a very good system to study putative tumour suppressors and oncogenes because it undergoes a well characterised progressive differentiation and a tightly regulated proliferation program Wolff and Ready (1991). Experiments performed in such a system confirmed that most of the cells belonging to the scribble mutant clones failed to

differentiate and exhibited abnormal expression of CycE and increased number of divisions Brumby and Richardson (2003). Thus, when confronted with wild type cells, scribble mutant cells showed phenotypes consistent with the documented role of scribble as a tumour suppressor. However, the size of the scribble mutant clones induced in a wild type background eye imaginal disc was considerably smaller than the size of control wild type GFP clones. This observation was intriguing, considering the increased proliferation observed in cells upon scribble knock-down, which in this study was measured by bromodeoxyuridine (BrdU) staining. Further observations revealed that this was due to increased cell death of scribble mutant cells within the clone. Indeed, expression of the caspase inhibitor p35 in scribble clones produced clones with larger size. Notably, the most significant rescue of scribble clonal size was achieved by expression of a dominant-negative version of the *Drosophila melanogaster* c-Jun N-terminal kinases (JNK) homolog, Basket (BskDN), induced specifically within the scribble mutant clone. This results suggested that the JNK induced apoptosis was responsible for the removal of Scribble mutant cells Brumby and Richardson (2003). In both mammalians cells and *Drosophila melanogaster*, JNK is known to induce a stress response leading to apoptosis Mcmahon et al. (2015). Finally, further experiments were performed to test whether JNK induced apoptosis was a cell-autonomous response to a loss of cell polarity or, alternatively, if it was induced by the surrounding wild type tissue. Therefore the wild type eye disc tissue surrounding the scribble mutant clones was removed by expression of the cell death inducer, Hid; this experiment resulted in increased viability of the scribble mutant clones, tissue overgrowth and lethality, thus demonstrating the importance of neighbouring cells in determining the fate of scribble mutants. Further studies demonstrated that the removal of scribble mutant clones from the eye imaginal disc epithelium is dependent on Eiger, the *Drosophila melanogaster* homologue of tumour necrosis factor alpha (TNFα) Igaki et al. (2002). Indeed, scribble/Eiger -/- double mutant clones had increased survival, suggesting that scribble mutant clones may be the source of Eiger. These data are consistent with other reports indicating Eiger as an activator of JNK signalling, which is required for elimination of scribble clones Igaki et al. (2002),Brumby and Richardson (2003).

In 2011, evidence of scribble induced competition was demonstrated in an *in vitro* mammalian model Norman et al. (2011). Indeed, Norman and collaborators showed that the fate of scribble knock-down MDCK cells was influenced by the presence of wild type cells in their neighbourhood. Wild type MDCK cells represent a good system to model a healthy epithelial tissue, with cells forming polarised and well connected monolayers which enable the study of cellular interactions happening between neighbours. For this study, Norman and collaborators

established an MDCK cell line stably expressing scribble shRNA in a tetracycline-inducible manner (*scribble*^{kd}) Norman et al. (2011). This strategy had been used before Hogan et al. (2009),Kajita et al. (2010), as it allowed the proper mixing of transformed cells with non-transformed cells, resulting in the production of a mosaic of epithelial cells. The use of this system also mimics the initiation of cancer, as it allows to have just one cell with the mutation surrounded by wild type cells. Therefore this system, aimed at emulating the chimeric tissue of *Drosophila melanogaster* epithelia, proved to be efficient for analysis of cellular processes at the interface between mutants and normal epithelial cells. By mixing in a 10:90 ratio *scribble*^{kd} with MDCK wild type cells, Norman demonstrated that only upon tetracycline induction, *scribble*^{kd} undergo apoptosis (as demonstrated by the expression of specific apoptosis markers, such as caspase 3) and subsequent apical extrusion from the monolayer (Figure 1.12 a). However, when cultured in pure populations, the *scribble*^{kd} cell line was still viable and able to form an epithelial monolayer. Indeed, when cultured at high density, *scribble*^{kd} mostly maintained a proper apico-basal polarity, as shown by localization of gp135 to the apical domain and the presence of ZO-1 at tight junctions (Figure 1.12 c) Norman et al. (2011). This study also investigated the mechanism by which apical extrusion happened and revealed that it occurs after apoptosis initiation. Indeed, by blocking the activity of Myosin II, which is required for the extrusion process Rosenblatt et al. (2001), many dead *scribble*^{kd} cells remained within the monolayer Norman et al. (2011). Following to the reports of JNK induced apoptosis of scribble mutants in *Drosophila*, JNK activity was evaluated by Norman and co-workers. Interestingly, no sign of JNK activity was found in *scribble*^{kd} undergoing apoptosis; conversely, it was found that the activity of p38 protein kinase was significantly increased in *scribble*^{kd} surrounded by wild type neighbours. This result suggested that p38 MAPK, which had also been shown to be activated in response to various cellular stresses and to induce apoptosis Zarubin and Han (2005), is responsible for the death of MDCK *scribble*^{kd} cells Norman et al. (2011).

Further investigations performed by Wagstaff and co-workers helped elucidate the mechanism playing a role in the MDCK scribble induced competition, moving from the important contribution given by Norman's work. Using the same inducible *scribble*^{kd} line, they demonstrated that the competition phenomenon was independent on the exchange of soluble factors between the two cell lineages, by performing experiments with conditioned medium and transwell assays Wagstaff et al. (2016). Interestingly, they found that the growth rate of *scribble*^{kd} cells was not affected by conditioned medium from competing cultures. They also showed no significant difference when *scribble*^{kd} cells were cultured in a transwell system together with co-cultures of competing (wild-type/*scribble*^{kd}) cells. This suggested

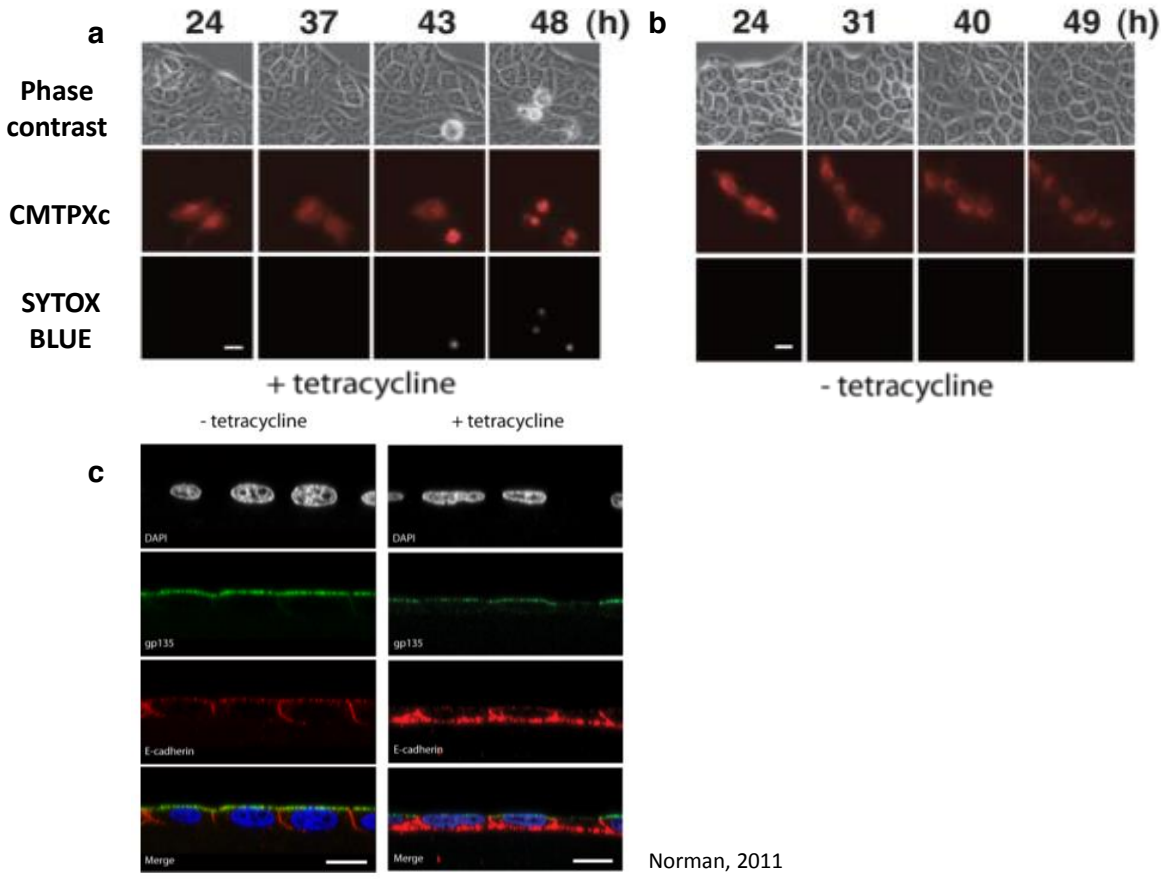

Figure 1.12: Scribble depletion induces cell competition in MDCK cells. Representative images from time-lapse movies of competition assays performed by mixing *scribble*^{kd} cells, fluorescently labelled with CMTPX dye (red), and wild type MDCK cells in a 1:10 relative ratio. Experiments were performed both in the presence (a) and absence (b) of tetracycline induction. Cells were stained with SYTOX Blue to label dead cells. Scale bar is 10 μm. Apoptosis of *scribble*^{kd} was only observed upon tetracycline induction. (c) Effect of scribble knock-down on cell polarity. *scribble*^{kd} cells were cultured in the absence (left) and presence (right) of tetracycline. Then immunofluorescence was performed using anti-gp135 (green) to mark the apical membrane and anti-E-cadherin antibodies (red), to label adherens junctions. Nuclei were stained with DAPI. Scale bars: 10 μm. All images are from Norman et al. (2011).

that soluble factors were not involved and shed a light on the potential role of cell-cell contacts and interactions. Indeed, Wagstaff and colleagues demonstrated that *scribble*^{kd} cells were outcompeted by MDCK wild-type cells by means of mechanical competition arising from differences in the tolerances of each cell type to density. By using micro-patterned substrates to confine cell growth on a pre-determined area and stretchable PDMS membranes to allow compression of confluent monolayer, they proved that *scribble*^{kd} cells are hypersensitive to crowding conditions (Figure 1.13). Indeed, when cultured in pure populations, the density in each cell population first increases before reaching a plateau (the homeostatic density). This homeostatic density was maintained over time because the rate of cell death exactly compensated the rate of cell birth. Notably, *scribble*^{kd} cells reached lower homeostatic densities than wild type cells because of a threefold larger apoptosis rate Wagstaff et al. (2016). However, when cultured in competitive conditions (10:90 *scribble*^{kd} and wild type ratio), the wild type cells are able to compact *scribble*^{kd} cells, causing an increase in their density and even a greater increase in death rates Wagstaff et al. (2016). These results suggested that changes in density induced increases in apoptosis events that alone might be sufficient to result in the elimination of the *scribble*^{kd} cells. Interestingly, Wagstaff and co-workers were able to identify the genes and pathways involved in this behaviour, by comparing transcriptional profiling of outcompeted *scribble*^{kd}, control wild type cells and an isolate of *scribble*^{kd} cells that was resistant to cell competition. They found that cells depleted of scribble showed an increased baseline level of p53, which is both necessary and sufficient to induce hypersensitivity to crowding and confer a mechanical loser status. Furthermore, they showed that compaction itself increased the already high p53 expression of *scribble*^{kd} cells and outlined the mechano-transduction cascade leading to elimination of *scribble*^{kd}. Indeed, they showed that the compaction of *scribble*^{kd} cells is responsible for activation of the Rho-associated kinase (ROCK). Following activation of ROCK, increased p38 levels were measured in *scribble*^{kd} cells, consistent with experimental results reported by Norman Norman et al. (2011), leading to further p53 elevation and cell death Wagstaff et al. (2016). Overall, this study demonstrated the existence of a mechanical cell competition, which had only been hypothesised before, where cell death is triggered by mechanical insults rather than molecular signalling. In addition to this, it indicated the important role of p53 activation in determining mechanical loser status, as p53 is required for both acquiring a low homeostatic cell density and hypersensitivity to compaction. Elimination of *scribble*^{kd} cells was effectively rescued by either a p53 depleted (*scribble*^{kd} p53-/-) version of the inducible cell line or by adding a p53 inhibitor to the culture medium. Such paradigm of p53-mediated mechanical cell competition

was also demonstrated in a mouse model, by using primary cultures of mouse tracheal epithelial cells (MTECs) Wagstaff et al. (2016). Indeed, when inducing mild p53 activation in these cells by addition of Nutlin-3, a remarkable decrease (26%) of homeostatic cell density and an increased number of extrusion events were observed. This is reminiscent of the hypersensitivity to crowding shown by $scribble^{kd}$ cells. Moreover, cell competition was observed when co-culturing MTECs wild type cells with MTECs deficient in p53 (p53-/-) following Nutlin-3 treatment. In such condition, cell death and extrusion of MTECs wild type cells was demonstrated. Interestingly, neither mechanical insults nor p53 inhibition were able to rescue the *Drosophila melanogaster* scribble depleted mutants from being eliminated by wild type cells Wagstaff et al. (2016), thus suggesting a different underlying mechanism of mechanical competition in Drosophila.

1.7 Machine learning and its application in biology

Automated image analysis of cells and tissues has been an active research field in computer science and biomedical informatics for decades. In recent years, it has experienced an exponential development thanks to the progress in microscopy hardware Wienert et al. (2012). In biological laboratories, the widespread use of motorised microscopes for time-resolved live imaging assays generates a huge amount of data, that can reach up to 10^5 images per day Conrad and Gerlich (2010). Such high-throughput systems dictate the need for implementation of automated data analysis for multiple reasons. Firstly, this facilitates the work of researchers and releases them from manual analysis of large datasets. Second and most important, automated image processing provides reliable and objective quantitative measurements. However, a common challenge in the development of an analytical work-flow consists in the complexity and diversity of image data. Analytical tools developed for a specific assay, when applied to different cellular types or simply to images of lower quality, often show poorer performances and require parameter tuning or adaptations of the software. Engineering pre-existing image analysis packages requires an accurate knowledge of the algorithm used in the software and can be quite difficult to achieve and time-consuming when approached by non experts.
The introduction of machine learning (ML) methods aims at overcoming similar obstacles and providing a universal analytical tool for analysis of biological images Bishop (2013),Hastie et al. (2001). The innovation of ML consists in the development of algorithms able to identify the best processing rules from the data provided as examples, rather than relying on manual adjustments. Therefore, ML links the problem of learning from data samples to the general concept of

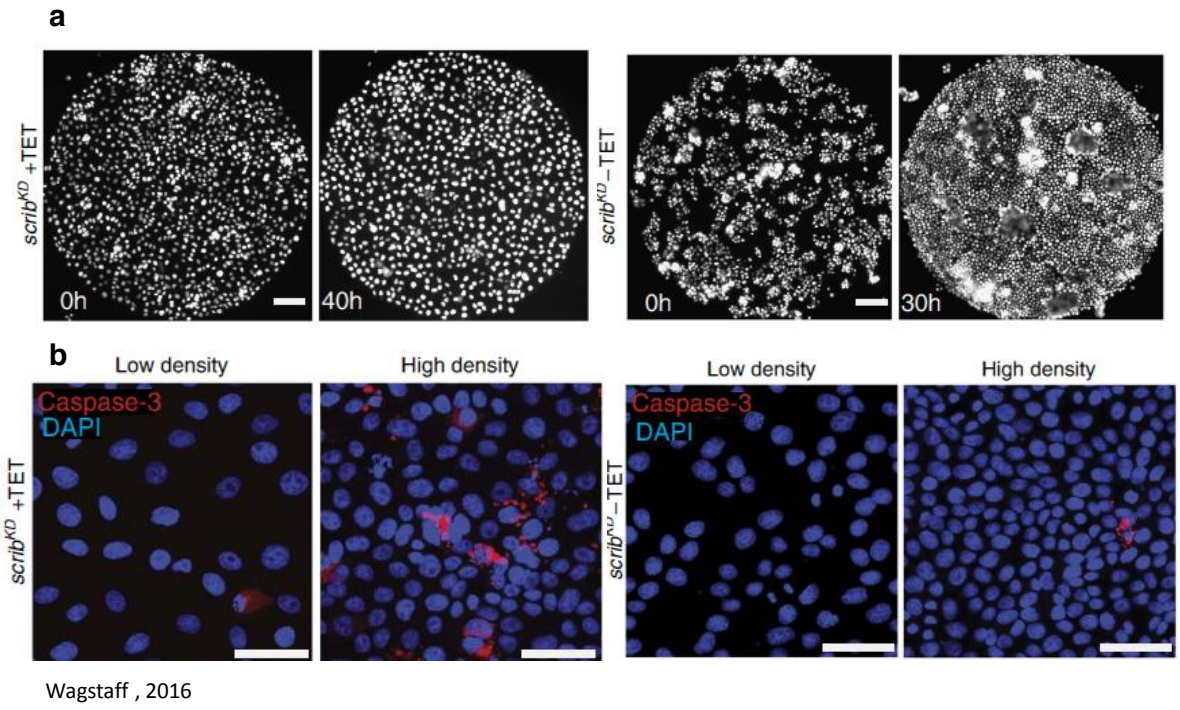

Wagstaff , 2016

Figure 1.13: Depletion of scribble induce sensitivity to crowding and lowers homeostatic density in MDCK cells. (a) Fluorescence images from time lapse movies representing growth of $scribble^{kd}$ cells labelled with GFP, cultured on micropatterned arenas (diameter 800 μm) in the presence (left) and absence (right) of tetracycline induction. Remarkably, cells cultured without addition of tetracycline reached higher density, as also confirmed by the presence of multicellular hemispherical structures known as blisters. Scale bar is 100 μm (b) Immuno histochemical staining of cleaved Caspase-3 (red) performed on non-induced (left) and induced (right) $scribble^{kd}$ cells staining with DAPI (blue nuclei) at both low and high density. These pictures show increased cell death of induced $scribble^{kd}$ cells at higher density. Scale bar is 50 μm. Images from Wagstaff et al. (2016).

inference. Every learning process consists of two phases: (i) a training phase, during which a dedicated dataset is used to implement a computer system from inherent structure and pattern within this data; (ii) the use of the computer system for making predictions on new dataset Bishop (2013),Hastie et al. (2001). There are two main types of ML methods: supervised (SML) and unsupervised (UML) learning. In SML, the user needs to manually annotate into distinct cate-

gories (classes) some features extracted from images of the training dataset. The learning algorithm automatically infers the rules to discriminate the classes, which can then be applied to the full data set (Figure 1.14). By doing so, SML is able to generalize from a few selected examples. As a consequence, the choice of the sample and its accurate classification are extremely important for the performance of the ML. To improve the classification accuracy of ML methods, a temporal model describing the biological process under investigation can be implemented Held et al. (2010). For instance, when looking at chromatin morphology changes during cell division, it is possible to define a clear direction for transition from one state (class) to another, given the large body of scientific knowledge available about cell cycle progression. Therefore, the formulation of a scheme defining the state transition allowed during a biological process can be used for correcting ambiguous morphologies. Such ambiguity often occurs at state transitions, when morphology of a state is subjected to a gradual change and single object-based classification can result relatively inaccurate.
SML is widely used in image-based screening for its ability to detect cell morphologies and phenotypes. Typically, the screening is aimed at determining whether an experimental perturbation (e.g. drug treatment, RNAi or genetic manipulation) produces a distinctive cellular phenotype, for instance characterised by a change in cell morphology or expression/ localisation of a fluorescent protein. SML has been successfully applied for analysis of various types of biological assays and large scale applications: high-content RNAi screening Conrad and Gerlich (2010),Held et al. (2010), drug development and proteomics Sommer and Gerlich (2013), cancer prognosis and prediction (reviewed in Kourou et al. (2015)). In this field, particularly, ML methods have become a popular tool for medical researchers, as they allow identification of recurrent patterns and discovery of unknown links between the multiple indicators (molecular, cellular and genetic) used for cancer prediction Kourou et al. (2015).

As mentioned above, SML is based on previous classification of representative phenotypes; hence, it cannot be used for discovery of new phenotypes, or in any situation where representative examples are not available. The second type of ML is unsupervised learning (UML), where no expected or known phenotypes are provided (Figure 1.14). In this case, the algorithm's task is to identify clusters, groups of objects sharing similar features with the input data, without prior user definition of the output Sommer and Gerlich (2013). In contrast with SML, the UML has not been frequently used for biological applications, especially because of the noisy nature of the input data.

Implementation of both SML and UML requires some pre-processing steps

needed to increase the quality of the data. Typical issues of time-lapse images can be fixed by removing artefacts produced by the microscope or camera: uneven illumination of the field of view or pixel noise resulting from low light exposure. Flat-field correction or application of smoothing filters can dramatically improve the quality of images (Figure 1.14). Following this, the second step in the workflow consists in segmentation of the objects of interest from the image background.

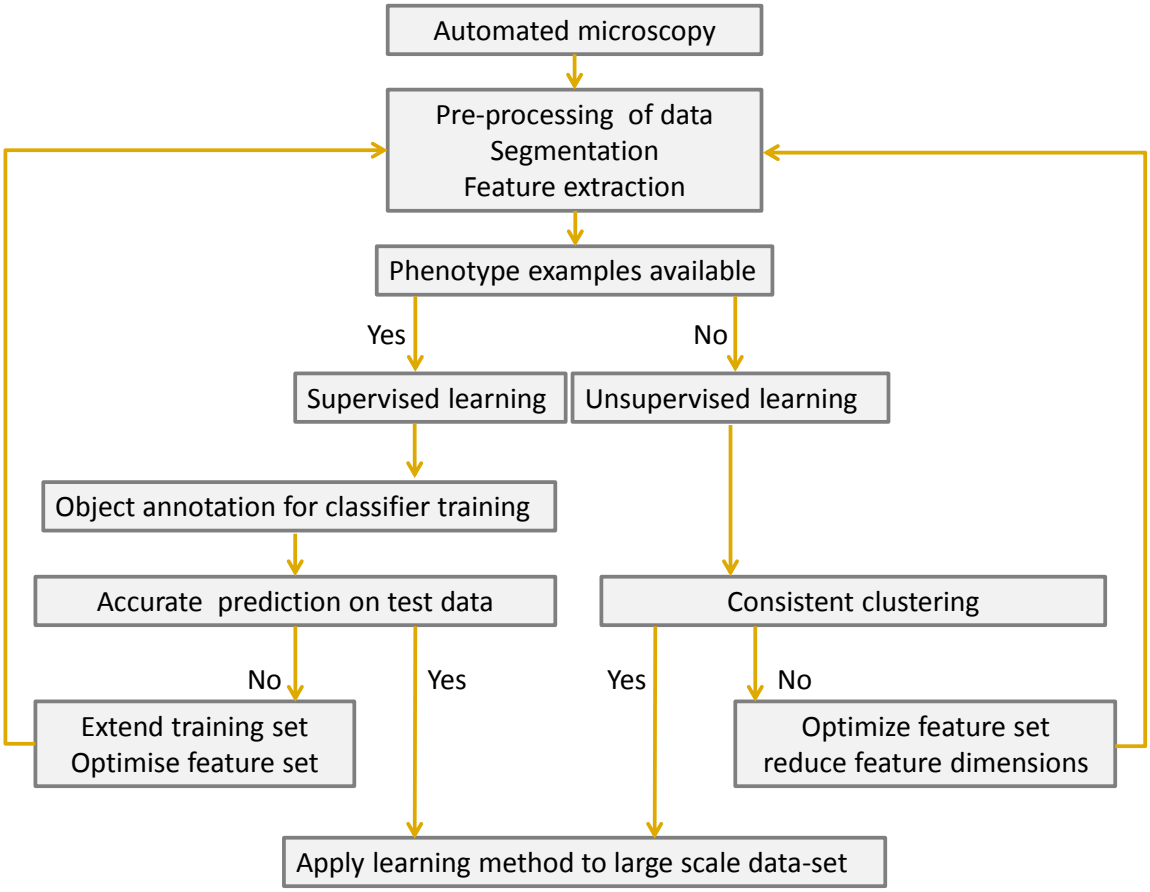

Figure 1.14: Machine learning pipeline in image-based screening. Diagram representing the typical machine learning work-flow for cell biological applications. The first step of the pipeline is aimed at increasing the quality of the data by performing some standard image pre-processing. Then segmentation is performed by separating foreground (e.g. cells) from background (object detection) and features are extracted according to different criteria. The choice of the leaning strategy is influenced by the *a prori* knowledge of the phenotypes under investigation. If this is available, then supervised learning will be implemented. To this extent, a classifier will be trained based on manual annotation by a human expert. Otherwise, when is not possible to annotate and define a training data set, unsupervised learning can be implemented, although this model is not frequently used in biological applications. Image adapted from Sommer and Gerlich (2013).

2 Aim of the thesis

The aim of this thesis is to determine the relationships, at the single-cell, level between normal and mutated epithelial cells proven to engage in mechanical competition. In particular, I examined how cellular interactions can lead to shifts in the make-up of cell populations.

To do this, I developed a novel quantitative approach that combines automated long-term microscopy with deep learning image analysis tools allowing examination of millions of individual cellular observations per experiment. These data enable the generation of phase diagrams that show how cell fate (death, division) depends on interactions with surrounding cells. By application of this method, it is possible to characterise how cell behaviour is modulated by the fraction of competitive interactions and how cell population evolves over time in a competitive environment. More specifically, my research was focus on three objectives:

1) Characterisation of pairwise interactions between wild type MDCK cells and cells of the same lineage depleted of the scribble protein, when mixed in 90:10 ratios;

2) Collaboration to the development of a quantitative mathematical model to investigate how the density dependence of cell division and apoptosis determine the time evolution of cell count and the overall population fitness;

3) Exploring how interactions between cancer cells are changed by varying the relative seeding ratios of the competing cell lines or the topology of the experimental assay.

3 Methods

3.1 Molecular biology and biochemistry techniques

3.1.1 Western Blotting

The level of expression of scribble and other adhesion proteins was evaluated using Western Blotting. Western Blotting was performed on MDCK H2b-GFP cells, non-induced MDCK *scribble*^{kd} H2b-RFP (tet-) and induced MDCK *scribble*^{kd} H2b-RFP (tet+) cells. Induction of scribble shRNA was carried out as described in Norman et al. (2011). Briefly, MDCK *scribble*^{kd} cells were induced with 1μg/ml doxycycline (Sigma-Aldrich, D9891) for 70 hours before lysis. Indeed, it had been previously demonstrated that a 72 hours-long doxycycline induction resulted in a significant depletion (greater than 90%) of scribble protein level Norman et al. (2011). For preparation of protein extracts, cells were placed on ice and washed with cold PBS. After removal of PBS, the cells were lysed using RIPA lysis buffer (Santa Cruz Biotechnology) to which protease and phosphatase inhibitors were added at appropriate concentrations. The lysates were clarified by centrifugation at 8,000g for 4 min at 4°C, diluted 1:1 with Laemmli buffer (Sigma-Aldrich), denatured for 5 min at 95°C and loaded onto NuPage 4 -20% gradient gels (Bio-Rad). Gels were placed in the electrophoresis apparatus and locked in place. Samples were loaded (30μl per well, 5μl marker) and running buffer added into the apparatus. Gels were run at 150 V for 1-2 hours. Proteins resolved with SDS-page were then transferred to a polyvinylidene fluoride (PDVF) membrane. Before transfer, membranes were soaked in 100% Methanol for 1-2 min, and then washed in transfer buffer. A transfer sandwich was prepared as follows: the PDVF membrane and the gel (that had been washed in transfer buffer) were placed between four sheets of transfer Whattman blotting paper and two sponges soaked in transfer buffer. After removing bubbles, the whole sandwich was placed in a chamber filled with transfer buffer. The blot was run at 220mA for 2 hours (longer for large proteins). Membranes were blocked with a mix of 5% Marvel in 1 x TBST for 30 min on a rocker at room temperature; then the primary antibody was added at the appropriate dilution in 2.5% Marvel/TBST and incubated overnight in the fridge. Next, membranes were washed 3 times with TBST for 5

min. The secondary peroxidase conjugated antibody was, then, added in 2.5% Marvel/TBST and incubated at RT for 1 hour, before being washed three times with TBST for 5 min. Peroxidase detection was performed by making a 1:1 mix of solutions of ECL detection reagents (GE Healthcare) and applying it onto the membranes.

Table 3.1: Western Blot solutions.

RIPA buffer	50 mM Tris-Hcl pH7.4	25 ml of 1M solution
	150 mM NaCl	15 mL of 5M solution
	1% NP-40 (IGEPAL)	5 mL
	0.5% Sodium deoxycholate	2.5 g
	0.1% SDS	0.5 g
	H2O	up to 500 mL
Running Buffer (RB)	250 mM Tris (base)	30.2 g
	1.92 M Glycine	144 g
	1% SDS	10 g
	H2O	up to 1L
	Heat and stir	-
Transfer Buffer (TB)	48 mM Tris-base	2.91 g
	39 mM Glycine	1.46 g
	10% SDS	1.87 mL
	Methanol	100 mL
	H2O	up to 500 mL
10x TBS	1.5M NaCl	87.6g
	100mM Tris base (Trizma)	12.1g
	H2O	up to 1L
	Adjust to pH8 with HCl	
TBST	1 x TBS + 0.1% Tween-20.	

3.1.2 Establishing MDCK cell lines stably expressing H2b-FP

In order to visualise the morphology of nucleic acids during the cell cycle, I established cell lines expressing fluorescently tagged histone markers in a stable manner. To enable accurate segmentation of the cells, I used different fluorescent proteins for distinguishing the two competing cell types, thus allowing for accurate determination of the composition of each cell's neighbourhood. I transduced MDCK wt cells with lentiviruses encoding H2b-GFP (Addgene, plasmid #25999) and the *scribble*^{kd} cells with lentiviruses encoding H2b-RFP (Addgene, plasmid

Table 3.2: Primary antibodies for WB and IF.

Antigen/Species	Company	Catalogue number	Dilution
E-cadherin (rat)	Thermo-Fisher	(ECCD-2) 13-1900	IF 1:100 WB: 1:500
Scribble (goat)	Santa Cruz	sc-11048	WB 1:500
GAPDH (mouse)	Novus Biologicals	NB300-221	WB 1:1000

Table 3.3: Secondary antibodies for WB and IF.

Antigen/Species	Company	Catalogue number	Dilution
(HRP)-anti-goat	Abcam	ab 97110	WB:1:10,000
(HRP)-anti-mouse	GE Healthcare	NXA931	WB:1:10,000

#26001).The infection was carried out by seeding 5x10^4 cells in 12 well-plate and adding to each well, in equal volume, the medium containing the viral particles together with the culture medium. The concentration of viral particles was calibrated so that the MOI <1 (500 μl of viruses and 500 μl of medium). Polybrene (Hexadimethrine bromide, Sigma) was added to the well at a final concentration of 8 μg/ml, in order to enhance the transduction of cells. Cells were infected soon after trypsinazion, and incubated with the mixture containing viral particles at 37°C and 5% $C0_2$ for 4-6 hours. A second round of infection was performed, following the same steps described for the first round. Finally, the viral mixture was removed and replaced with culture medium. Infected cells were grown for 2-3 weeks, until reaching confluency in T75 flask. Cells were finally sorted using fluorescence activated flow cytometry based on GFP or RFP fluorescence to yield populations with homogeneous levels of fluorescence.The sorting was performed at the UCL ICH/GOSH Flow Cytometry Core Facility, with assistance from Dr.Ayad Eddaoudi and Stephanie Canning. Plasmid and lentiviruses used for establishing the cell lines were kindly provided by Dr.Pedro Monteiro and Dr. Susana Godinho (Queen Mary, University of London) and, at a later stage, by Dr. Ana Lisica.

3.2 Cell biology techniques

3.2.1 Cell culture

Madin-Darby Canine Kidney (MDCK wt) cells were cultured in Dulbecco's Modified Eagle Medium (DMEM, Thermo-Fisher) supplemented with 10% foetal bovine serum (FBS, Sigma-Aldrich), GlutamaxTM (Gibco, 1%), Hepes buffer 25 mM (Sigma-Aldrich) and penicillin/streptomycin (PAA Laboratories GmbH, 1%). MDCK pTR Scribble shRNA ($scribble^{kd}$) cells were grown in DMEM supplemented with 10% tetracycline free foetal bovine serum (Clontech, 631106), GlutamaxTM (Gibco, 1%), penicillin/streptomycin (Gibco, 1%), Hepes buffer 25 mM (Sigma-Aldrich). Mixed MDCK wt/$scribble^{kd}$ cultures were grown in DMEM containing 10% tetracycline free foetal bovine serum, 1% GlutamaxTM and 1% penicillin/streptomycin. When required, doxycycline (Sigma-Aldrich, D9891) was added to cells at a final concentration of 1μg/ml.

3.2.2 Cell passaging

Cells were typically grown in T25 flasks (VWR) to approximately 70-80% confluence before splitting in order to avoid overcrowding, thus preserving the maintenance of a correct epithelial morphology. I performed passaging of cells by aspirating the growth medium and rinsing cells with an equal volume of sterile phosphate buffered saline (PBS). After aspirating PBS, 1 ml trypsin EDTA solution (0.05% trypsin, 0.53 mM EDTA) was added to the flask and cells were incubated in an atmosphere containing 5% CO_2 in a humidified incubator at 37 °C for 20-30 minutes. When cells detached from the bottom of the flask and from each other, pre-warmed culture medium was added to the trypsinised cells, and the suspension was strongly pipetted up and down in order to break down any remaining clumps of cells. Finally, an aliquot of the suspended cells (500-1000) μl was added to 5 ml of fresh medium and seeded into a new T25 flask.

3.2.3 Freezing/thawing of cells

The freezing of cells for long-term storage was performed by trypsinising cells as described above. At the end of the trypsin incubation, cells were re-suspended in fresh medium, transferred to a 15 ml tube (BD Biosciences) and spun for 3 minutes at 1500 RPM. The supernatant was discarded while the pellet was re-suspended into culture medium supplemented with 10% dimethyl sulphoxide (DMSO, Sigma Aldrich) and 20% FBS. Cells were then aliquoted into cryotubes

and frozen to -80 °C for 2 days prior to transferring to liquid nitrogen for long term storage.

The thawing procedure was performed by removing the cryotube from liquid nitrogen and rapidly thawing cells in a 37°C water bath. Cells were, then, diluted into pre-heated culture medium in a 15 ml tube and centrifuged for 3 minutes at 1500 RPM. After centrifugation, the supernatant was aspirated, the pellet was gently resuspended in complete growth medium and cells transferred in a T25-T75 (VWR) flask, depending on the number of cells frozen in the cryovial.

3.2.4 Wide-field microscopy

To perform long-term imaging while maintaining steady environmental condition, I assisted Dr Alan Lowe in the design and assembly of an automated epifluorescence microscope built inside a standard CO_2 incubator (Thermo Scientific Heraeus BL20). The microscope is composed of a high performance motorized stage (Prior Proscan III, H117E2IX), a motorised focus controller (Prior FB201 and PS3H122R) and a 9.1MP CCD camera (Point Grey GS3-U3-91S6M). Three different LEDs provide brightfield and fluorescence illumination. Brightfield illumination is provided using a green LED (Thorlabs M520L3, 520nm) while GFP and mCherry/RFP fluorescent channels illumination use respectively a blue (Thorlabs M470L3, 470nm) or yellow (Thorlabs M565L3, 565nm) LED. The blue and yellow LEDs are combined using a dichroic beamsplitter (Semrock), and focussed onto the back focal plane of a 20x air objective (Olympus 20x, 0.4NA) in an epifluorescence configuration. The LEDs and camera firing were synchronised via TTL pulses from a DAC (Data Translation DT9834), ensuring minimal light exposure. To prevent evaporation from the imaging dishes over the duration of the experiment, a custom built humidified chamber was fabricated and fitted with a thermocouple and humidity sensor to continuously monitor the environment (Figure 3.1). Dr. Lowe wrote Python and C++ software to operate the microscope.

3.2.5 Long-term live imaging and competition assay

Cells were seeded in 35 mm glass bottom Petri-dishes (WillCo), at an initial density of 1x10^{-3} cells/μm^2. In most competition assays, MDCK wt cells expressing H2b-GFP were mixed with scribble^{kd} H2b-RFP cells at a ratio of 90:10. In some experiments, the expression of scribble shRNA had been induced in scribble^{kd} cells by exposure to doxycycline for 70 hours before seeding. In other experiments, the cells were maintained in tetracycline free medium to prevent scribble shRNA induction. Imaging was started 2- 3 hours after seeding. The imaging medium

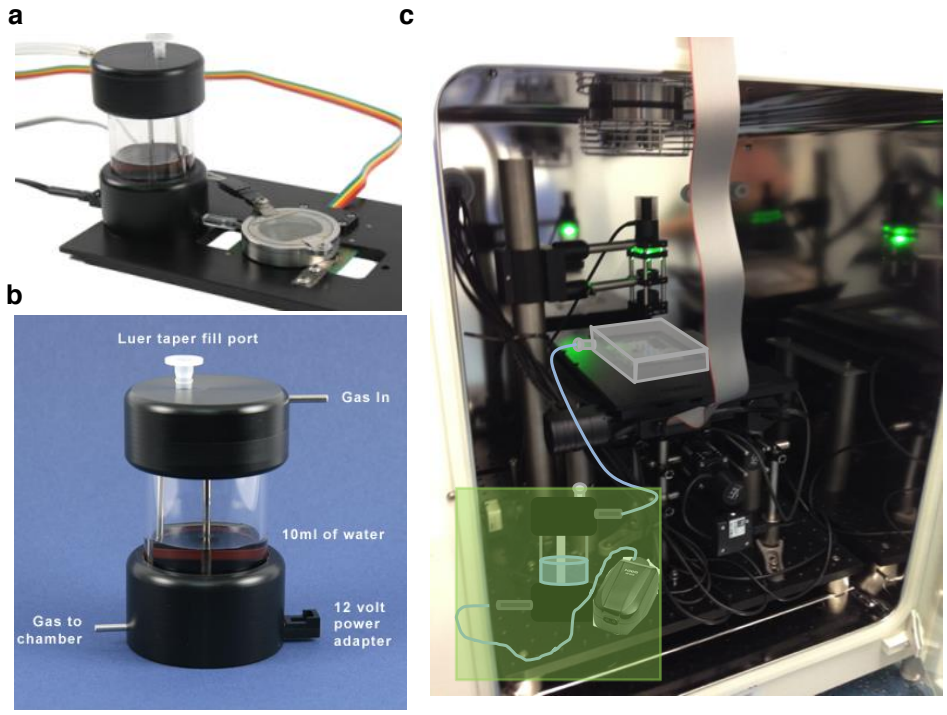

Figure 3.1: Long-term imaging setup Wide-field fluorescence microscope for long-term imaging built inside a standard $C0_2$ incubator (c) equipped with a humidifier system (green shaded rectangle). The humidifier design was inspired by the micro-humidification system (Bioptech) a-b),and adapted to fit the incubator space. Such system was coupled to a small silent air pump (Hidom), to bubble the water vessel; the out flowing water vapour is coupled to the plexiglass cell chamber.

used during the assay was phenol red free DMEM (Thermo Fisher Scientific, 31053) supplemented with tetracycline-free bovine serum, Hepes, antibiotics and, for experiments involving induction, doxycycline at the dose indicated above. Multi-position imaging was performed inside the incubator-scope for a duration of 80 h, on three different imaging dishes. Typically, 12 regions (4 per dish) of (530 x 400) μm^2 were imaged sequentially, using a 20x objective and every 4 min. A competition experiment was typically run side-by-side with two controls, in identical conditions.

3.2.6 Immuno fluorescence

Cells were seeded onto glass coverslips in 12 well-plates. Paraformaldehyde (PFA) fixation was performed at room temperature; cells were washed with

PBS before 4% PFA/PBS was applied for 20 min. Cells were then washed 3 times with PBS and permeabilised with 0.5% Triton X100/ PBS for 5 min on ice. After having removed the permeabilisation solution, unreacted fixative was passivated by incubating with 5% BSA/PBS solution at room temperature for 30 min. Primary antibody was added, after having been diluted appropriately in 1%BSA/PBS in a minimal volume (50-100μl). Incubation was either performed at room temperature for 1 hour or overnight at 4°C. Cells were then washed 3-4 times in PBS and the secondary fluorophore-conjugated antibody was diluted 1:200 in 1%BSA/PBS and the cells were incubated with this at room temperature for 1 hour. Phalloidin-TRITC (dilution 1:50 from 6.6 μM stock) and DAPI (1 μg/ml) were also included with the secondary antibody to allow for visualization of F-actin and nucleic acids, respectively. Primary antibodies used are listed in table 3.2.

3.3 Computational strategy for the analysis of cellular interactions

All image processing was performed on a Dell Precision workstation running Ubuntu 16.04LTS with 32 Gb RAM and an NVIDIA GTX1080 GPU, and all code used for image processing was developed by Dr. Lowe Bove et al. (2017).

3.3.1 Image processing

The images acquired by the incubator-scope were analysed by detecting and segmenting fluorescent nuclei. The segmentation was performed by distinguishing foreground (cells) from background. Prior to segmentation, several pre-processing steps were implemented to restore images and increase the signal/noise ratio. In particular, flat-field illumination correction was performed and 'hot pixels' of the CCD camera were removed. Following image restoration, segmentation of the fluorescent nuclei was performed applying a method based on the Gaussian mixture model (GMM). The histogram intensity of three images taken from the beginning, middle, and end of the movie were combined and fitted to a GMM using the expectation maximization algorithm (EM) to determine the appropriate parameters Xu and Jordan (1996). The intensity distribution was described as a weighted sum of n normal distributions:

$$P(X|\Theta) = \sum_{k=1}^{n} \lambda_k N_k(\mu_k, \sigma_k^2) \tag{3.1}$$

where Θ represents the learned parameters for the N models: λ_k is the normalized weight, μ_k the mean intensity, and σ_k^2 the variance for each normal distribution

in the mixture model Prince (2013). Typically, the number of distributions used was three. Images from the GFP and RFP channels were segmented separately; therefore different parameters were learned for the GFP and RFP fluorescence movies. The three normal distributions generally reflected the intensity distributions of background, interphase, and mitotic/apoptotic cells. When the segmentation process is correctly performed, it returns as output a binary classification of the image into background (dark) and cells (clear). As the time-lapse experiments run for several days, cells proliferate and, as a consequence, the resulting images present very crowded and cell-dense regions. Such high confluence images represent a challenge for segmentation because it is more difficult to discriminate single cells boundaries when cells are highly compacted. In order to improve segmentation at high density, multiple strategies were implemented: a marker-controlled watershed transform, a custom-written object-splitting algorithm based on calculating regions of concavity in convex objects Wienert et al. (2012), or a hybrid of both methods. A further issue arose from the oversegmentation of nuclei having a weak fluorescence signal. A multi-step merging algorithm was used to recombine fragments of nuclei. This algorithm was optimized so that it does not combine apoptotic fragments with non apoptotic nuclei.

3.3.2 Classification of mitotic states and apoptosis

Chromatin morphology visualized through H2b-FP markers was used to classify cell cycle states and apoptosis (Figure 3.2 a). Following segmentation, split/merge steps, each detected object (nucleus) was assigned one of five different classes (interphase, pro(meta)phase, metaphase, anaphase/telophase, and apoptosis.), according to its position in the cell cycle. Object classification was performed via a computer vision approach. To do so, both a support vector machine (SVM) for supervised learning and a deep convolutional neural network (CNN) for deep learning were implemented and trained. The non-linear SVM (with Radial Basis Function) used quantitative image features describing brightness (fluorescence intensity, intensity gradient), texture and shape (aspect ratio, orientation, eccentricity, histogram of oriented gradients features) for classifying detected objects. For training the SVM, two data sets were generated: (i) training (ii) validation (Figure 3.2 d). Each set contained an equal number of images (100 frames taken from four different experiments) taken from both GFP and RFP movies. For CNN, three datasets were generated: (i) training, (ii) test, and (iii) validation, with the test data set fed to the algorithm while it is learning. As opposed to SVM, the training images for CNN were manipulated and augmented (rotations, noise, translations), in order to yield a large number of

training examples. Another difference between SVM and CNN consists in the use of BF images, that contribute to the classification of nuclei status but are not used in SVM. To provide ground truth, I manually annotated the training data,using a Fiji ImageJ plugin (*https://github.com/quantumjot/impy-tools/blob/master/ImageJ/IJClassifier.py/*). The accuracy of both SVM and CNN classification was measured by determining a confusion matrix, which compares a ground truth based on human operator classification and the SVM/CNN prediction. After training steps, the CNN achieved an overall accuracy of >99%, remarkably higher than SVM performance (80%). The poorer performance of the latter was due to a poor apoptosis detection (Figure 3.2 b). Hence, CNN was used for all data analysis presented in this work. All code was implemented in Python and C/C++ using CVXOPT, GLPK, Numpy, Scipy, TensorFlow, and Caffe libraries. CNNs were implemented in Caffe and TensorFlow.

3.3.3 Cell tracking

Following segmentation and classification, objects were assembled into tracks. Tracking cells over several rounds of division is not a trivial task. First, sections of tracks not containing division events (tracklets) were linked and assembled into one sequence. Each tracklet is associated with a probabilistic model, where the prediction of future state and error associated to the state was evaluated via application of a Kalman filter. Hence, tracklet linking was performed by calculating posterior probabilities of each potential linkage for all possible scenarios. When linking tracklets, occasional classification errors came to light, and were corrected using a temporal model of the cell cycle Held et al. (2010) implemented as a hidden Markov model (HMM). Such a temporal model allowed defined directional transitions between the five classes used for describing the cell cycle state of each object (interphase, prometaphase, metaphase, anaphase and apoptosis) (Figure 3.2 e). Transition probabilities fed into the model were manually determined (Table 3.4). Following HMM correction of mislabelled trajectories, tracklets containing a metaphase to anaphase transition were split into separate tracks. This step is functional for labelling of division events in later steps of the algorithm. Finally, lineage trees were plotted by using multiple hypothesis testing and integer programming Al-Kofahi et al. (2006), after identification of a globally optimal solution connecting all tracklets. Such a global solution found a sequence of high-likelihood hypotheses, considering all observations. The following hypotheses were introduced and computed for some/ all of the tracklets 1) true positive track, 2) false positive track, 3) initializing at the beginning of the movie or near the edge of the field of view (FOV), 4) termination at the end of the movie or near

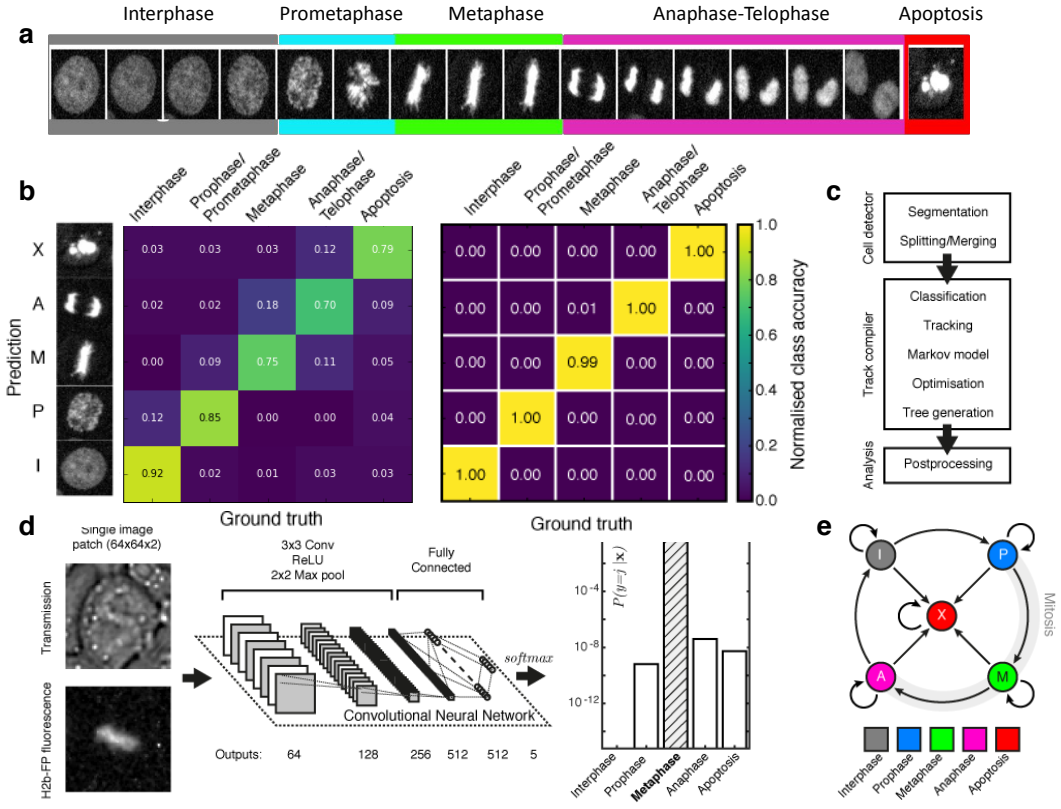

Figure 3.2: Classification of cell cycle states via computer vision approaches (a) Chromatin morphology was used to classify different mitotic stages, as well as apoptosis (b) Confusion matrix showing the matching of human annotations vs. the annotation of the SVM (left) and CNN system (right). The CNN resulted in better performances, thus was chosen for performing all data analysis. (c) Schematic of the computational pipeline implemented for the study of competition dynamics, based on three major steps: segmentation of individual cells (cell detector), automatic annotation of morphological classes related to cell cycle state and apoptosis (track compiler), and post-processing analysis of single-cell tracking data. (d) CNN for object classification. The CNN inputs are single-object patches, both in the transmission (BF) and fluorescence channels (left). Schematic of CNN architecture, as combination of different types of layers: convolutional/ReLU/max-pooling, and fully connected layers (middle). The CNN transforms the input image layer by layer from the original pixel values to the final class scores with the highest score reflecting the most probable classification of the image data (right). (e) HMM temporal model. The figure depicts the allowed directional transitions between the five classes considered.

the edge of the FOV, 5) a merge between two tracklets, 6) a division event, or 7) an apoptotic event.

Following identification of the global solution, tracks were merged, division

events labelled and daughter cells assigned with a new cell ID. For each newly born cell, information on the lineage was stored (Movie 1). Apoptosis events were, likewise, accounted for. Cell cycle state, eventually, was automatically updated for single tracks. Therefore, the final output of the tracking software is a list of unique cell IDs containing information on xyt-position, cell cycle state, and lineage of each ID.

Table 3.4: Transition Probabilities for HMM.

State	Interphase	Prometaphase	Metaphase	Anaphase	Apoptosis
Interphase	0.9943	0.0047	0	0	0.0008
Prometaphase	0	0.7288	0.2770	0	-
Metaphase	0	0	0.7595	0.2402	-
Anaphase	0.1623	0	0	0.8375	-
Apoptosis	0	0	0	0	1

3.4 Post processing of segmented cell tracks

3.4.1 Determination of the cellular interaction network

A custom-written MATLAB (MathWorks) code was optimized to calculate the number and type of neighbours each cell had during its entire life. The algorithm used the built-in Voronoi function Barber et al. (1996), taking as input the location of cell centroids in each frame (Figure 3.3 a,left). Such calculation excluded cells closer than 10 μm to the edge of the FOV, because their entire neighbourhood could not be determined. A threshold for describing the maximum distance between two cells in contact at low density was defined by manually measuring the cell diameter in pre-confluency conditions (i.e. free space remained in the FOV). The definition of such a threshold was crucial for removing nuclei from the Voronoi diagram that cannot be considered neighbours because they are separated by a distance greater than the maximum value aforementioned. In both pure MDCK wt populations and in the competition co-culture, the average cell diameter was 33 μm; in 100% scribble^{kd} induced (tet+) experiments, cells exhibited a larger cell area with an average diameter of 60 μm. Both values were chosen as our thresholds to determine true neighbours in the different scenarios.

3.4.2 Measurement of single cell density

The local cellular density was measured by implementing a custom-written MATLAB script based on the Delaunay triangulation of cell centroids in each image frame (Figure 3.3 a, right). Local cellular density (ρ) was defined as the sum of inverse areas of the triangles that share a common vertex with the centre of the target cell:

$$\rho = \sum_{i=1}^{N} \frac{1}{A_i} \tag{3.2}$$

where A_i is the area of each triangle i sharing a vertex with the target cell. Such a definition of cellular density has the disadvantage of under-estimating the true cell surface area, but, conveniently, the error in this metric is systematic (it is not affected by low or high density conditions). Hence, for the purpose of this project, it provides a robust measure for comparing density at the single cell level within a spatially heterogeneous population. Local cellular density was computed for each cell ID and averaged among cells of the same lineage at each time point. Cells closer than 10 μm to the edge of the FOV were excluded from the density calculation, due to the incomplete knowledge of their neighbourhood. The average of ρ was plotted as a function of time for each cell type, in both pure and mixed populations.

3.4.3 Measurement of division and apoptosis probability as a function of density

The effect of density on proliferation and apoptosis was investigated by determining the probability of division and death as function of cell density. A custom-written MATLAB (MathWorks) code was optimised for this. As first step, the algorithm discretised the local density for each cell ID at each time frame into 20 bins. The bins were chosen so that the middle bin represented the mean local density of all cells, while the first and last bins corresponded, respectively, to the minimum and maximum local density measured across the population. The number of bins chosen was found appropriate to optimize the statistics of the plot, while ensuring that there was a sufficient number of cells in each bin (for *scribble*^{kd} N> 134,000 per bin, for MDCK wt n> 405,000 per bin). The probability of cells undergoing mitosis/apoptosis per cell per frame was then calculated for each bin as:

$$p^{div/apo}(\rho) = \frac{\sum_{\rho} f^{div/apo}}{\sum_{\rho} f} \tag{3.3}$$

with $f^{div/apo}$ being the number of observed events (division or apoptosis) in each bin and f being the total number of observations in that bin. Given equation 3.3, the net growth per cell per frame $p^{netgrowth}$ is then defined as:

$$p^{netgrowth}(\rho) = p^{div}(\rho) - p^{apo}(\rho) \tag{3.4}$$

Once computed, f^{div}, f^{apo} and $p^{netgrowth}$, they were plotted as function of local density for induced *scribble*^{kd} (tet+), non-induced *scribble*^{kd} (tet-) and MDCK wt in both pure populations and competition assays.

3.4.4 Measurement of division and apoptosis probability as function of neighbourhood

Single cell analysis was performed to investigate the impact of local neighbourhood composition on population dynamic during competition. Knowing, for each cell ID, the total number of neighbours and the number belonging to each cell lineage from previous calculations, it was possible to categorise each division and apoptosis event as a function of the number of neighbours of each type. A MATLAB (MathWorks) code was developed to colour code the probability of division, apoptosis, net growth and as function of neighbourhood by colour coding it in a grid, where the x-axis and y-axis represented the number of *scribble*^{kd} and MDCK wt neighbours, respectively. The measurement within each grid position was computed from > 500 observations. Grid positions populated by more than 500 cells where no event (apoptosis/division) was observed were annotated with an asterisk. In these positions, an upper bound (1/Nobservations) was provided for the probability of the event. To determine if some neighbourhood were more prone than others to division or death, I defined a metric for asymmetry, computed as:

$$s = \sum U - \sum L \tag{3.5}$$

where U and L are the upper and lower triangular matrices of the neighbourhood plot.

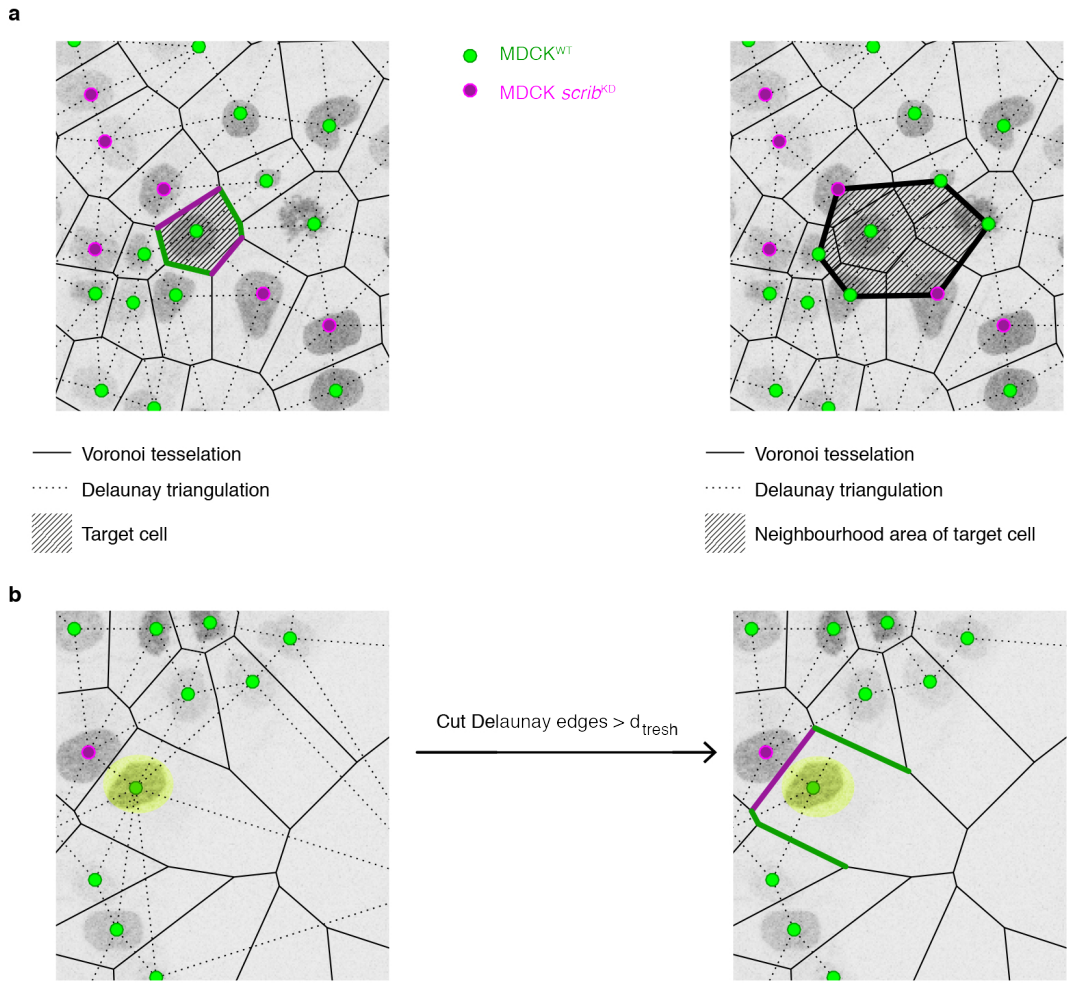

Figure 3.3: Definition of cellular neighbourhood and local cellular density. (a) Definition of local neighbourhood (left). The centre of the nucleus of each cell is marked with a filled circle (green for MDCK wt; magenta for $scribble^{kd}$). The position of nuclei is used to construct a Voronoi tessellation (solid lines). The composition of the cellular interaction network is determined by the number of junctions the target cell (striped pattern) has in common with the MDCK wt cells (junctions shown in green) or $scribble^{kd}cells$ (junction shown in magenta). Once determined the neighbours of a target, we can measure its local density (right). For doing so, centres of mass of nuclei are used to construct a Delaunay triangulation (dashed lines). Local density is defined as the sum of inverse areas of the triangles sharing a common vertex at the nucleus of the cell of interest (included in the striped pattern). (b) Definition of true neighbours based on threshold. True neighbours share a common edge with the Voronoi polygon of the target cell (highlighted in yellow), and are separated from the target cell by a distance below a threshold value. Dotted lines link the centroid of neighbours. After culling of nuclei located at greater separation distance than the threshold (right), the interaction network of the target cell consist of four neighbours, three MDCK wt (green) and one $scribble^{KD}$ (magenta).

4 Effect of scribble knock-down on proliferation and apoptosis of MDCK cells

4.1 Introduction

In this chapter, I present data showing the effect that scribble knock-down has on proliferation and apoptosis rates of MDCK cells.
Polarity and morphology of the pTR MDCK scribble shRNA cell line, cultured in the presence or absence of tetracycline, had been rigorously characterised by other groups Norman et al. (2011). Previous studies have focussed on the dynamics of these aspects, given the key role of scribble protein in maintaining apico-basal polarity, and considering how relevant the loss of polarity could be when studying cellular interactions. According to their findings, upon prolonged tetracycline induction (72 hours), pTR MDCK scribble shRNA lose their typical epithelial cobblestone morphology, exhibiting a flattened morphology and covering a larger area. The only major polarity disruption was observed in the E-cadherin localization, which exhibited greater localization to the basal domain rather then the baso-lateral one in control conditions Norman et al. (2011).
Although having been examined in previous studies, the effect of scribble knock-down on proliferation is less understood. Previous work has demonstrated that scribble is an important protein for both maintenance of cell polarity and regulation of cell motility, however it is also involved in the regulation of cell division. In *Drosophila melanogaster* imaginal discs, for instance, scribble works as a suppressor of Cyclin E, thus regulating entry in the S phase Humbert et al. (2008). Experimental evidence in both *Drosophila melanogaster* Brumby and Richardson (2003) and mammals Vaira et al. (2011) have shown that loss of function of scribble is commonly associated with uncontrolled proliferation. Conversely, over-expression of scribble was shown to repress proliferation in various mammalian in vitro models Takizawa et al. (2006). In this chapter, I look at growth and death rates of cells cultured in pure populations. I will describe, at both the tissue and single-cell level, how proliferation is affected by scribble knock-down. This

detailed analysis was made possible by the combination of long-term imaging with the image analysis pipeline I developed. I will also quantitatively characterise the apoptosis rate upon depletion of scribble. After having assessed the effect on pure populations, I will present the proliferation and apoptosis profiles measured when MDCK cells depleted of scribble protein are mixed with MDCK wt cells in a 10:90 ratio. Overall this analysis, together with confirming the competitive interaction between the two cell types, also validated the pipeline used for measuring division and apoptosis during long-term imaging, confirming the efficiency of the analytical approach for providing reliable automated quantification of single-cell events.

4.2 Induction of pTR MDCK scribble shRNA cell line and nomenclature

In the absence of tetracycline, the expression of scribble sh RNA in pTR MDCK scribble shRNA cells is inhibited by the tet repressor Hillen and Berens (1994). In this work, the induction of shRNA was induced with doxycycline, a more stable analogue of tetracycline. Western blotting with an anti-scribble antibody was performed to validate the efficacy of knock-down of scribble in induced pTR MDCK scribble shRNA. For subsequent experiments and analysis, the pTR MDCK scribble shRNA line was stably labelled with H2b-RFP, and will be referred to as $scribble^{kd}$. Likewise, the MDCK wild type line used in all experiments stably expressed H2b-GFP and will be referred to as MDCK wt. When scribble depletion was not induced (tet-), the $scribble^{kd}$ cell line expressed scribble at a level comparable to that in MDCK wild type. Addition of doxycycline reduced scribble protein level so that, after 72 hours of induction, the scribble protein is barely detectable (Figure 4.1 a, top). E-cadherin expression was also assessed, and was found to be enhanced by scribble knock-down (Figure 4.1 a, bottom). Surprisingly, non-induced $scribble^{kd}$ cells also displayed higher E-cadherin expression than MDCK wt. This result is not what I was expecting, but it might be due to incomplete repression of the promoter by the tet repressor. These experiments also confirmed the previously observed change in epithelial morphology upon scribble depletion, resulting in flat cells with higher surface area and apparently larger nuclei (Figure 4.1 c), Movie 4. Therefore, addition of doxycycline to $scribble^{kd}$ efficiently knocked-down the level of scribble protein.

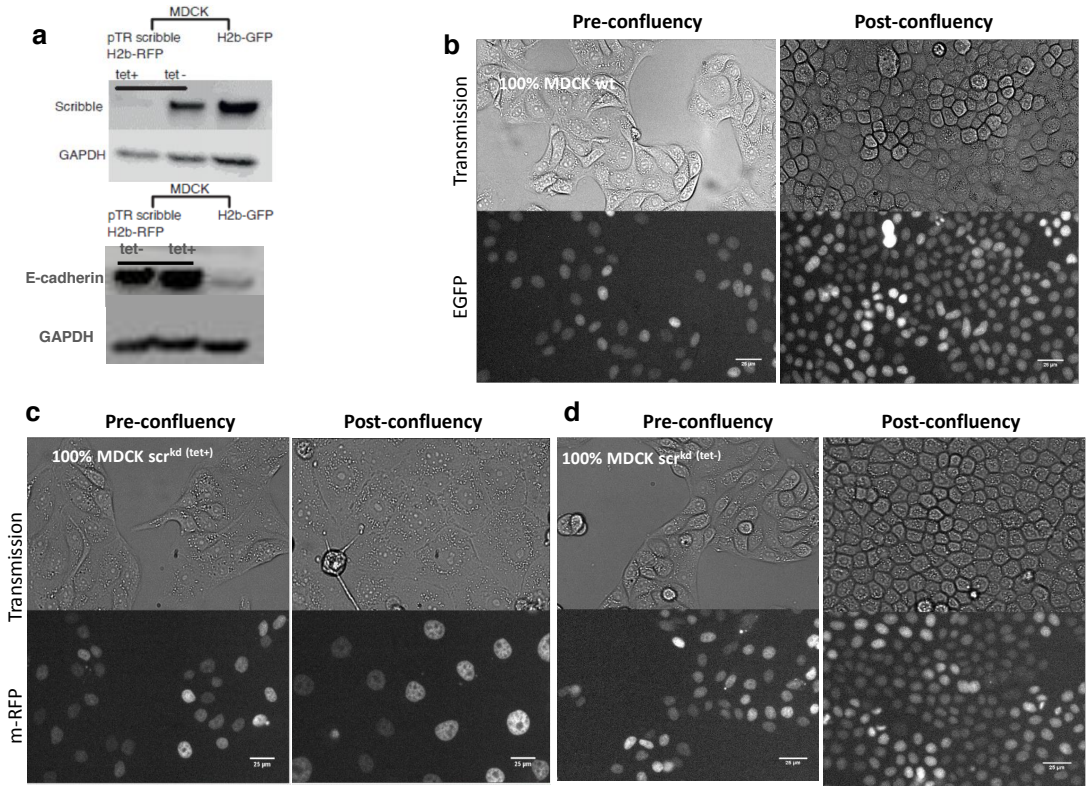

Figure 4.1: Effect of scribble knock-down on epithelial cell morphology and E-cadherin expression (a) Top: Immunoblot showing scribble and GAPDH expression for induced (tet+) $scribble^{kd}$ cells, non-induced (tet-) $scribble^{kd}$ cells, and MDCK wt cells expressing H2b-GFP. Induction of scribble shRNA expression results in a significant depletion of scribble levels. The $scribble^{kd}$ were incubated with doxycycline for 72 hours. Bottom: Effect of scribble depletion on E-cadherin expression. GAPDH control is shown. (b) Transmission (top) and EGFP (bottom) images of MDCK wt cells stably expressing H2b-GFP. (c) Transmission (top) images of $scribble^{kd}$ cells expressing H2b-RFP (bottom), after 72 hours incubation with doxycycline. (d) Transmission (top) images of $scribble^{kd}$ cells expressing H2b-RFP (bottom) cultured in the absence of doxycycline (tet-). At both low and high density, these cells show a classic epithelial cobblestone morphology, resembling to the MDCK wt control (compare b-d). Conversely, the $scribble^{kd}$ (tet+) no longer show an epithelial cell morphology, appearing larger and flatter, especially in post confluency conditions. Scale bars are 25 μm.

4.3 Effect of scribble shRNA on proliferation

The effect of scribble knock-down on cell proliferation was evaluated by plotting cell counts for 72-hours induced (tet+) and non-induced (tet-) $scribble^{kd}$ cells grown in pure populations. Cells were seeded at an initial density of 10^{-3} cells/μm^2

and imaged for 50 h (Movie 4, Movie 5). Normal MDCK were also imaged and used as control (Movie 2). Over the course of the experiment, the plots for *scribble*^{kd} count in the absence and presence of doxycycline differed markedly (Figure 4.2 a); the *scribble*^{kd} (tet-) and the MDCK wt showed a fivefold increase in cell count (Figure 4.2 b) while the *scribble*^{kd} (tet+) population increased 1.5 fold. Such large-scale quantification of growth rate is consistent with previous work Wagstaff et al. (2016) and demonstrates that the growth of MDCK cells is slowed down by scribble knock-down. To better understand the effect of scribble knock-down on MDCK proliferation, I analysed the duration of the cell cycle at single-cell resolution by measuring the temporal separation between the birth of a cell and that of its daughters on a lineage tree (Figure 4.3 c). Indeed, the reduced proliferation could be due to either a lower number of cell division or to an increase in cell cycle time due to scribble depletion. To compare induced and non-induced cells, I plotted the cell cycle duration distribution for both populations (Figure 4.2 c). This analysis showed that, despite the differences in cell count, the average duration time of the cell cycle for the *scribble*^{kd} induced and non-induced cells are very similar, 18.5 $\pm$ 6 hours. For comparison, the cell cycle time measured for a population of MDCK wt displayed a mean value of 22 $\pm$ 6 h (Figure 4.2 c). Thus, it appears that cell cycle duration changes are not the cause of the differences in cell count after 72 hours. It is important to note that, despite accurate estimation of cell cycle duration for the vast majority of the population, some errors subsist due to identity swaps at high cell densities or triple divisions that lead to underestimation of the cell cycle time. Single-cell analysis confirmed that no significant difference is shown in cell cycle duration time upon induction of scribble. Moreover, MDCK wt cells seemed to have a slightly longer cell cycle time. All division times are consistent with other reports Gudipaty et al. (2017).

4.4 Effect of scribble shRNA on apoptosis

The data collected from pure population experiments were analysed to determine the change in death rates caused by scribble knock-down. For this purpose I plotted the cumulative apoptosis count, averaged across all FOVs imaged during an experiment. Data used for these plots were pooled from two biological replicates, each one having 5-6 imaged FOVs. As expected, the apoptosis count increased over time for induced *scribble*^{kd} cells (magenta), non-induced (green) *scribble*^{kd} cells and wild type cells (grey) (Figure 4.3 d, right). However, when scribble was knocked-down, the average number of apoptotic nuclei was larger than the one observed for non-induced cells at all time points, and resulted in

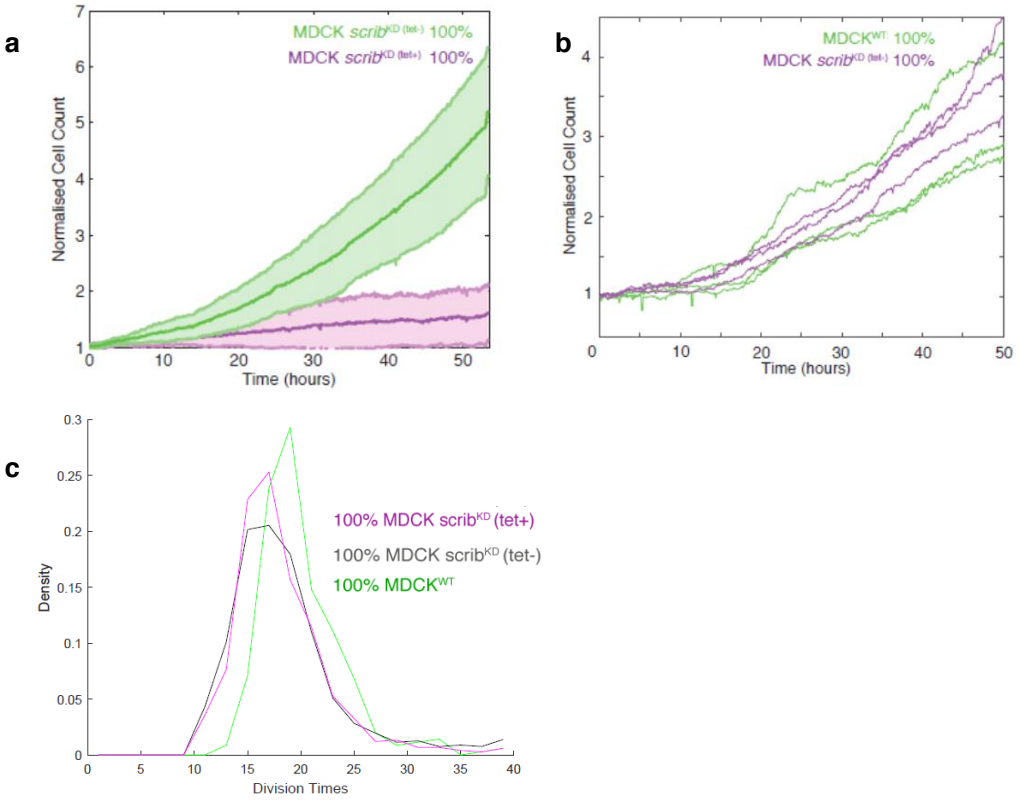

Figure 4.2: Effects of scribble knockdown on proliferation of pure cultures (a) Growth curve for pure non-induced *scribble*^{kd} (tet-, green) and induced *scribble*^{kd} (tet+, magenta) populations. Plots are normalised to the initial cell count and are pooled from three biological replicates, imaging three fields of view each. The solid line indicates the mean of the experiments and the shaded area indicates the standard deviation.(b) Proliferation profiles of non-induced *scribble*^{kd} (tet-, magenta) and MDCK wt (green) cells in pure populations. The three lines show the cell count in each field of view imaged during one control experiment. (c) Probability density of cell-cycle time measured for a pure population of MDCK wt (green), *scribble*^{kd} in the presence (magenta) and absence (grey) of tetracycline. The distribution represents a population of at least 250 cells in the same field of view followed for minimum time of 50 h. Data are pooled from two biological replicates.

a 2.5 fold increase after 50 hours (Figure 4.3 d, right). Notably, the cumulative apoptosis count of *scribble*^{kd} (tet-) reproduced accurately the curve obtained for pure MDCK wt. These results suggested that the *scribble*^{kd} (tet+) line has a higher apoptosis baseline when cultured in pure populations. The comparison between non-induced *scribble*^{kd} and MDCK wt also confirmed that increased apoptosis is effectively caused by the depletion of scribble protein, consistent with observations from other studies. Indeed, as it was demonstrated by Wagstaff et al.

(2016), the higher apoptosis level observed in induced *scribble*^{kd} cells was due to an over-expression of p53 levels, which, per se, was shown to promote apoptosis through transcription-dependent and independent mechanisms, as reviewed in Fridman and Lowe (2003). Moreover, Wagstaff and colleagues demonstrated that the increased p53 levels in *scribble*^{kd} cells cause the hypersensitivity to crowding through the proposed model that I described in paragraph 1.6.3.

4.5 Effect of scribble depletion on proliferation and apoptosis in mixed cultures

Next, the fate of *scribble*^{kd} induced cells surrounded by MDCK wt cells was determined, and growth and death rates calculated as explained in the previous paragraphs.
Mixed cultures of *scribble*^{kd} and MDCK wt were plated in 10:90 relative ratio. The *scribble*^{kd} line was induced 72 hours prior to seeding via addition of doxycycline to the culture medium. The two lines were mixed after trypsinization in the appropriate proportions, to produce a cell suspension with final density of 10^{-3} cells/μm^2. Cells were imaged for 80 h (Movie 3). Control experiment were performed using the same experimental condition but mixing the two lines without doxycycline induction. This seeding protocol reliably produced isolated or very small groups (from 2 to maximum 4 cells) of *scribble*^{kd} cells surrounded by MDCK wt cells (Figure 4.3 a), (Movie 3).

Over the course of 80 h, *scribble*^{kd} (tet+) and MDCK wt proliferation showed very different growth trends, with the *scribble*^{kd} cell count peaking around 40 hours at 1.85 fold the initial count before decreasing to 1.5 fold (Figure 4.3 b, inset), whereas the MDCK wt increased sevenfold (Figure 4.3 b, left). In contrast, control experiments of MDCK wt co-cultured with non induced *scribble*^{kd} (tet-) in a 90:10 ratio showed a two fold increase in cell count for *scribble*^{kd} and a three fold increase in MDCK wt cells after 50 h (Figure 4.3 b, right). Such growth rates were comparable to those recorded in pure populations of each cell type, for similar durations (Figure 4.2 a). Therefore, scribble depletion affected the growth of knock-down cells mixed with wild type cells, resulting in a cell count that is different from the proliferation profile measured for pure *scribble*^{kd} (tet+) populations.

The drop of cell count of *scribble*^{kd} (tet+) cells in the presence of MDCK wt cells could be due to either a reduced division rate or to an increased cell death of MDCK cells upon scribble depletion. To answer this, I quantified the cell death

during time laps assays of both competition and control experiments by plotting the cumulative count of apoptosis events for each cell type (Figure 4.3 d). The average cumulative apoptosis count demonstrated that, in co-cultures, *scribble*^{kd} cells had significantly higher apoptosis counts than MDCK wt cells, despite being far scarcer (Figure 4.3 d, right). In contrast, when mixing the MDCK wt and *scribble*^{kd} non-induced lines, the number of apoptoses evolved in proportion to the initial seeding ratio (Figure 4.3 d, middle). Hence, when cultured in the presence of MDCK wt cells, *scribble*^{kd} (tet+) undergo a sustained cell death, which is 4.5 fold higher than the apoptosis baseline measured for *scribble*^{kd} pure populations.

Moreover, the long-term imaging assay allowed to qualitatively investigate in which conditions such context-dependent cell death took place. Particularly, the parallel acquisition of both transmission and fluorescence images enabled to discriminate whether dying cells were apically eliminated from monolayers prior to or after apoptosis. I found that *scribble*^{kd} cells would undergo apoptosis before being eliminated in most of the cases, as suggested by the nuclear fragmentation and cytoplasmic condensation mostly observed within the monolayer followed by the acquisition of a rounded up morphology and apical extrusion (Figure 4.3 a), (Movie 4).

4.6 Discussion

In the first part of the chapter, I have presented data showing the different effects of scribble knock-down on morphology, proliferation and apoptosis of MDCK cells. From transmission and fluorescence images, *scribble*^{kd} cells grown in standard 2D conditions inside the incubator scope in the presence of doxycycline (Movie 4) manifested a loss of the epithelial cobblestone morphology characteristic of MDCK wild type cells (Movie 5). *Scribble*^{kd} (tet+) cells appeared to spread more and to assume a flatter morphology reminiscent of a mesenchymal cell type. However, upon induction, *scribble*^{kd} maintained intercellular contacts (Movie 4), suggesting that cell-cell adhesions were maintained. To reinforce this observation, I measured E-cadherin expression of both induced, non-induced *scribble*^{kd} and wild type cells and I found that the *scribble*^{kd} (tet+) cells were enriched in E-cadherin compared to both non-induced (tet-) and wt MDCK cells. This result confirmed the effects shown by previous reports Qin et al. (2005),Norman et al. (2011). Indeed, other groups focused on the characterisation of the effects of scribble knock-down on the morphology and polarity of MDCK cells finding that, despite the different morphology, the *scribble*^{kd} (tet+) cells kept a correct 2D polarity, as indicated by the apical localization of the membrane marker gp135 and the fact that tight junction formation is preserved (as demonstrated by the correct localization of

ZO-1) Norman et al. (2011). Consistent with our Western Blot analysis, Norman and colleagues observed, via immuno-fluorescence, an increased accumulation of E-cadherin at cell-cell contacts in *scribble*^{kd} (tet+). Such increased expression resulted in a mislocalization of E-cadherin, which was found to be more localised in the basal domain rather then the baso-lateral one.

I showed that knock-down of scribble has a dual effect on the proliferation rate of MDCK cells, when looking at either tissue and single-cell scale. Particularly, the proliferation analysis detected a significantly lower cell number of *scribble*^{kd} (tet+) cells compared to non-induced cells. To test the hypothesis that this could be caused by a slower growth rate induced by scribble depletion, I measured the cell cycle time of both induced and non-induced *scribble*^{kd} populations by means of single-cell analysis. However, the distribution of cell cycle duration time did not revealed any significant difference between *scribble*^{kd} (tet+) and *scribble*^{kd} (tet-) cells. Another consideration is that both lines have a slightly shorter division time when compared to MDCK wt. An increased division rate upon induction of scribble depletion is what one might expect, as loss of scribble has being reported to cause aberrant proliferation (and loss of tissue size control) in *Drosophila melanogaster* Brumby and Richardson (2003); Humbert et al. (2008) and in various mammalian cell types scribble activity was found to negatively regulate the cell-cycle progression from G1 to S phase Nagasaka et al. (2006). To explain the discrepancy between single cell (distribution of cell cycle duration) and tissue scale (cell count over time) proliferation analysis, I quantified changes in cell death (identified by detection of nuclear fragmentation as a marker of apoptosis) upon scribble depletion. I measured the apoptosis profile of *scribble*^{kd} (tet+) cultured in pure populations (magenta)(Figure 4.3 d, right) and found that it reached 3 fold larger final value when compared to *scribble*^{kd} (tet-) and MDCK wt populations. This suggested a cell-autonomous increase in apoptosis rate (+35%) upon scribble silencing. This effect could compensate for the unchanged cell cycle time, and explain the cell count trend observed.

In the final section of this chapter, after having assessed the effect of scribble knock-down on MDCK in pure populations, I examined the fate of *scribble*^{kd} when in the presence of wild type neighbours (Movie 3). Work of other groups revealed increased cell death in *scribble*^{kd} cells when in the presence of MDCK wt cells Norman et al. (2011), Wagstaff et al. (2016). Such phenomenon was described as cell competition, due to the dramatically enhanced apoptotic rate of *scribble*^{kd} (tet+) in mixed cultures. Interestingly, in this particular cell competition scenario, the apoptotic rate of losers (induced *scribble*^{kd}) was found to be greater than

the death rate of non-induced $scribble^{kd}$ (tet-) in pure populations too. I found that cells depleted of scribble were effectively outcompeted by wild type cells because of decreased growth rates. I demonstrated that this was due to increase of cell death of $scribble^{kd}$, which reached higher rates than for pure population. Thus, the increase of cell death of $scribble^{kd}$ (tet+) has the characteristic of a non cell-autonomous, context-dependent phenomenon, a hallmark of cell competition. Previous experiments performed with addition of blebbistatin to the cell culture medium Norman et al. (2011) showed that competition-induced apoptosis happened independently of apical extrusion. Qualitative observation of time-lapse data supported this evidence, as apoptosis systematically preceeded extrusion.

In this section, division and death rates were displayed in time, and characteristic proliferation and apoptosis curves were retrieved for both pure and mixed populations. These data will be important to consider in the following chapters where, to further investigate the underlying mechanism of cell competition, proliferation and apoptosis will be analysed as functions of other variables (i.e. local density and neighbourhood).

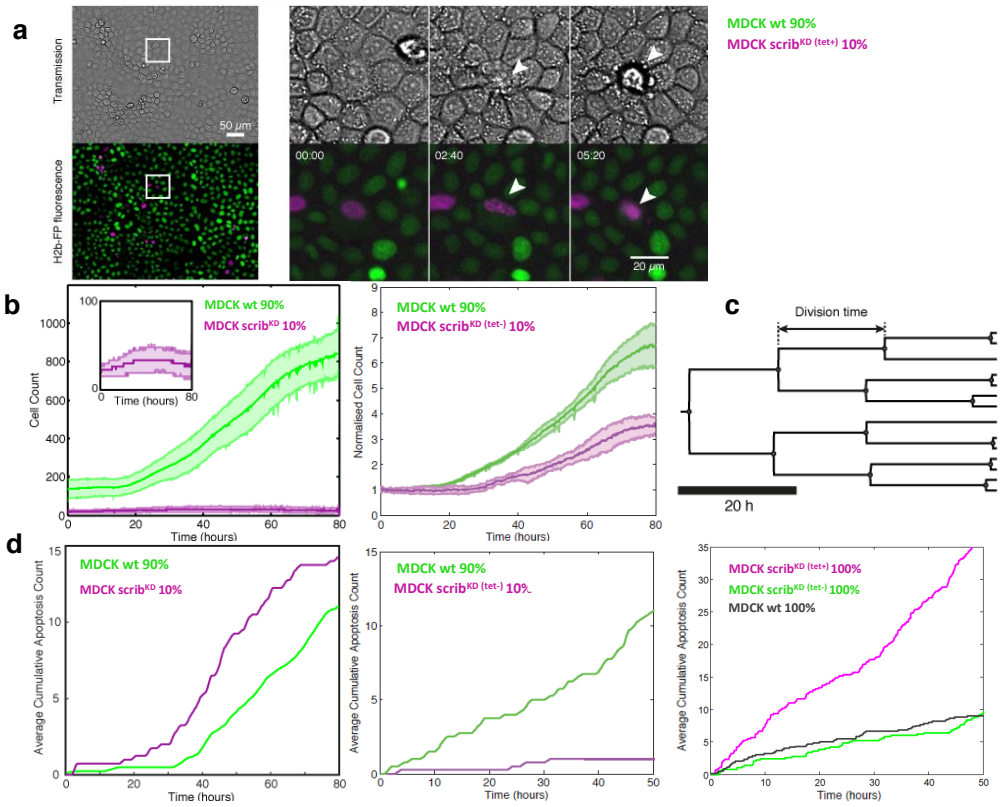

Figure 4.3: Knock-down of scribble triggers cell competition in MDCK cells (a) Left: Representative image containing MDCK wt (green) and *scribble*^{kd} (magenta) cells mixed in an initial 90:10 ratio. The image corresponds to one FOV (530 x 400) μm acquired by wide-field epifluorescence using 20x magnification. Scale bar = 50μm. The region of interest in the white rectangle is shown to the right. Right: Time series from the competition assay. The white arrow head indicates a *scribble*^{kd} cell undergoing apoptosis. Scale bar = 20μm (b) Left: Proliferation profiles of MDCK wt (green) and induced *scribble*^{kd} (magenta) during a competition experiment. The inset shows the evolution of cell count in the *scribble*^{kd} cells on a smaller scale. Right: Proliferation profiles of a control experiment, where MDCK wt cells (green) were mixed with non-induced *scribble*^{kd} (tet-). In both plots, data are pooled from three biological replicates imaging 4 fields of view for each replicate. The solid line indicates the mean of the experiments and the shaded area the standard deviation.(c) Representative lineage tree, obtained from classification and tracking of MDCK wt cells. The diagram shows how to compute cell cycle time at single cell level, by measuring the temporal separation between the birth of a cell and that of its daughters on a lineage tree (d) Left: Quantification of apoptosis for MDCK wt (green) and *scribble*^{kd} (magenta) during competition. Middle: Quantification of apoptosis for a control experiment, where MDCK wt cells (green) were mixed with non-induced *scribble*^{kd} (tet-) in the same relative proportions 90:10. Right: Apoptosis quantification for 100% *scribble*^{kd}, cultured in the presence (magenta) or absence(green) of tetracycline and for 100% MDCK wt (gray). The number of apoptoses is detected and averaged across 5-6 areas imaged during an experiment. Data are pooled from two biological replicates. Image from Bove et al. (2017).

5 Effect of local cellular density on the probability of division and apoptosis

5.1 Introduction

Previous experiments showed that *scribble*^{kd} cells are less tolerant to high density than MDCK wt cells. Wagstaff and co-workers have proved this by seeding cells on micro-patterned arenas with a well defined area and measuring the total density by dividing the number of DAPI stained nuclei by the area of the arena. In this way, they demonstrated that non-induced *scribble*^{kd} (tet-) cells, when plated at both low and high initial density, proliferated until reaching a typical maximal density value of 4 x10^{-3} cells/μm^2. Conversely, *scribble*^{kd} (tet+), if plated at high density, decreased their number in time as an effect of increased apoptosis and extrusion. However, if plated at low density, *scribble*^{kd} (tet+) cell count didn't drop, but fluctuated around the initial value of 4 x10^{-3} cells/μm^2. Therefore they concluded that, upon depletion of scribble, the MDCK cells become hypersensitive to crowding and, if forced to higher cell density, respond via activation of apoptosis. They hypothesised that such different tolerance to density is the key to explaining the loser status of induced *scribble*^{kd} cells in competition. Furthermore, they demonstrated that changes in density may induce increases in apoptosis events that alone are sufficient to result in the elimination of the *scribble*^{kd} (tet+) cells during competition. However, a detailed characterisation of the influence of density on apoptosis is lacking to quantitatively test this hypothesis. Moreover, the influence of cell density on division rate was not examined, although changes in division rate could also play a role during cell competition.

This chapter will describe how division and apoptosis probabilities are influenced by local cellular density. Similarly to the first chapter, analysis on pure populations was used as a comparison to better understand the effects observed in competition assays, where the *scribble*^{kd} cells are mixed with MDCK wt. I applied the single-cell density measure defined in equation 3.2 to characterise quantitatively

the exact relationship between cell density and probability of apoptosis. The application of this analytical pipeline quantitatively confirmed some previous observation that scribble knock-down cells are more sensitive to high cell density leading to apoptosis Wagstaff et al. (2016). Competition-specific changes relative to density-regulated division were also found. Such effects were of particular interest, because they did not fit with the hypothesis that cell density is the main predictor of competition outcome. This observation led me to consider other factors that may participate to competition, and this will be topic of the following chapter.

5.2 Scribble knock-down cells have lower homeostatic density than wild type cells in pure populations

To characterise division and apoptosis dependence on density, I developed an algorithm for computing the cellular density that a given cell senses. Such method is based on the Delaunay triangulation of cell centroids in each image frame (Figure 3.3 a, right) for identification of neighbouring cells. However, in sub-confluent conditions, this algorithm might identify false positives by linking the nuclei of cells which are separated by free space. Therefore it was necessary to define a threshold describing the maximum inter-nuclear distance separating two neighbours cells. I assessed the accuracy of the distance threshold by comparing the number of neighbours determined from the Voronoi diagram (number of Voronoi edges) based on the distance threshold to the number of neighbours determined by manual count of the E-cadherin delimited edges of a single cell (ground truth). To do so, I fixed and imaged MDCK cells stably expressing the H2b nuclear marker stained with an E-cadherin antibody, to detect the presence of an adherens junction and hence the presence of a true neighbour. I seeded cells at both high and low density (Figure 5.2). I performed a correlation analysis between the edges detected via the Voronoi method and the number of manually determined neighbours, calculating the Pearson coefficient (r). I obtained a correlation coefficient r=0.832 for high density and r=0.951 for low density. These results suggested that the experimental threshold applied to the Voronoi method provides a reliable estimate of the number of neighbours of each cell. Hence, I used the algorithm for computing the local cellular density for each cell ID from time-lapse data of 100% $scribble^{kd}$ (tet+) and $scribble^{kd}$ (tet-). I then averaged such parameter among cells of the same lineage, at each time point, and plotted the mean cellular local density in time for each population of

cells investigated. When computing density, I verified that the distance threshold experimentally determined D_{tresh} was accurate by computationally calculating the edge lengths of the Delaunay graph constructed from each cell centroids (Figure 5.1 b). The evolution in time of such measure effectively represents the inter-nuclear separation. As expected, the average inter-nuclear distance decreased over time and, notably, it was larger than the threshold values only at low density (i.e. when cells are sub-confluent and still separated by some free space). Remarkably, the larger D_{tresh} value used for *scribble*^{kd} (tet+), as opposed to that used for *scribble*^{kd} (tet-) and MDCK wt cells, reflected the increase in cell spreading observed upon scribble depletion, displayed in the previous chapter (Figure 4.1).

Consistent with previous descriptions Wagstaff et al. (2016), the mean local density of non-induced *scribble*^{kd} (tet-) and MDCK wt cells cultured in pure population increased with time, reaching a plateau (homeostatic value) after 80 hours. Conversely, the density of induced *scribble*^{kd} (tet+) had a flat trend, fluctuating around the initial density value (Figure 5.3 a, left). The maximal density value of both non-induced *scribble*^{kd} and MDCK wt was several fold higher (3.6 and 3-fold, respectively) than the maximal density of induced *scribble*^{kd}. Therefore, it is possible to conclude that induced *scribble*^{kd} (tet+) cells have a lower homeostatic density than MDCK wt or non-induced *scribble*^{kd} (tet-) cells.

5.3 Scribble knock-down cells reach higher cellular densities than surrounding wild type neighbours during competition assays

The evolution of mean local density was measured for induced *scribble*^{kd} cells in competition with MDCK wt cells. Strikingly, the temporal evolution of *scribble*^{kd} cells density changed dramatically compared to their behaviour in pure populations. In particular, competing *scribble*^{kd} cells reached a final density that surpassed the homeostatic value of surrounding MDCK wt cells by a factor of 1.4 (Figure 5.3 a, middle), with the maximal density value of MDCK wt following exactly the same trend as observed for pure populations. Such an increase in local density displayed by *scribble*^{kd} cannot be explained by considering it as a reflection of the density of the mixed culture. If that was the case, *scribble*^{kd} would be forced to reach a cellular density similar or comparable to that of the majority of surrounding cells. To test if this phenomenon was specific to the interaction of MDCK wt cells with *scribble*^{kd} (tet+), I performed experiments on mixed populations in the absence of doxycycline and plotted the local density

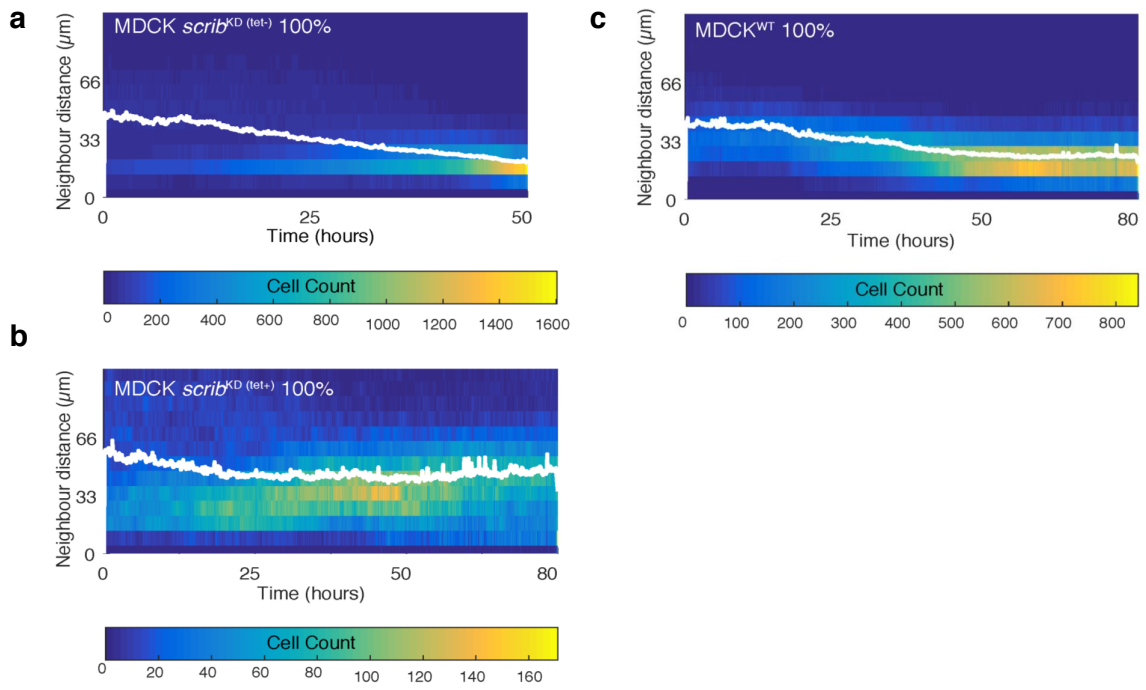

Figure 5.1: Distance threshold for interacting cells used in neighbourhood and density estimation. Two-dimensional histograms of distance between centroids for non-induced (a) and induced (b) *scribble*^{kd} and MDCK wt (c) cells. The mean value of inter centroid distance over time is displayed as solid white line. The time evolution is used to calculate the threshold value (D_{thresh}) for interacting cells used in neighbourhood estimation. From experimental measurement, the D_{thresh} was determined to be 30 μm for non-induced *scribble*^{kd}(tet-), 60 μm for *scribble*^{kd} (tet+) in which knock-down of scribble had been induced, and 30 μm for MDCK wt. Such values correspond to the respective average cell diameter in pre-confluency conditions. Any distance larger than this would imply the presence of free space between cells, signifying they cannot be classified as neighbours. In all of the three plots, the threshold value chosen is always below the average internuclear distance. Image from Bove et al. (2017).

for both lineages (Figure 5.3 a, right). The mean cell density of non induced *scribble*^{kd} also increased, but the curves representing the average cellular density of non-induced (tet-) and MDCK wt populations have very comparable trends and values. Finally, the results showed by the time resolved single-cell density analysis are fully consistent with the global density analysis previously performed

by other groups Wagstaff et al. (2016) by means of single time-point quantification. Furthermore, they proved the efficacy of the cellular density definition, given by equation 3.2, to estimate density heterogeneity in co-culture.

5.4 Scribble knock-down and wild type MDCK cells regulate their homeostatic density differently

Having validated the computational approach for calculating cellular density, I tried to rigorously explain the evolution of cell density as result of changes in both apoptosis and division rates.
Changes in population composition can, indeed, arise not only from increases in apoptosis but also via changes in division rates; despite this consideration, previous studies have mainly described apoptosis changes. I investigated the dependency of proliferation and apoptosis probability on local cellular density, using equation 3.3.
In pure populations, MDCK wt cells showed a high baseline probability of division; such proliferation rate was negatively regulated by density, as it decreased when the density increased beyond $\rho \sim 10^{-2}\mu\text{m}^{-2}$. Conversely, the division probability of pure *scribble*^{kd} cells (tet+) remained approximately constant through all the range of densities explored, at a 4-fold lower level than the MDCK wt cells (Figure 5.3 b, left). Probability of apoptosis for both cell types increased with density; however, the *scribble*^{kd} had a higher apoptotic rate than MDCK wt at all densities. Notably, the apoptosis rate of both *scribble*^{kd} and MDCK wt was approximately 10-fold smaller than their division rate (Figure 5.3 b, middle). Overall, this resulted in net growths that were positive and relatively insensitive to density until $\rho \sim 10^{-2}\mu\text{m}^{-2}$ after which they decreased (Figure 5.3 b, right). Altogether, these data suggested that the homoeostatic density was set differently for MDCK wt and *scribble*^{kd}. MDCK wt cells controlled population size by a density-dependent decrease in proliferation, whereas *scribble*^{kd} cells maintained a constant division rate and regulated their homeostatic density through a density dependent increase in apoptosis rate.

5.5 Apoptosis of scribble knock-down cells increases with density during cell competition

I analysed the contribution of division and apoptosis rates to the population shifts observed when co-culturing the *scribble*^{kd} induced cells in the presence of MDCK wt, in 10:90 proportion. This analysis confirmed what was hypothesised before by

Wagstaff et al. (2016), that the *scribble*^{kd} cells increase their apoptosis rate when forced to a density higher than their homeostatic value. Particularly, I found that the probability of apoptosis of competing *scribble*^{kd} cells undergoes a dramatic density-dependent increase for ρ>4*10^{-3} μm^{-2} (Figure 5.3 c, middle). As for the apoptosis rate of MDCK wt cells in competitive conditions, I found that it was comparable to that observed in pure populations until $\rho \sim 10^{-2}\mu m^{-2}$, after which it increased sharply. From an accurate analysis of the density dependent apoptosis profile, it emerged that when $\rho>10^{-2}\mu m^{-2}$, the probability of apoptosis for *scribble*^{kd} cells was $\sim$ 6-7 fold higher than that measured in MDCK wt cells. At the lowest densities instead, when ρ<3*10^{-3} μm^{-2}, the probability of apoptosis for *scribble*^{kd} was similar both in competitive and pure populations (Figure 5.3 b and c, middle). Remarkably, the local density observed during competitions assays covered a larger range than in pure populations (Figure 5.3 c). This effect could be due to the fact that, when cultured in pure populations, *scribble*^{kd} cells maintained their homeostatic density by exactly compensating proliferation with cell death. Hence, these results confirmed that apoptosis is upregulated with increasing density, as hypothesised previously Wagstaff et al. (2016).

5.6 Division of scribble knocked-down cells increases with density during cell competition

From the comparative analysis of division probabilities in pure populations and competitive conditions, some clear differences in behaviour between *scribble*^{kd} and MDCK wt cells emerged. On the one hand, the birth rate of MDCK wt cells showed a similar trend in both pure population and co-culture conditions: the division probability stayed constant with density until $\rho>10^{-2}\mu m^{-2}$ (Figure 5.3 b-c, left, green). Conversely, the p^{div} of *scribble*^{kd} cells exhibited a density dependent behaviour during competition assays. Indeed, at low density, the p^{div} of *scribble*^{kd} was comparable to the value measured for pure population; however, for $\rho>10^{-2}\mu m^{-2}$, a sharp increase was observed (Figure 5.3 b-c, left, magenta). Such behaviour is interesting, especially when compared to the constant trend (at both low and high density) of p^{div} measured for *scribble*^{kd} cells in pure populations, where the value registered is 4 folds lower than the wt curve. Therefore, at high density ($\rho>10^{-2}\mu m^{-2}$), the division rate for competing *scribble*^{kd} cells is higher than the division rate of MDCK wt and non competing induced *scribble*^{kd} cells.

5.7 Net growth of wild type cells is greater than that of scribble knock-down cells at all densities

The implementation of an algorithm to compute both apoptosis and division dependence on density allowed me to precisely quantify the net growth of each competing population within the density range explored, as formulated by equation 3.4. For both *scribble*^{kd} and MDCK wt cells, the net growth was generally decreasing with increasing density, as expected. A sharp net growth reduction was observed for densities $\rho > 10^{-2}\mu m^{-2}$, and resulted from the combination of a density dependent increase in apoptosis and decrease in division (Figure 5.3 c, right). Despite the higher p^{div} of *scribble*^{kd} cells at high density, their net growth was still lower than that of the competing wild type cells, due to the dramatic increase in p^{apo} observed in the same density regime. MDCK wt cells dominated the competition, with a net growth 4 fold higher than that of *scribble*^{kd} cells, at low density. However, when density increased, the MDCK wt cells' net growth dropped to 0.025%, thus converging to the net growth measured for *scribble*^{kd} cells. Still, in the range of density explored in our experiments, there was no regime where *scribble*^{kd} cells have higher net growth than MDCK wt cells, indicating that they are losers of this competition.

5.8 A purely density dependent model does not reproduce the experimental cell count

Previous work has suggested that mechanical competition may be the result of cell-autonomous increases in apoptosis with increasing density Wagstaff et al. (2016). To test this hypothesis, I collaborated with a PhD student in the Charras lab, Daniel Gradeci, who developed a quantitative model on the basis of the experimental results I have described so far. The model, based on coupled rate equations, investigated how the density dependence of cell division and apoptosis determine the time evolution of cell count in the competing populations and the overall population fitness. In this model, the density of the MDCK wt cells (WT) and *scribble*^{kd} cells (KD) increases at a rate proportional to a density-dependent division rate (f^{wt}_{div}, f^{kd}_{div}), and decreases proportionally with a density-dependent death rate (f^{wt}_{apo},$f^{k}_{apo}d$), as given by equation 5.1 and equation 5.2. The functions describing dependence of birth (f^{wt}_{div}, f^{kd}_{div}) and death (f^{wt}_{apo},$f^{k}_{apo}d$) rates of MDCK wt and *scribble*^{kd} cells were obtained by fitting an analytical function to the density dependent birth and death rates determined experimentally in Figure 5.3. In particular, it was found that birth rates followed a Gaussian behaviour whereas

apoptosis rate displayed a negative logistic behaviour (Figure 5.4 a). The coupled equations (5.1 - 5.4) were solved numerically to predict the temporal evolution of cell counts of MDCK wt and *scribble*^{kd} cells (Figure 5.4 b), subject to the experimental initial conditions for the cell count and density of the two cell types. By formulating the equations in such way, we tested the hypothesis that division and apoptosis rate are equally affected by the densities of the MDCK wt and *scribble*^{kd} cells, such that $f(\rho) \equiv f(\rho_{wt} + \rho_{kd})$. This hypothesis implies that cells cannot recognise which type their neighbours belong to but can determine their local density. MDCK wt and *scribble*^{kd} cells contribute equally to the measured density. However, this model failed to quantitatively reproduce the experimental cell count, predicting a lower count of MDCK wt cells (Figure 5.4). This suggests that alterations in cell behaviour due to density alone are not sufficient to explain the outcome of my experiments.

$$\frac{\partial \rho_{wt}}{\partial t} = f^{wt}_{div}(\rho_{wt} + \rho_{kd}) \cdot (\rho_{wt} + \rho_{kd}) - f^{wt}_{apo}(\rho_{wt} + \rho_{kd}) \cdot \rho_{wt} \tag{5.1}$$

$$\frac{\partial \rho_{kd}}{\partial t} = f^{kd}_{div}(\rho_{wt} + \rho_{kd}) \cdot (\rho_{wt} + \rho_{kd}) - f^{kd}_{apo}(\rho_{wt} + \rho_{kd}) \cdot \rho_{kd} \tag{5.2}$$

$$\frac{\partial N_{wt}}{\partial t} = \left[f^{wt}_{div}(\rho_{wt} + \rho_{kd}) - f^{wt}_{apo}(\rho_{wt} + \rho_{kd})\right] \cdot N_{wt} \tag{5.3}$$

$$\frac{\partial N_{kd}}{\partial t} = \left[f^{kd}_{div}(\rho_{wt} + \rho_{kd}) - f^{kd}_{apo}(\rho_{wt} + \rho_{kd})\right] \cdot N_{kd} \tag{5.4}$$

5.9 Discussion

Cell competition induced by loss of scribble had been characterised as an example of mechanical competition Norman et al. (2011), where loser cells are eliminated by winner cells due to their lower tolerance to high cellular density.
In this chapter, I have quantitatively described the relationship between division, apoptosis and net growth probabilities as a function of local cellular density, which I measured by means of the novel single-cell approach image analysis which I developed.
Indeed, when cells are cultured in pure populations, the density in each cell population first increases before reaching a plateau (homeostatic density). The homeostatic density is strongly affected by scribble depletion. I measured the time-course of mean cellular density of both *scribble*^{kd} and MDCK wt populations, either in pure culture and in competitive conditions. The density analysis confirmed that induced *scribble*^{kd} cells have a lower homeostatic density value than that of MDCK wt cells and non-induced *scribble*^{kd} cells. I also found that, when

placed in competitive conditions, *scribble*^{kd} cells showed a three-fold increase in their local density compared to the average value measured in pure population culture. Notably, the relative difference of homeostatic values among the three pure populations and the increase of density during competition matched up with values reported by other groups Wagstaff et al. (2016), where density measurement were performed at a single-time point. Hence, the efficacy of the density definition we proposed was validated.

Consequently, I tested the hypothesis that density had an influence on the apoptosis rate by measuring the probability of apoptosis as function of local density. I found that *scribble*^{kd} (tet+) cells set their homoeostatic population size by increasing apoptosis with increasing density. Such effect, present in pure population, is dramatically exaggerated during competition, as a result of the higher density values that cells are exposed to due to compaction by their wild type neighbours.

In addition to this, I characterised the sensitivity of cell division to density, as it could also affect population dynamics. It emerged that birth rate is, likewise, density regulated; specifically, MDCK wt cells decrease their mitotic rate as density increases. This result is not surprising, and it proves the transition to a contact-inhibition regime for cellular density greater than $10^{-2}\mu\text{m}^{-2}$. MDCK wt cells are, indeed, well known to exhibit contact inhibition of proliferation in *in vitro* culture Atala (2012). Interestingly, such behaviour was not observed for *scribble*^{kd} cells; their division rate was approximately constant when cultured in pure populations. A similar lack of proliferation control fits with loss of scribble function, as scribble is an important negative regulator of cell cycle progression Nagasaka et al. (2006). Surprisingly, during competition, *scribble*^{kd} cells showed an increase in their proliferation rate for densities greater than $10^{-2}\mu\text{m}^{-2}$. This observation raised the question of whether division was also density regulated, as an effect of scribble induced competition. The importance of examining division is clear, especially when considering that the probability of division was approximately one order of magnitude larger than the probability of apoptosis. As a consequence, any effect on division will be likely to dominate the competition outcome.
Having quantified specific density dependence of birth and death rates for both MDCK wt and *scribble*^{kd} cells, I asked if such density related changes were sufficient to predict the temporal evolution of cell count and the overall population fitness that I measured with the single-cell approach. This question was addressed by collaborating with Daniel Gradeci, a Physics PhD student, who developed a

quantitative model based on the experimental results that I found. Interestingly, the model could not efficiently reproduce cell counts of MDCK wt cells, when assuming that cells can only determine their local density but not the cell type of their neighbourhood. This observation further emphasised the importance of considering division as well as apoptosis when studying cell competition, and suggested that factors other than density might be involved in setting the competition outcome.

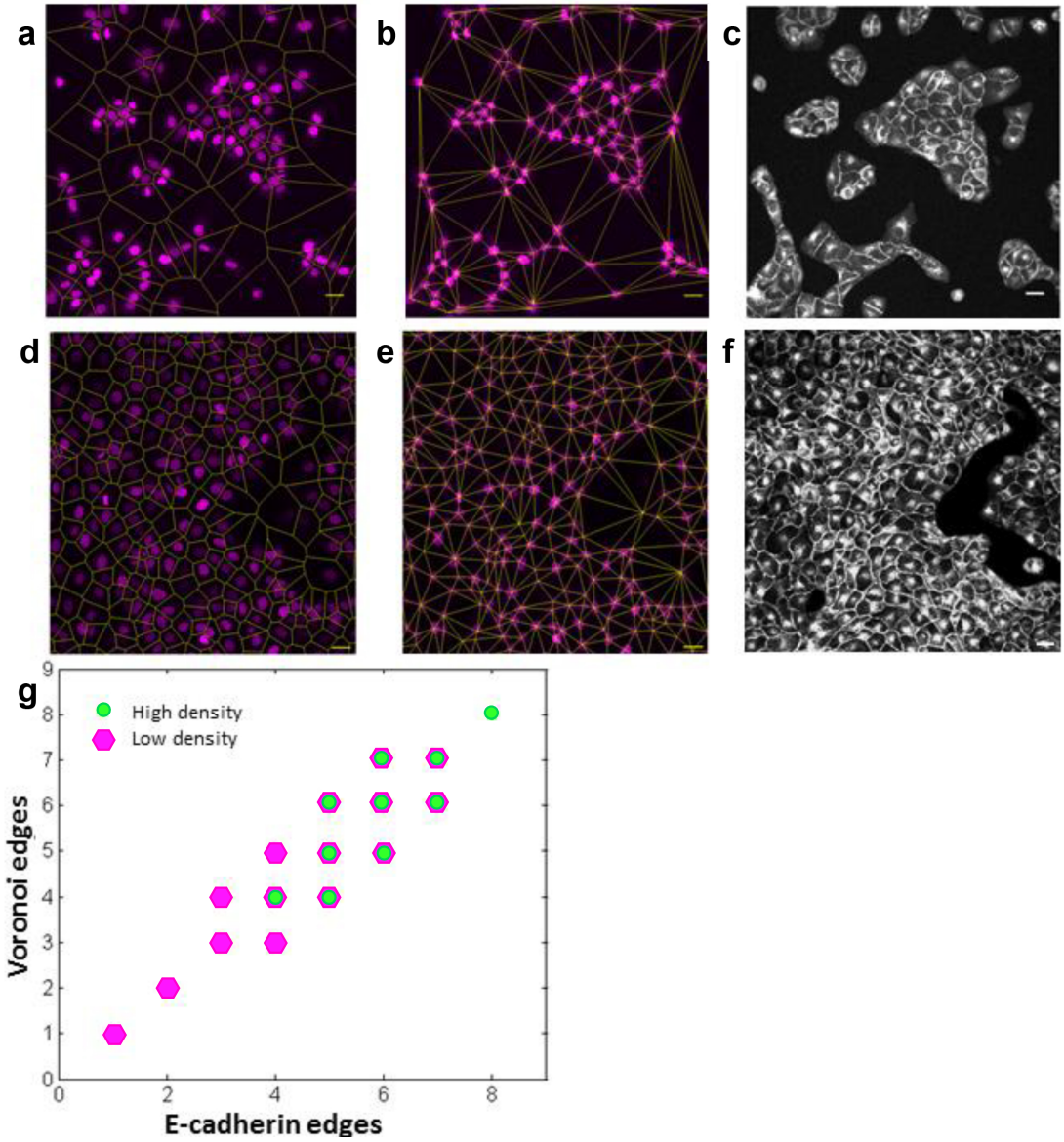

Figure 5.2: Validation of neighbourhood analysis using the Voronoi method. High density (d,e) and low density (a,b) images of MDCK stably expressing H2b-RFP (magenta, a-b, d-e) and E-cadherin GFP (grey, c,f). Scale bar = 25μm. I applied the Voronoi tessellation and Delaunay triangulation algorithms to the nuclei images (a-b, d-e). The Voronoi diagram and the Delaunay triangulation are highlighted in yellow. I manually scored the number of E-cadherin delimited edges for each cell as a ground truth. (g) I determined the correlation between the edges detected via the Voronoi method and the manually detected edges, at high (shown in green circle) and low densities (displayed in magenta markers). I calculated the Pearson coefficient (r) and obtained r=0.832 for high density and r=0.951 for low density, indicating that the Voronoi method provides a reliable estimate of the number of neighbours. Image from Bove et al. (2017).

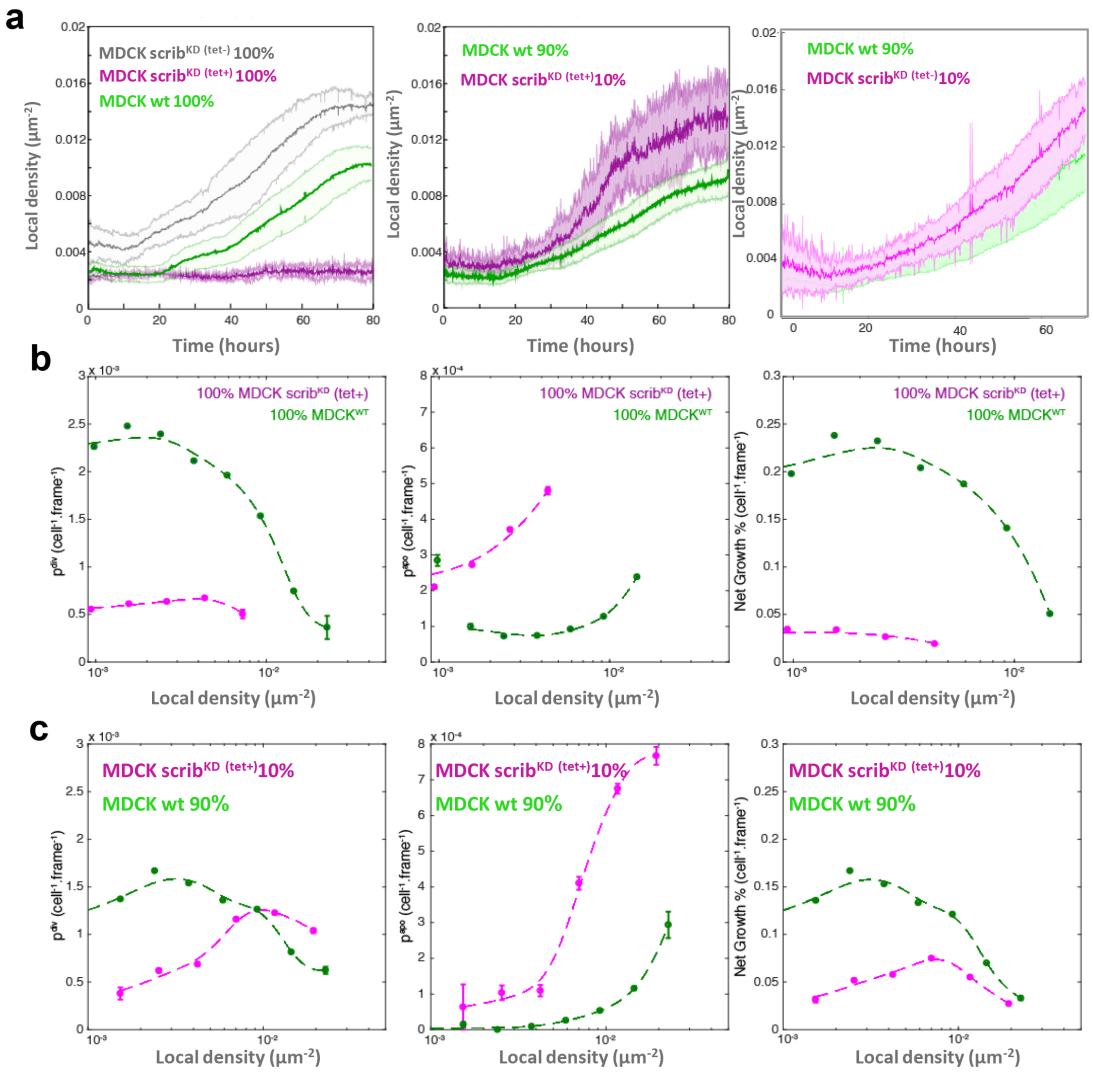

Figure 5.3: Probability of apoptosis and division are sensitive to local density in pure and competitive conditions. (a) Evolution of local density for MDCK wt and *scribble*^{kd} cells cultured both in pure and mixed populations. The solid line indicates the mean of the experiments and the shaded area indicates the standard deviation. Data are pooled from three biological replicates. Left: Temporal evolution of local density for pure populations of MDCK wt (green), non-induced *scribble*^{kd} (tet-, black), and induced *scribble*^{kd} (tet+, magenta). Middle: Temporal evolution of local density for MDCK wt (green) and *scribble*^{kd} (magenta) seeded at a 90:10 ratio during a competition assay. Right: Temporal evolution of local density for MDCK wt (green) and non induced *scribble*^{kd} (magenta) seeded at 90:10 ratio. (b) Probability of division (p^{div}), apoptosis (p^{apo}), and net growth (p^{div}-p^{apo}) per cell per frame as function of local density computed for induced *scribble*^{kd} (tet+, magenta) and MDCK wt (green) pure populations. (c) Probability of division, apoptosis, and net growth per cell per frame for MDCK wt and induced *scribble*^{kd} during competition. Data are pooled from 8 fields of view from two biological replicates. (b-c) Data points are indicated by solid circles. Trend lines computed using smoothing splines are plotted as dashed lines. Image from Bove et al. (2017).

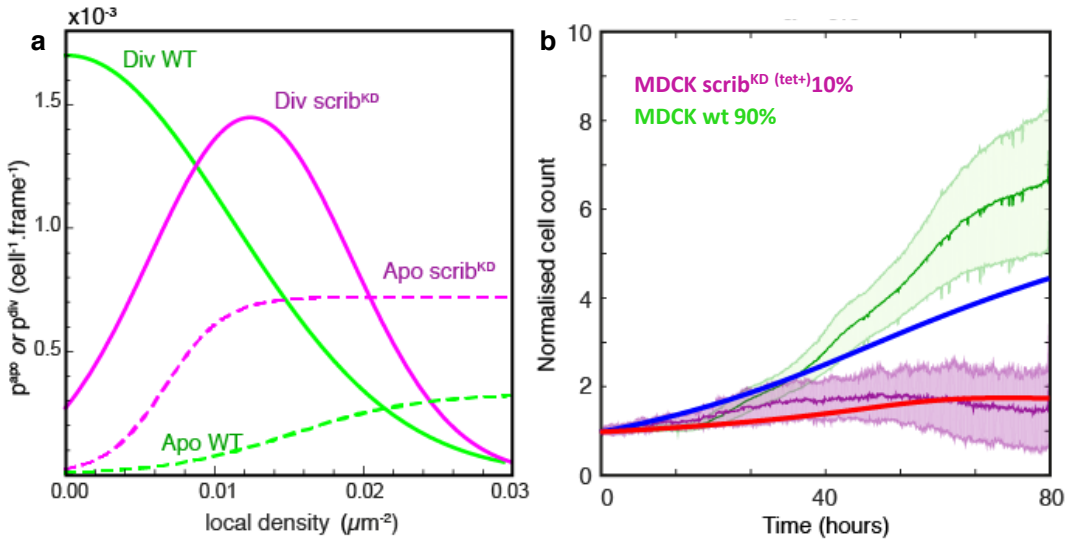

Figure 5.4: A density dependent rate equation model for cell competition cannot predict the evolution f cell count. (a) Probability (per unit time per cell) of apoptosis (dashed lines) and probability of division (solid lines) for MDCK wt (green lines) and *scribble*^{kd} (magenta lines) cells determined the rates f_{apo} and f_{div} for our model. These functions were fitted to the experimental data in (5.3). (b) Temporal evolution of cell count predicted by the symmetric interaction model initialised with the mean experimental cell count at t=0 for MDCK wt (solid blue line) and *scribble*^{kd} (solid red line). The model curves are overlaid with the experimental cell count from (4.3 b) for MDCK wt (green) and *scribble*^{kd} cells (magenta). Image from Bove et al. (2017).

6 Effect of local cellular neighbourhood on the probability of division and apoptosis

6.1 Introduction

In the previous chapter, I described some competition-specific changes relative to division and apoptosis rates discovered for $scribble^{kd}$ cells. Such changes came to light after investigation of proliferation and death density dependent probabilities. The working hypothesis was that the competition phenomenon observed was triggered by mechanical cues and, accordingly, cell density was the main predictor of its outcome. However, the density induced mitotic behaviour of $scribble^{kd}$ cells was difficult to understand within the mechanical competition framework, and suggested that other factors could have a role. Indeed, the numerical simulation resulting from the implementation of a coupled rate equation model, where rates of division and apoptosis depended on cell density, failed to reproduce the experimentally observed cell count of MDCK wt cells. Therefore, I asked if contact-mediated biochemical interactions between loser and winner cells might have an impact on the population evolution. The induction of behaviour in one cell lineage in response to interaction with another one is a key concept in cell competition Vincent et al. (2013). To address this question, I used the single-cell analysis approach to generate neighbourhood plots, which display how the probability of apoptosis or division depends on the number and type of neighbours. To provide a negative control, I performed time-lapse experiments on co-cultures of MDCK wt H2b-GFP cells mixed with MDCK wt H2b-RFP cells in 90:10 relative seeding ratio. The neighbourhood analysis of these controls was very different from neighbourhood plots of competition assays, thus elucidating that cellular interactions could be players in scribble induced competition.

6.2 Apoptosis of scribble knock-down cells increases with number of neighbours

To detect inductive behaviours during cell competition, each apoptosis event was categorised as a function of the number of neighbours of each type. This analysis was made possible by the implementation of a neighbourhood-based distance algorithm to retrieve the interaction network for each cell at each time point. I generated neighbourhood plots, where the probability of apoptosis is colour-coded and placed in a grid as function of the number of $scribble^{kd}$ and MDCK wt neighbours, respectively on the x-axis and y-axis. Each grid position typically grouped 10^4 - 10^5 observations (cells per frame) (Figure 6.2). Grid positions representing less than 500 observations were not considered in the computation, and are displayed in the plots as grey boxes. Grid positions for which many observations were made but no division or apoptosis event was detected are marked by an asterisk and coloured as 1/N observations to provide an upper bound for the probability in that position.
I used neighbourhood plots to elucidate the role of cellular neighbourhood in the apoptosis of $scribble^{kd}$ cells observed during competition (Figure 6.1, middle). Briefly, an apoptosis diagram with uniform colour indicates a behaviour independent on the composition of the cell neighbourhood, whereas a diagram showing asymmetry about the diagonal identifies a behaviour dependent on neighbourhood.

Notably, the probability of apoptosis is higher in $scribble^{kd}$ cells than MDCK wt cells for most grid positions. The diagram relative to MDCK wt apoptosis (Figure 6.1 a, middle) was approximately uniform with low apoptosis probabilities and therefore coloured in cold colours, whereas the $scribble^{kd}$ plot (Figure 6.1 b, middle) showed some higher apoptosis probabilities and was therefore coloured in warmer colours. This was apparent especially on the upper quadrant. In summary, the neighbourhood analysis revealed that apoptosis is increased in $scribble^{kd}$ cells possessing many neighbours, this observation is highly consistent with the results already presented that apoptosis increases at high density. In addition, apoptosis in $scribble^{kd}$ is slightly more sensitive to neighbourhood than apoptosis in MDCK wt cells. However, this feature is not clearly displayed in the (Figure 6.1 d). This is due to the lack of detected apoptosis events in some positions in the first row of both grids (Figure 6.1), as demonstrated by the presence of asterisks. The probability value assigned to those positions was 1/N observations, therefore, although providing an upper bound, it affected the value of the s parameter. The comparison of these results with those retrieved from control experiment, where MDCK wt cells expressing both fluorescent nuclear markers are co-cultured in

a 90% H2b-GFP and 10% H2b-RFP mixture, are very informative. Indeed, in control experiments, the p^{apo} of MDCK wt labelled with GFP and RFP nuclear marker showed very similar patterns, when plotted in the neighbourhood plots (Figure 6.4, middle). Particularly, both cell lineages displayed apoptosis diagrams with uniform colour distribution and very low (average) values of $p^{apo} \sim 0,3x10^{-3}$-$0,4x10^{-3}$ $(frame^{-1})$, consistent with average value observed for the MDCK wt in competition (Figure 6.1, a middle). Such analysis provides an example of how the neighbourhood plot would look like when confronting two non competing populations. Similarly, neighbourhood plots for mixed populations of MDCK wt mixed with non induced $scribble^{kd}$ (tet -) in 90:10 showed low sensitivity to neighbourhood, and a much lower degree of asymmetry in apoptosis (Figure 6.3). Nevertheless, these diagrams are not identical to those shown in (Figure 6.1 a, middle), probably because of an incomplete repression of the promoter by the tet repressor, as suggested in section 4.2. Altogether, the evidences I presented here reinforce the concept that the increase in apoptosis of $scribble^{kd}$ is, indeed, a signature of mechanical cell competition.

6.3 Division of MDCK wild type cells increases in scribble knock-down enriched cellular neighbourhoods

I investigated the effect of neighbourhood on the division probability p^{div} using a similar algorithm as the one I described in the previous paragraph. Division events were categorised according to the number of neighbours of each lineage. This enabled me to generate neighbourhood plots where p^{div} $(frame^{-1})$ is colour-coded and placed in a grid as function of the number of $scribble^{kd}$ and MDCK wt neighbours, respectively on the x-axis and y-axis.
Interestingly, I found that the probability of division of MDCK wt is strongly influenced by cellular neighbourhood, as displayed by the warm colour patch in the lower quadrant (red arrow Figure 6.1 a). In contrast, p^{div} for $scribble^{kd}$ cells is insensitive to neighbourhood, as suggested by the uniformly coloured diagram displayed in (Figure 6.1 b, left). The asymmetric distribution of probability, quantified by means of the s parameter (equation 3.5), is displayed in (Figure 6.1 d): when it comes to p^{div}, MDCK wt have a three fold higher value of s than $scribble^{kd}$ cells. To test if such effect is specifically induced by cell competition, I plotted neighbourhood diagrams of p^{div} for MDCK wt labelled with green H2b (90%) mixed with MDCK wt tagged with red H2b (10%)(Figure 6.4, left). In contrast to the marked asymmetric behaviour found in (Figure 6.1 a, left), these

neighbourhood plots showed a very low degree of asymmetry; particularly, the division probability of MDCK wt H2b-GFP is quite constant (uniform blue colour) across all grid positions. It is important to note that the scale used for Figure 6.1 and Figure 6.4 are the same. Overall, these results indicate a non cell-autonomous behaviour that positively regulates proliferation of the MDCK wt (winner) cells in the presence of a majority of $scribble^{kd}$ cells.

6.4 Net growth of both cell lineages is dominated by the contribution of division

Shifts in the composition of a cell population arise from imbalance, at the single-cell level, of both proliferation and cell death rates. Hence, in order to gain insight into the dynamics of the cell competition process and how it shapes the population make up, I combined the contribution of apoptosis and division in one single parameter, the net growth ($frame^{-1}$) computed, in analogy to the definition provided in equation 3.4, as the difference between p^{div} ($frame^{-1}$) and p^{apo} ($frame^{-1}$). Thus, $p^{netgrowth}$ describes the fitness of a cell in a particular neighbourhood. The analysis on p^{div} and p^{apo} presented in this chapter indicates that, for both cell lineages, p^{apo} is lower than p^{div} by approximately an order of magnitude. This results, valid for both competitive (Figure 6.1) and non-competitive (Figure 6.4) scenarios, was not surprising, as it confirmed what was found in (Figure 5.3 b-c). Accordingly, the net growth neighbourhood plots reflect the prevalent contribution of division (Figure 6.1 a-b, right). Indeed, net growth is positive and highest in the lower quadrant of the neighbourhood diagram for MDCK wt cells (Figure 6.1 a, right). In contrast, $p^{netgrowth}$ of $scribble^{kd}$ cells is very low, either zero or negative in the upper quadrant, which represents the region dominated by MDCK wt (Figure 6.1 b, right). Net growth diagrams plotted from non competitive assays (Figure 6.4, right) showed a net growth quite uniform for both GFP and RFP labelled MDCK wt, with a trend that negatively correlates to the number of total neighbours (the lower net growth, the greatest the number of total neighbours). No particular symmetry to the diagonal was detectable, so no neighbourhood effect was found, as one would expect for a non competitive control.

6.5 An asymmetric model for describing the density dependent division of MDCK wt cells

Following from the model discussed in the paragraph 5.8, the hypothesis that the division rate of MDCK wt cells is non cell-autonomous was tested by adding an asymmetric dependency term to equation 5.1 and equation 5.3, such that $f(\rho) = f(\rho_{wt} + (1-a)\rho_{kd})$. Such addition was used to modify only the terms describing density depended division rate of MDCK wt cells, based on our experimental finding that the MDCK wt cells exhibit an asymmetric neighbourhood dependence of division rate (Figure 6.1 a, left). Such formulation allows to model the situation where the local cell density of MDCK wt cells is lower if there are *scribble*^{kd} cells in their neighbourhood. The coupled rate equations were changed, as reported below:

$$\frac{\partial \rho_{wt}}{\partial t} = f^{wt}_{div}(\rho_{wt} + (1-a)\rho_{kd}) \cdot (\rho_{wt} + \rho_{kd}) - f^{wt}_{apo}(\rho_{wt} + \rho_{kd}) \cdot \rho_{wt} \tag{6.1}$$

$$\frac{\partial \rho_{kd}}{\partial t} = f^{kd}_{div}(\rho_{wt} + \rho_{kd}) \cdot (\rho_{wt} + \rho_{kd}) - f^{kd}_{apo}(\rho_{wt} + \rho_{kd}) \cdot \rho_{kd} \tag{6.2}$$

$$\frac{\partial N_{wt}}{\partial t} = \left[f^{wt}_{div}(\rho_{wt} + (1-a)\rho_{kd}) - f^{wt}_{apo}(\rho_{wt} + \rho_{kd})\right] \cdot N_{wt} \tag{6.3}$$

$$\frac{\partial N_{kd}}{\partial t} = \left[f^{kd}_{div}(\rho_{wt} + \rho_{kd}) - f^{kd}_{apo}(\rho_{wt} + \rho_{kd})\right] \cdot N_{kd} \tag{6.4}$$

The introduction of the asymmetric term enabled to model different types of competitive interactions. For instance, if a=0, the model returns the symmetric dependence, characteristic of a cell-autonomous behaviour, as described in paragraph 5.8. Conversely, if a>1, the birth rate of MDCK wt is positively influenced by the presence (i.e. the density) of *scribble*^{kd} cells, as the term $(\rho_{wt} + (1-a)\rho_{kd})$ decreases. This described the enhancement of division rate of MDCK wt when in neighbourhoods with high proportions of *scribble*^{kd} cells, as observed in my experiments (Figure 6.1). Therefore, numerical simulations were performed, setting a>1 and treating "a" as a parameter which was varied to reproduce the experimental cell count evolution (Figure 6.5 b). Interestingly, the numerical simulations performed after implementation of equation 6.1 and equation 6.3 showed that the scenario that most accurately reproduced the experimental cell counts assumed an asymmetric dependency of the birth rate of MDCK wt on the density of *scribble*^{kd} cells. Indeed, the value of a=2.6 enabled to quantitatively reproduce the experimental cell count (Figure 6.5 a-b), accounting for the increased birth rate of MDCK wt cells in *scribble*^{kd} populated neighbourhoods. This result reinforced the notion that the MDCK wt cells exhibited division induction dependent on local neighbourhood.

6.6 Discussion: Single cell analysis revealed non-autonomous behaviours in scribble competition

In this chapter, I described how I used the sophisticated single cell approach developed for characterising, at tissue scale level, the cell-cell interactions occurring during loss of scribble induced competition. The aim was to gain further insight into the mechanism underlying such competition, to determine the cellular events leading to the final population shift outcome. Despite the considerable number of suggested mechanisms Wagstaff et al. (2016), Merino et al. (2015), Vincent et al. (2011) potentially responsible for competition events, some common features in the mode of competition were recently identified: (i) slower division rate of loser cells, (ii) increased proliferation of winner cells and (iii) non-autonomous apoptosis of loser cells Kucinski et al. (2017). The distinctive factor of (i-iii) is the induction of non-autonomous cell behaviour. A preliminary description of scribble induced competition highlighted only one of the features listed above: the increase of apoptotic rate of loser cells in the presence of winner cells, accordingly to (iii). No emphasis was laid on the role of cellular interactions, as this result was mostly characterised as function of sensitivity to cellular density. By analysing the dependence of death rates of both MDCK wt and $scribble^{kd}$ on neighbourhood composition, I was able to discriminate neighbourhood effects from density effects, thus adding quantitative evidence to mechanism (iii). Firstly, the analysis of apoptosis diagrams suggested that death of $scribble^{kd}$ increased with increasing number of total neighbours, consistent with the notion that it increases at high density. In addition, by looking at the colour of grid positions in (Figure 6.1 middle, b), the apoptosis of $scribble^{kd}$ cells was found to be more sensitive to neighbourhood than the apoptosis of MDCK wt cells. Globally, I found that apoptosis plots were generally more symmetric than division plots (Figure 6.1 d). This suggested that the apoptosis rate was more influenced by the number rather than the cell-type of neighbours, and highlighted the need to consider the contribution of division effect.

The most striking dependence was, indeed, revealed in neighbourhood plots of division of competing MDCK wt cells. I found that the probability of division of MDCK wt cells was significantly increased in neighbourhoods mostly populated by $scribble^{kd}$ cells. Proliferation of the winner cell type seemed affected (specifically up regulated) by local cellular neighbourhood. Therefore, I was able to identify another non-autonomous behaviour of scribble competition, which is reminiscent of mechanism (ii). With the help of my collaborator, Daniel Gradeci, I investigated the dependence of apoptosis and division on neighbour cell-type, evident from our

experimental data, by introducing an asymmetry parameter in the coupled rate equation model for the evolution of cell count. Indeed, the scenario that enabled accurate simulation of the experimental outcomes relied on the assumption that the local cellular density seen by MDCK wt cells decreases due to the presence of *scribble*^{kd} cells. Such effect caused the proliferation rate of MDCK wt to be higher in neighbourhood populated by *scribble*^{kd} cells. This model was able to quantitatively reproduce the experimentally observed cell counts of both MDCK wt and *scribble*^{kd}, conversely to the symmetric interaction model discussed in paragraph 5.8 which failed to do so.

An interesting question arising from the analysis of these data is to investigate the causality relationship between death of *scribble*^{kd} cells and proliferation of MDCK wt cells during competition. Winner cell proliferation can be attributed to different events: winners -loser recognition signals or compensatory mechanisms triggered by loser cell death Levayer and Moreno (2013). Previous studies showed that dying cells were able to secrete mitotic signals, thus increasing proliferation of neighbouring cells Ryoo et al. (2004). Such apoptosis induced proliferation seemed to respond, in *Dropophila melanogaster*, to cellular injuries or stress and was mediated by JNK pathway Mcmahon et al. (2015). This mechanism was called the "active model", as apoptotic cells actively signalled to neighbour cells by secretion of growth stimulating factors, both dpp and wg Vincent et al. (2011), as opposed to a passive model, where proliferation would occur as an indirect results of physical changes at the cell-cell boundaries due to empty space left by the dead cells. Further experiments will be needed to understand the molecular mechanisms underlying the sensitivity of mitotic behaviour of MDCK wt cells to density and neighbourhood in the *in vitro* model I examined. For instance, this could be done by inhibiting the apoptosis of *scribble*^{kd} cells using specific p53 inhibitors; this approach has already been validated by Wagstaff et al. (2016). If the division rate of MDCK wt measured in neighbourhoods dominated by *scribble*^{kd} cells is comparable to that observed in MDCK wt neighbourhood, then one must conclude that the increased proliferation was caused by the previous death of *scribble*^{kd}, thus demonstrating the apoptosis-induced mechanism (either active or passive). Otherwise, if the non-autonomous cell division of MDCK wt cells is still observed, then one could argue that this is caused by some other signalling interplay between loser and winners cells. Then, a dynamic characterisation of the molecular changes occurring at the interface between cell types would be necessary, together with the establishment of genetic or pharmacological tools for controlling the expression or the activity of the main pro-mitotic candidates.

Division of *scribble*^{kd} cells did not show any particular dependence or symmetry,

being quite constant in all neighbourhood. Many studies performed in *Drosophila melanogaster* had outlined slow division rate of loser cells as a hallmark of competition, notably showing that it was due to JNK activity. Beyond inducing losers' cell death, JNK had been noted to inhibit growth of neoplastic tumour suppressor (Lgl,Dgl, Scrib) mutant cells Brumby and Richardson (2003), and Minute Kucinski et al. (2017). However, JNK activity in $scribble^{kd}$ cells was analysed by previous groups Norman et al. (2011), and found to be unaltered during competition with MDCK wt, as well as not required for apoptosis of outcompeted cells. This could explain the absence of such competition feature.

In conclusion, I was able to outline more precisely the experimental/cellular signature of scribble competition, revealing the presence of non-autonomous behaviour affecting both proliferation of winner cells and apoptosis of loser cells.

6.7 Future directions

Further insight into the dynamics of competition events will be gained by generation of time-resolved neighbourhood plot. Time-resolved neighbourhood plots may enable comparison of competition at low and high density, or before and after drug treatment. With the help of my collaborator Daniel Gradeci, I developed the code to perform such analysis and I have tested it on the MDCK wt: $scribble^{kd}$ competition (Figure 6.6). Nevertheless, for this analysis to be informative, a larger number of observation and events is required, to collect sufficient statistics for each condition that we want to compare. However, such considerations must be included early on in experimental design, for instance starting from very sparse initial density conditions. Results displayed in Figure 6.6, although showing evident differences between low (Figure 6.6 a,d) and high density (Figure 6.6 b,e), are difficult to interpret because epithelial cells grow in colonies. Growth in colonies may explain why, even at low densities, some cells have a large number of neighbours. Indeed, my data shows that the majority of cells, both belonging to MDCK wt and $scribble^{kd}$ cells, at low density have an average number of four neighbours, which is quite large considering that, in confluent monolayers, the average number of neighbour a cell has is six. This may be because the cells that I used grow in colonies; therefore cells fully surrounded by neighbours exist from early on in the experiment. Indeed, the most striking asymmetry in the division neighbourhood plot of MDCK wt is observed at low density, where cells are at the periphery of a colony. This data is interesting, as it can help clarifying the role that proliferation of winner cells have in the competition outcomes. The numerical simulation was used to make prediction on how the net growth of the competing

cell lines varies with the densities of MDCK wt and $scribble^{kd}$ cells. Plots (Figure 6.5, c) shows that $scribble^{kd}$ cells may outcompete MDCK wt cells in regions of high $scribble^{kd}$ density and low MDCK wt density (bottom right hand corner of Figure 6.5 c). Such a regime is never observed in our experimental conditions and would require external manipulation for it to be attainable. Finally, a series of different experimental designs will be employed for performing competition assays under tightly controlled micro- environmental conditions, and are discussed in the following section.

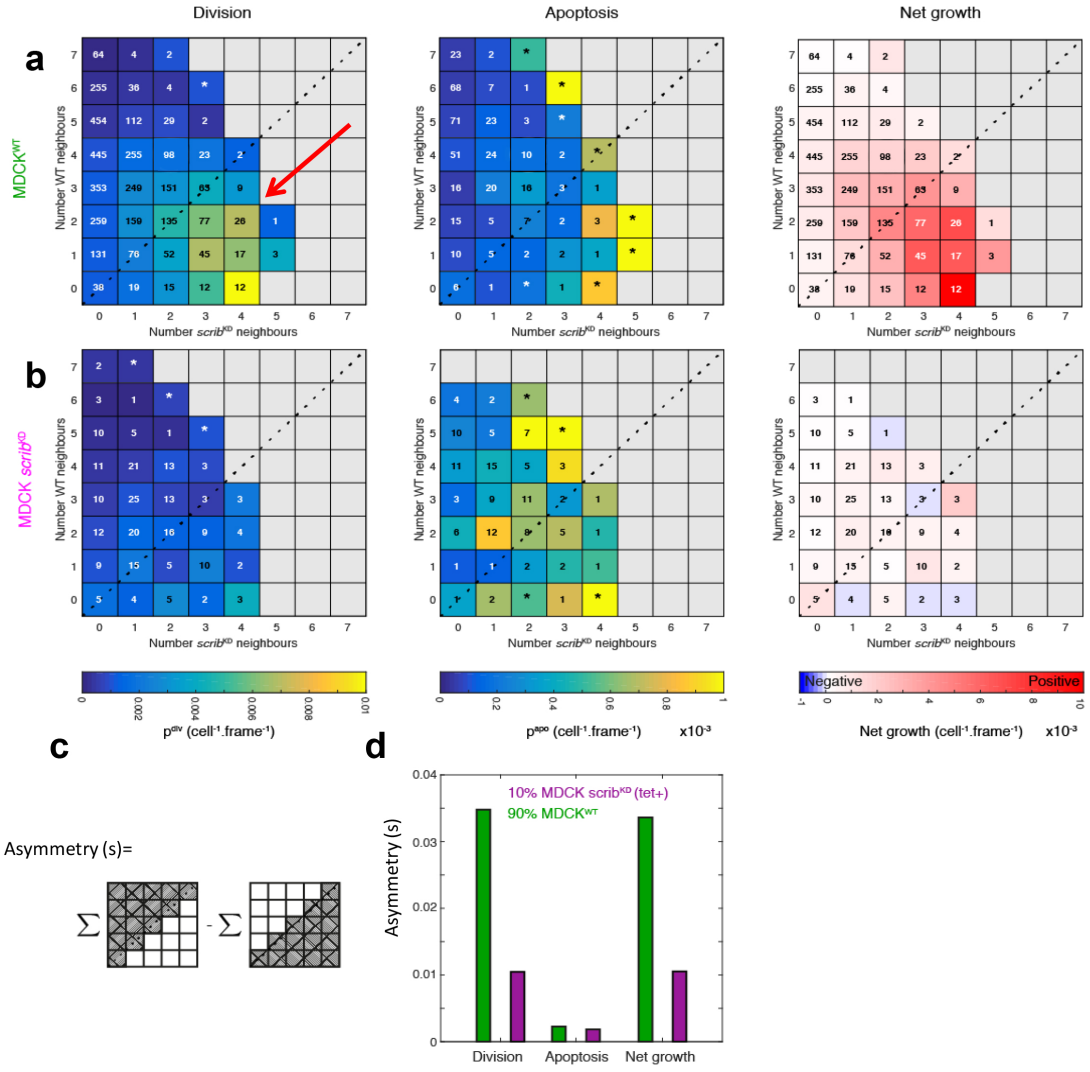

Figure 6.1: Probability of apoptosis, division, and net growth are sensitive to the composition of local neighbourhood. Neighbourhood plots showing the colour coded probability per cell per frame of division, apoptosis and net growth for MDCK wt (a) and *scribble*^{kd} (b) during competition. The diagonal (black dashed line) indicates grid positions with equal numbers of MDCK wt and *scribble*^{kd} neighbours. Numbers in each grid position indicate the number of detected events (division or apoptosis). Measurements for each grid position are typically computed from observations of >500 cells. Grid positions for which many observations were made but no event detected are marked by an asterisk and coloured as 1/N observations to provide an upper-bound for the probability in that position. Data are pooled from 12 time-lapse movies from three biological replicates. The red arrow indicates a warm colour patch in the lower quadrant of MDCK wt division plot, where probability of division is influenced by the presence of neighbours belonging to the other cell type. (c) Definition of the parameter s used for calculating the asymmetry of neighbourhood plots around the diagonal (d) Calculation of asymmetry performed on neighbourhood plots shown in a-b. The asymmetry defines whether the behaviour is cell-autonomous (low s values) or dependent on the cell-type of neighbours (high s values).

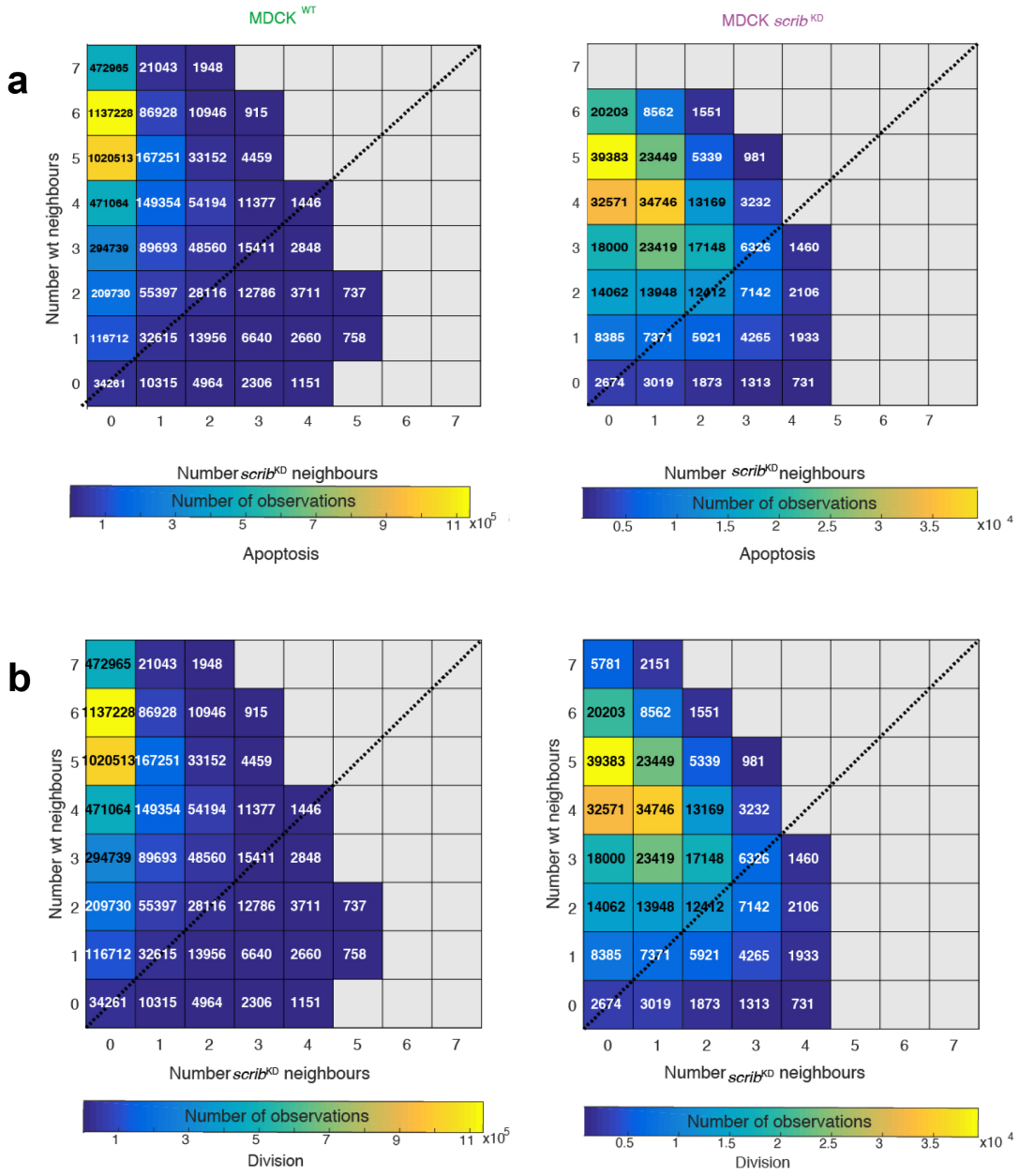

Figure 6.2: Number of observations in each position of neighbourhood plots (a,b) Neighbourhood plots showing the colour coded number of observations for MDCK wt (left panels) and *scribble*^{kd} (right panels) during competition. The number of *scribble*^{kd} neighbours is shown on the x-axis and the number of MDCK wt neighbours is shown on the y-axis. The diagonal (black dashed line) indicates grid positions with equal numbers of MDCK wt and *scribble*^{kd} neighbours. Numbers in each grid position indicate the number of observations for MDCK wt and *scribble*^{kd} cells with that particular neighbourhood. Data are pooled from 12 time-lapse movies from three biological replicates. Only grid positions with more than 500 observations are included.

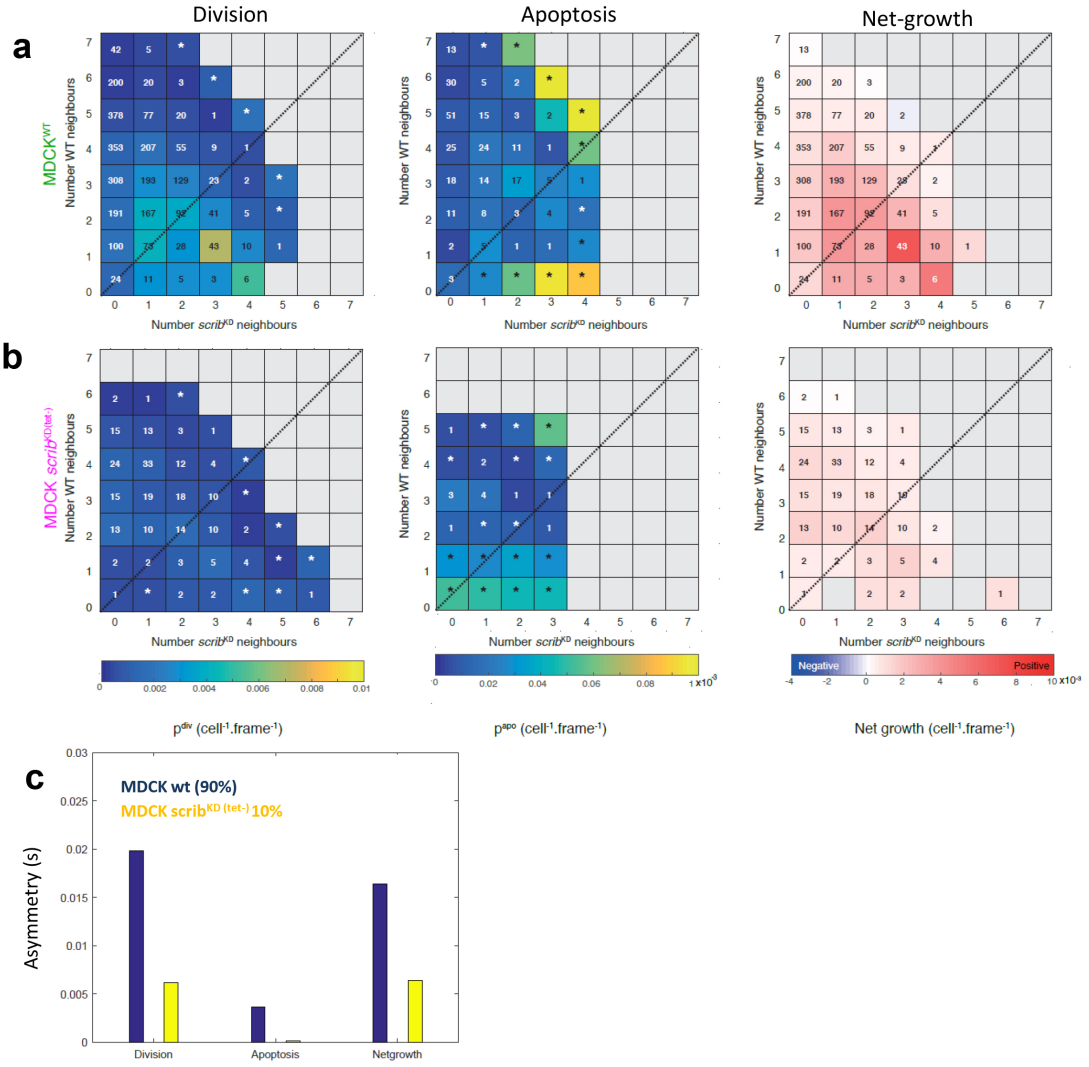

Figure 6.3: Probability of apoptosis, division and net growth are not affected by neighbourhood in the absence of tetracycline induction Neighbourhood plots showing the probability per cell per frame of division, apoptosis and net-growth for MDCK wt (a) and non-induced *scribble*^{kd} (b) co cultured in 90:10 ratio. The number of *scribble*^{kd} neighbours is shown on the x-axis and the number of MDCK wt neighbours is shown on the y-axis. The diagonal (black dashed line) indicates grid positions with equal numbers of green and red neighbours. Numbers in each grid position indicate the number of detected events (division or apoptosis). Measurements for each grid position are typically computed from observations of >500 cells. Grid positions for which many observations were made but no event detected are marked by an asterisk and coloured as 1/N observations to provide an upper-bound for the probability in that position. Data are pooled from 9 time-lapse movies from two biological replicates.(c) Asymmetry calculation performed neighbourhood plots in a and b. The parameter s defines whether the behaviour is cell-autonomous (low s values) or dependent on the cell type of neighbours (high s values).

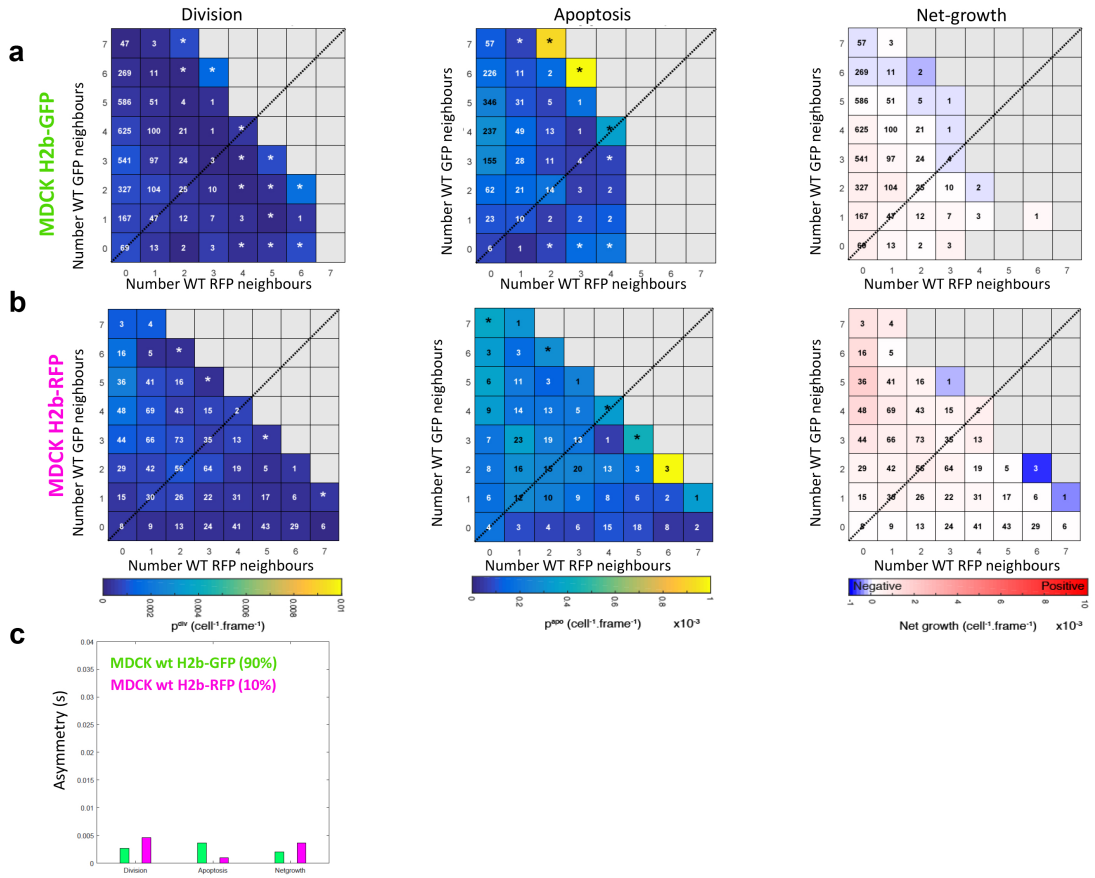

Figure 6.4: Probability of apoptosis, division and net growth are not affected by neighborhood for co-coltures of MDCK wt H2b-GFP admixed to MDCK wt H2b-RFP. Neighbourhood plots showing the colour coded probability per cell per frame of division, apoptosis and net-growth for MDCK wt labelled with H2b-GFP (a) and MDCK wt expressing H2b-RFP(b) when co-cultured in 90:10 ratio. The number of red neighbours is shown on the x-axis and the number of green neighbours is shown on the y-axis. The diagonal (black dashed line) indicates grid positions with equal numbers of green and red neighbours. Numbers in each grid position indicate the number of detected events (division or apoptosis). Measurements for each grid position are typically computed from observations of >500 cells. Grid positions for which many observations were made but no event detected are marked by an asterisk and coloured as 1/N observations to provide an upper-bound for the probability in that position. Data are pooled from 17 time-lapse movies from three biological replicates. (c) Calculation of asymmetry performed on neighbourhood plots shown in a-b. The asymmetry defines whether the behaviour is cell-autonomous (low s values) or dependent on the cell-type of neighbours (high s values).

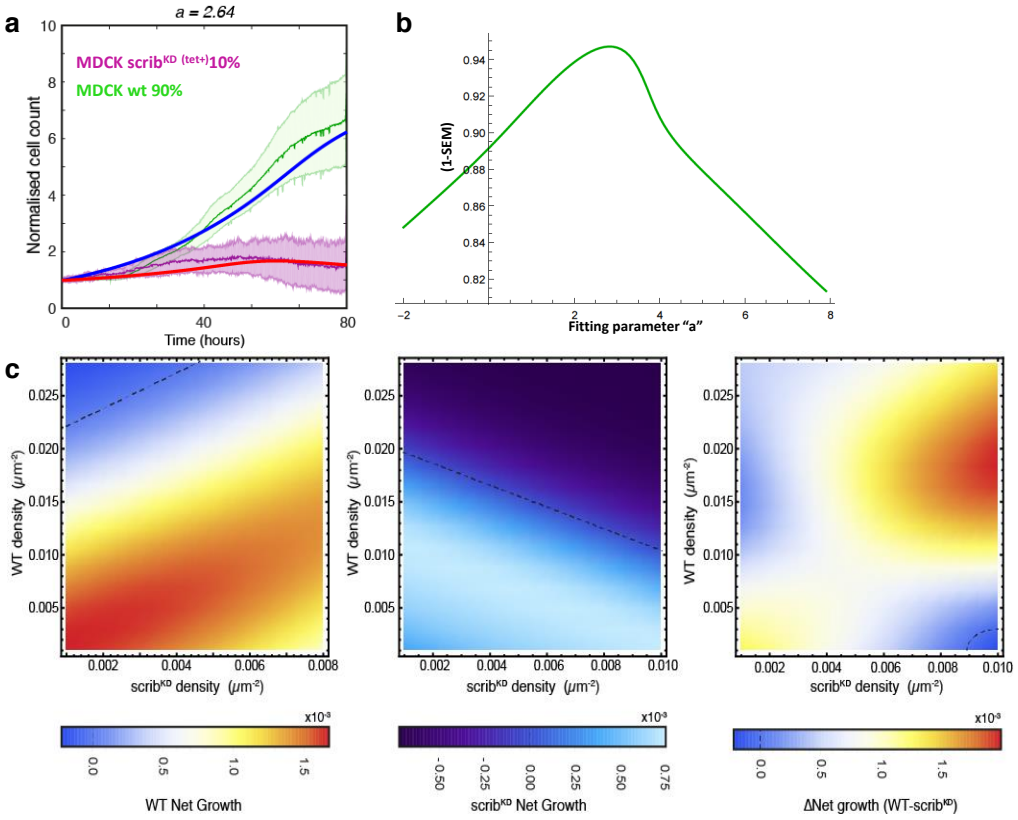

Figure 6.5: Asymmetric interaction model for cell competition (a) Temporal evolution of cell count predicted by the asymmetric interaction model (a=2.64) initialised with the mean experimental cell count at t=0 for MDCK wt (solid blue line) and *scribble*^{kd} (solid red line).(b) Error (1-Standard Error of Mean, S.E.M.) between numerical simulation and experimental data as function of the fitting parameter a. The model most accurately matches the experimental data for a=2.64. However, the broadness of the peak shows that the model outcome is not very sensitive to changes in a in the vicinity of 2.6.(c) Heat maps of net growth as a function of local density of MDCK wt cells on the y-axis and local density of *scribble*^{kd} cells on the x-axis for the asymmetric interaction model (a=2.64) for MDCK wt cells (left) and *scribble*^{kd} cells (middle). Warm colours indicate high net growths while cold colours indicate low net growths. Dashed line indicates the contour of zero net growth, or density homeostasis. Right: Relative fitness landscape for the asymmetric density dependent model (a=2.64), defined as the net growth of the MDCK wt cells minus the net growth of the *scribble*^{kd} cells. MDCK wt cells have a higher fitness than *scribble*^{kd} cells everywhere, except within the region delineated by the dashed line

.

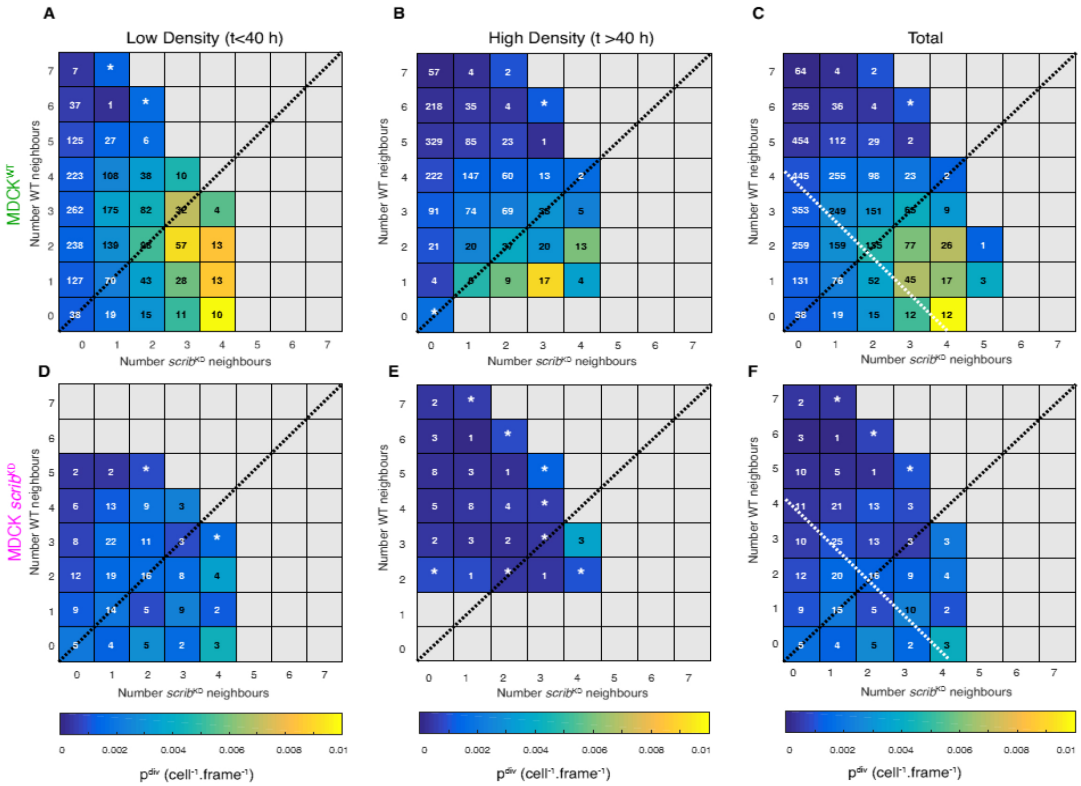

Figure 6.6: Time-resolved neighbourhood analysis Neighbourhood plots showing probability of division for MDCK wt (a, b) and *scribble*^{kd} (d,e). Data were split between low (t<40 h, a,d) and high (t>40 h, b,e) density; the resulting plots are displayed alongside with neighbourhood plots taking into account the whole duration of the experiment as shown in the original version of the manuscript (c,f). (a-f) The diagonal (black dashed line) indicates grid positions with equal numbers of MDCK wt and *scribble*^{kd} neighbours. (c,f) The white dashed line separates grid positions representative of the low density (lower quadrant) from those representative of high density (upper quadrant).

7 Development of cell assays for deciphering the role of micro-environment during cell competition

7.1 Influence of topology and seeding ratios on competition outcomes

Cell competition was initially thought to take place only at the interface between cell lineages; nevertheless, the discovery of mechanical competition revealed that direct contact is not necessary and that extrusion may take place several cell diameters away from this interface. For instance, mechanical competition was initially described as consequence of a fast growing population, compressing a slower growing one Levayer et al. (2016). In this hypothesis, when competition can arise several cell diameters away from the interface between the two populations, one would expect that cell density should be the single most important parameter. However, from the analysis I presented in this chapter, I was able to characterise induction of specific cell behaviours in both the $scribble^{kd}$ and the MDCK wt cell lineage, as a result of the contact with the other lineage. The experimental signature of scribble competition revealed a more sophisticated underlying mechanism than the sole dependence on density hypothesised for a mechanical competition. The evidence gathered and described so far showed how initial seeding density is a key parameter in scribble competition. All of the experiments I presented in the previous chapters were performed starting from identical initial conditions: the initial density of the cell suspension was 10^{-3} cells/μm^2 and the relative seeding density of MDCK wt and $scribble^{kd}$ lines was 90:10. In addition to this, the protocol I adopted for seeding mixtures of cells for competition assays robustly resulted in isolated, doublets or very small (up to 4 cells) clusters of $scribble^{kd}$ cells surrounded by MDCK wt cells. Therefore, in such configuration, the $scribble^{kd}$ cells mostly have interactions with the MDCK wt

neighbours since the beginning of the experiment. Topology was shown to have an important role in determining the outcomes of cell competition. Indeed in 2015, Levayer and colleagues Levayer et al. (2015) demonstrated that winner-loser cell mixing resulting from cell intercalation is crucial for promoting elimination of wild type cells by myc over-expressing clones. Increased surface of contact between winner and loser cells was shown to be the result of junction remodelling and preferential stabilization of winner-loser interfaces. Notably, shared surface between losers and winners correlated with the probability of elimination of loser cells in this "fitness fingerprint" model of cell competition Levayer et al. (2015). A larger surface of contact correlated with an increased probability of apoptosis. Therefore, to further characterise how cell behaviour is modulated by the fraction of cellular interactions and to gain more insight on the role of such interactions in the temporal evolution of cell population, I decided to investigate different experimental designs.

Firstly, I asked whether *scribble*^{kd} cells would be outcompeted by MDCK wt cells when changing the relative seeding ratio of the mixtures to be, respectively, 50:50 or 90:10 (Movies 6 and 7). These movies proved to be more difficult to analyse through the processing pipeline described in paragraph 3.3, due to the presence of GFP cytoplasmic fluorescence in the *scribble*^{kd} cells. Such cytoplasmic fluorescence was, indeed, hard to segment and distinguish from the nuclear fluorescence of MDCK wt cells. However, qualitative conclusions could be made; *scribble*^{kd} apoptosis was frequent and caused, in both 50:50 and 90:10 assays, a significant decrease of the population sizes. Strikingly, in such competitive environment, *scribble*^{kd} cells were not compacted by the MDCK wt cells. In contrast to the 90:10 condition, their surface area increased during the assay, similarly to what observed in pure *scribble*^{kd} (tet+) assays. To determine the experimental signatures in these competitive environments and compare them to the one characterised previously, Dr Lowe is developing deep learning tools that will enable this more complex segmentation. Therefore, by analysing growth and death rates, it will be possible to retrieve the rate of population evolution in the epithelium. Calculation of p^{div} p^{apo} as function of local cellular density, neighbourhood dependent apoptosis and division will help investigate the importance of density and the duration/extent of interactions needed for competition to occur, elucidating their role. It will also allow me to determine if competition in 50:50 or 10:90 occurs through different mechanisms than for 90:10 initial seeding densities. As discussed above, the topology produced from my seeding protocol was characterised by small clusters of *scribble*^{kd} cells surrounded by MDCK wt cells. This resulted in *scribble*^{kd} cells surrounded and sharing contact areas mainly with MDCK wt neighbours since the very first frames. According

to the results of Levayer et al, if 50% of interactions are not competitive (i.e. half of the neighbouring cells belong to the same lineage), then cells thrive and can escape competition Levayer et al. (2015). This suggests that colony shape plays a important role in survival. Therefore, an intriguing question to ask is if there are some colony shape and spatial arrangements able to promote survival of *scribble*^{kd} cells. To this extent, I developed an experimental assay where cells belonging to one lineage are present in well defined, 10-15 cell diameters large colonies, and are surrounded by the other lineage. To do so, I firstly seeded the non-induced *scribble*^{kd} cells very sparsely, and let them grow in clusters as epithelial cells typically do. Later, I seeded MDCK wt cells at high density to fill the empty space in between *scribble*^{kd} cells colonies. Furthermore, I induced *scribble*^{kd} cells one day prior imaging, with the addition of doxycycline. Such differential seeding protocol produced interesting cluster topology, with smooth boundaries, which have been suggested to favour survival (Figure 7.1). The *scribble*^{kd} cells maintained a compact morphology, reaching very high density within their colony (Figure 7.1 a). Such experiment allowed to detect where apoptosis occurred relative to the centre of the *scribble*^{kd} cells' colonies. For instance, from comparing the perimeter of colonies at the beginning (Figure 7.1 a) and at the end of the assay (Figure 7.1 b), it is evident that the areas most affected by apoptosis were close to the interfaces between the two cell populations. Colony boundaries retracted, as an effect of progressive cell death of *scribble*^{kd} starting from the edges. Space left empty by *scribble*^{kd} cell death was taken over by the MDCK wt cells. A rigorous single cell analysis will allow to detect any induced behaviour in which one of the physical/biological variables is altered by contact with competing cells. Furthermore, it will allow to investigate if the mechanism of competition is the same as in the 10:90 relative seeding scenario.

A topological configuration like the one displayed in (Figure 7.1) is suitable for a mechanical characterisation of the events happening within the tissue, with single cell resolution. The detection of regions where competition takes place can be performed by borrowing concepts from fluid dynamics. The movement of cells can, indeed, be approximated to a fluid flow on time-scales of hours. As each cell trajectory is known from image analysis, it is possible to determine the velocity field over the whole area of imaging and hence calculate the divergence in each region. A positive divergence indicates a local expansion in the fluid, which in a cell monolayer might be due to clonal expansion as during mechanical competition (Figure 7.1 d-e top). A negative divergence indicates a local contraction, which could be due to a cell extrusion event, or to removal of apoptotic bodies (Figure 7.1 d-e top). Performing experiments as illustrated in (Figure 7.1) enables focusing

on the dynamic interplay between MDCK wt and *scribble*^{kd} cells, combining the density dependence analysis of proliferation and death described previously with motion analysis. This will allow to show any potential role for collective behaviours of one of the cell lineages. Indeed, although mechanics has been hypothesized to play a crucial role in mechanical competition, little characterisation exists for lack of a good experimental and analytical system. Generation of neighbourhood plots of divergence will enable the detection of conditions in which mechanical competition occurs. Therefore, such information will complement the neighbourhood division and apoptosis dependence for combining physical and biological characterisation of the competitive environment.

7.2 Development of BioMEMs based techniques to use in competition assays

Tumours grow in conditions where space and nutrient availability tend to be limited Hanahan and Weinberg (2011). An intriguing follow up to this study is to evaluate the impact of micro-environmental conditions on cell lineages interactions, thus mimicking *in vitro* a more physiologically relevant scenario. To do so, new culture techniques are needed for controlling both geometrical confinement and biochemical environment (in particular the nutrient supply) during the competition assay. In recent years, micro-fabrication technologies have been extensively used to investigate fundamental question in cell biology, due to the several advantages offered in terms of geometry, surface chemistry and fluid control at micrometer scale. Therefore, during my PhD, I explored the biological application offered by micro-electromechanical based techniques (BioMEMs) to use in competition assays. Particularly, I designed and fabricated micro-patterned substrates (in collaboration with Dr Julien Gautrot, QMUL) that allow to mimick the physical confinement observed in tumours. To simulate spatial constraint, I confined cells in arenas of 400 μm diameter by covalently coupling PEG brushes to areas outside the arenas, where we want to prevent cell adhesion. The robustness and high chemical stability (during storage and cell culture conditions) of brushed-based micro-patterns made this technique the most suitable for long-term bioassays. Our preliminary data indicates that this successfully maintains confinement over more than 4 days (Figure 7.3 b). The set-up of competition assays in such devices offered the advantage of not having to worry about edge effects and cells escaping the FOV. Furthermore, it represents a condition where cells have an excess of nutrient availability. Indeed, the number of cells cultured in the dish is considerably lower compared to standard culture in Petri dishes (given the large portion of non adhesive area). Nevertheless, the

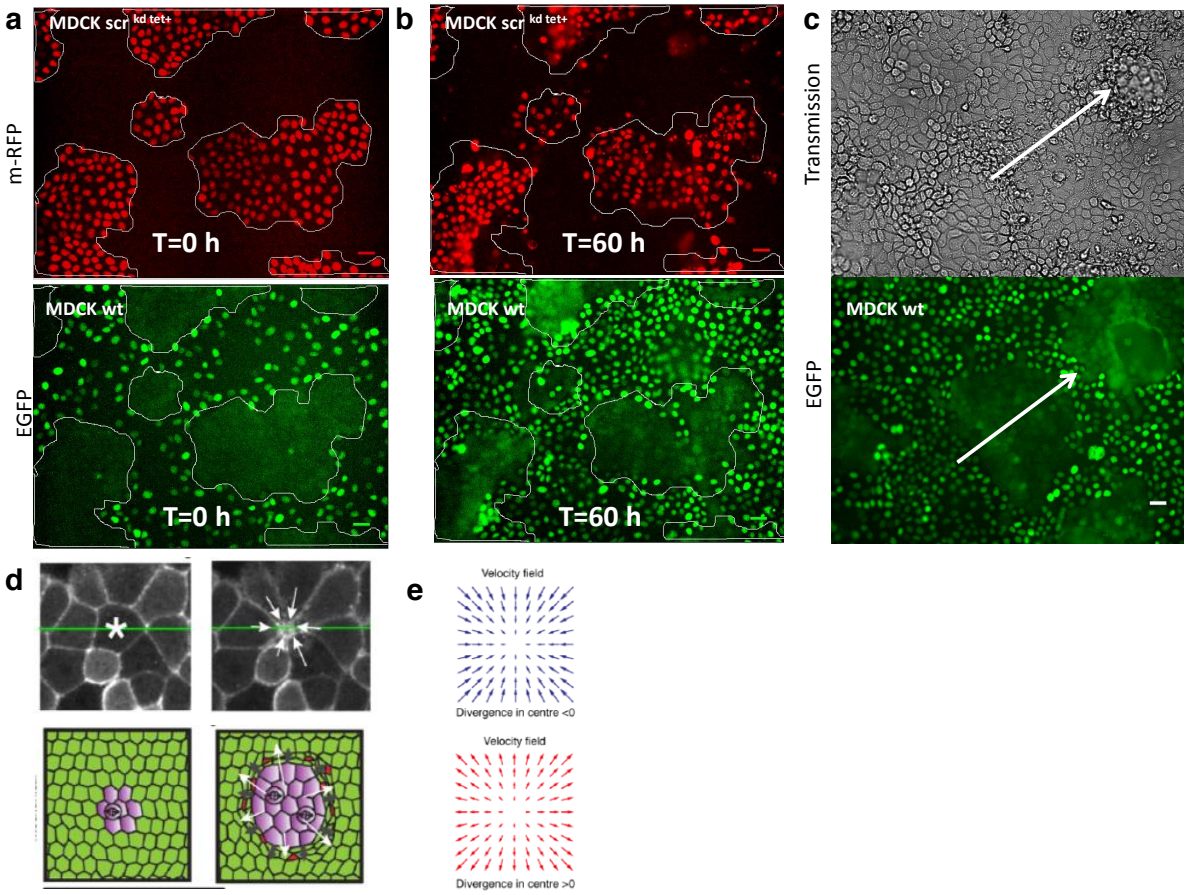

Figure 7.1: Assessing the influence of colony topology on cell competition. (a-b) m-RFP and EGFP images of *scribble*^{kd} (red) and MDCK wt (green) cells co-cultured by using a differential seeding protocol in order to obtain colonies of one cell lineage (in this case *scribble*^{kd}) with smooth boundaries. Apoptosis of *scribble*^{kd} at the interface within the two populations caused the colonies' area to decrease, while MDCK wt cells take over and expand (b). The *scribble*^{kd} maintained compact morphology and high density throughout the assay, as demonstrated by the constant area of the nuclei. Time indicating the start (t=0 h) and the end (t=60 h) of the time-lapse experiments are shown in a and b. (c) The MDCK wt also reached very high density, as demonstrated by the formation of blisters (white arrow). (d) Top: schematic diagram of cell extrusion event leading to inward movement of the neighbouring cells in the epithelial monolayer. Such local contraction is detected by negative divergence of the cell velocity field (e, top). Conversely, clonal expansion (d, bottom) of a lineage would be displayed by a positive divergence of the cell velocity field (e, bottom). (d) Image at the bottom was adapted from Levayer et al. (2016).

volume of culture medium provided is the same. To look more closely at the role of cell-cell interactions, I performed preliminary experiments on a different

micro-patterned geometry, where 1-2 cell diameters wide epithelial sheets are cultured on ring-shaped substrates (Figure 7.3 c). This situation provides a simplified one dimensional system, ideal to test hypotheses on induced behaviour due to cellular interactions.
Lastly, in order to determine the impact of nutrient limitations, I optimised cell culture in micro-fabricated culture chambers of 400-1000 μm in diameter and 40 μm in height based on previously published devices Hung et al. (2005), (Figure 7.2 a,c). Such microfluidic culture chamber offered the advantage of controlling the amount of nutrients available. Indeed, the limited height of the column of fluid provides an effective nutrient limitation. In this device, cells were seeded in each chamber through a seeding line. Once they adhered to the substrate, they were fed through a separate feeding line connected to a syringe pump (Figure 7.2 a). Feeding frequency was controlled by the image acquisition software. For instance, growth medium was replenished at chosen intervals. In my preliminary experiments, replenishing culture medium every 6 hours was sufficient to maintain healthy cell growth in the micro-wells (Figure 7.2 b). Conversely, cells died if medium was not replenished at least every 24h. This system enables to determine how interactions between competing cells are changed by micro-environmental conditions and drug/inhibitor treatments.

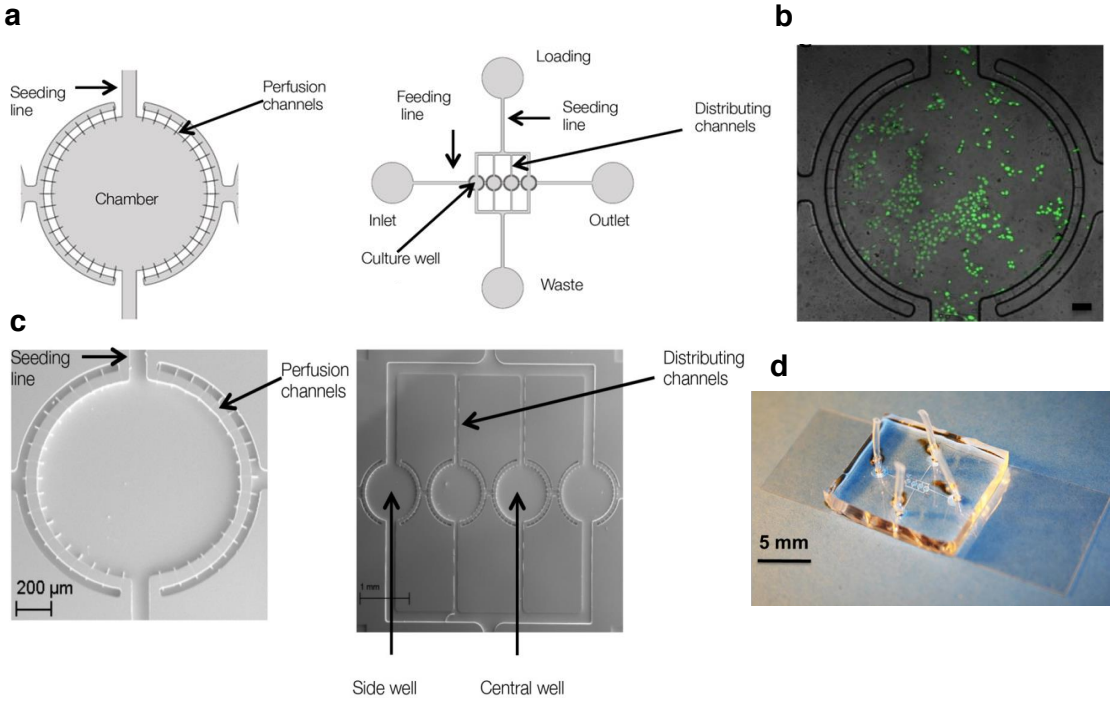

Figure 7.2: Microfluidic cell culture device for controlling the soluble environment. (a) Schematic of the microfluidic device for long term cell culture. Four cell culture chambers (each 1 mm diameter) are connected by two main fluidic channels (200 μm in width). The vertical seeding line is split into 4 distribution channels and used for injecting cells into the chambers. The horizontal feeding line carries the culture medium. Each chamber is surrounded by a polar array of narrow perfusion channels. (b) Representative composite image of a culture chamber seeded with MDCK wt cells. (c) SEM images of the silicon master used to cast the PDMS mould. Left: Detail showing a single cell culture chamber surrounded by the polar array of perfusion channels, used for feeding cells. Right: SEM image of the entire microfluidic platform, showing the four C-shape culture chamber wells and the distributing channels used for seeding cells into each chamber (black arrow). (d) Image of the fully assembled microfluidic device, where the PDMS culture chamber was bonded to a glass cover slip via plasma treatment.

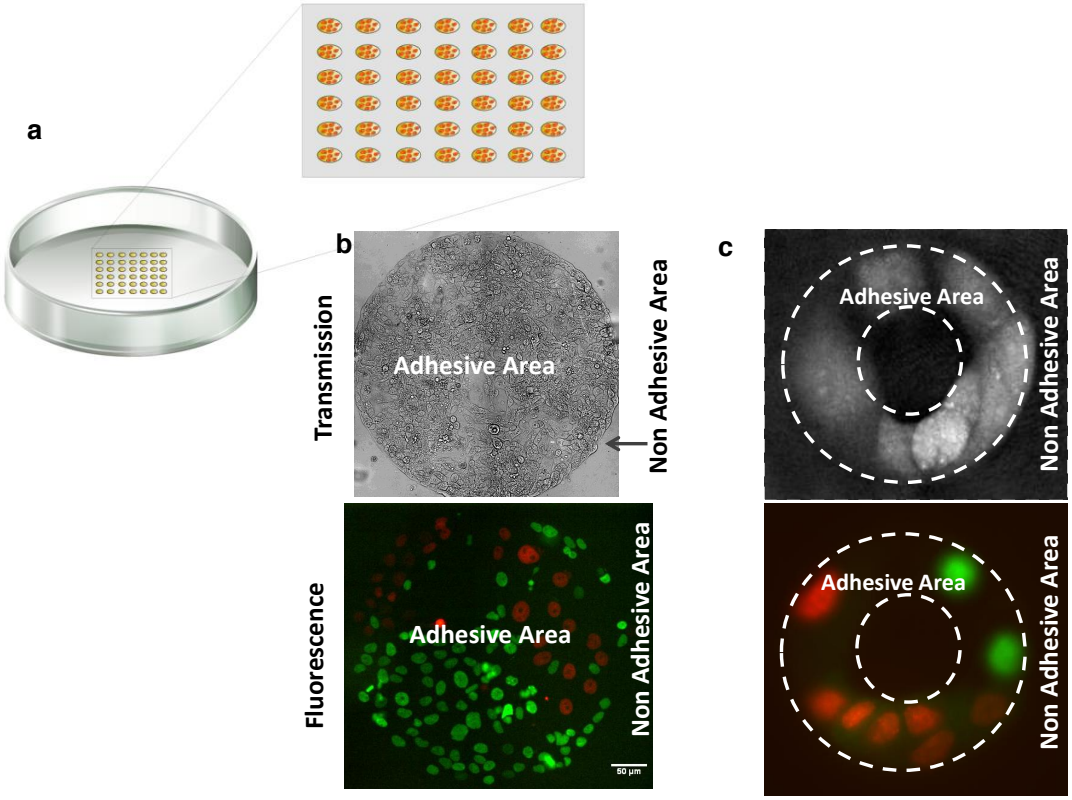

Figure 7.3: Micro patterning for developing cell competition assays under geometrical confinement (a) Schematic of a cell culture device assembled by gluing micro-patterned glass to the bottom of Petri-dishes. (b) Representative transmission (top) and fluorescence (bottom) images of competition assays performed by seeding MDCK wt and *scribble*^{kd} on the micro-patterned arenas. Cells adhere and grow only within the circular confined area. (c) Representative phase (top) and fluorescence (bottom) images of competition assays performed by seeding MDCK wt and *scribble*^{kd} cells on the micro-patterned rings substrate.

8 Final discussion

8.1 Summary of data presented

In this thesis, I presented results that highlight two dominant factors in scribble cell competition, that were not noticed in any previous study because of the qualitative nature of the analysis approaches utilised. First, I showed that the probability of division depends strongly on cell density (as would be expected for contact inhibition of proliferation) and that the probability of division is always several fold larger than that of apoptosis, except at the highest densities. Second, I showed that the probability of net growth of MDCK wt cells is highest in regions where they are in contact with $scribble^{kd}$ cells and that this effect is not caused by an increase in apoptosis of the $scribble^{kd}$ cells in that region of the diagram. I concluded that such effect was effectively driven by an increase in proliferation of MDCK wt cells in those regions. Most previous studies of competition concentrated on apoptosis; this results demonstrates that attention also needs to be paid to cell proliferation. Such observations were made possible by the unbiased approach in which analysis of cell competition was performed, with high-throughput at the single-cell level. I will now discuss the implication of such findings in the broader context of cell competition .

8.2 Is it correct to define cells depleted of scribble as loser cells?

The analysis of experimental data, supported by the computational model I presented, suggested an asymmetric density dependence for MDCK wt and $scribble^{kd}$ cells. Indeed, the numerical simulation (Figure 6.5) demonstrated that the $scribble^{kd}$ cells are equally influenced by the presence of cells of the same lineage (ρ_{kd}) and by interaction with other cell type neighbours (ρ_{wt}). Therefore, $scribble^{kd}$ cells proliferation and death is affected by the total cell density rather than the cell type. Mechanical competition postulated that the competing cell types have different sensitivities to density, with the cell type more tolerant to density (winners) growing to reach its homeostatic density. In doing so, winner

cells expose the less tolerant cell type to densities beyond its homeostatic density. This increased cell density is sufficient to cause increased apoptosis of the loser cells. In turn, the increased apoptosis allows the more tolerant cell type to grow further. Thus, it appears that each cell type is ignorant of the identity of its neighbours and only sensitive to changes in density. As the current definition of cell competition implies sensing of the other cell type in presence, one could argue that the elimination of $scribble^{kd}$ cells is not due to cell competition in the strictest sense and hence that it may not be correct to label them as loser cells. For instance, competition could take place between $scribble^{kd}$ cells that, for some reason, acquire different sensitivity to density. Indeed, Wagstaff et al demonstrated that it is possible to induce hypersensitivity to density by simply activating in a dose dependent manner the activity of p53 in wild type MDCK by addition of Nutlin-3 Wagstaff et al. (2016). This demonstrated that it is possible to induce the mechanical loser status only by increasing activity of p53.

The phenomenon of mechanical competition does need further characterisation to elucidate the exact role of cellular interactions. Investigations are needed, especially for finding more physiological occurrences of such phenomenon. In light of what discussed so far, the competition triggered by scribble depletion seems to perfectly fit in the definition of mechanical competition, as far as the behaviour of the $scribble^{kd}$ (loser) cells is concerned. As discussed in paragraph 6.6, the analysis of division probability as function of neighbourhood composition highlighted an important non cell-autonomous behaviour of MDCK wt cells. The increase in winner cells' proliferation induced by the presence of the loser cell type reveals a more subtle feature of scribble cell competition, which goes beyond the definition of mechanical competition given above. Indeed, the mitotic response of winner cells in the presence of loser cells indicates that these cells must sense the presence of neighbours with a different identity. Notably, such behaviour was not observed when they were surrounded by a comparable number of similar wild type neighbours. Further investigations are required to prove the existence of a similar unidirectional recognition (MDCK wt sensing the presence of $scribble^{kd}$ cells) and to establish what pro-mitotic factors are activated in MDCK wt cells when they come into contact with $scribble^{kd}$ (loser) cells. This could be done, for instance, by comparing the transcriptional profile of MDCK wt cells in contact with $scribble^{kd}$ cells with that of MDCK wt cells surrounded by wild type neighbours. Another possibility to address this question is to perform competition assay between $scribble^{kd}$ cells and MDCK cells stably expressing the Fucci sensor, which enables live monitoring cells transitioning from G1 to S phase during cell cycle progression Sakaue-Sawano et al. (2008). Furthermore,

the temporal sequence in which these events (apoptosis of losers and proliferation of winners) take place is another important feature to assess. This observation will be discussed in the following section.
Levayer and colleagues showed that, in Minute and Myc dependent competition (which are the best described examples of the fitness fingerprint model), the probability of elimination of loser cells correlates with the surface of contact shared with winner cells Levayer et al. (2015). Assessing this effect would contribute to delineate the complete signature of scribble competition which, from the considerations discussed so far, seems to lie in between the fitness fingerprint and the mechanical competition. In particular, a rigorous study of changes in actin organization and tension at the interface of loser-loser, winner-winner and loser-winner junctions needs to be performed. Coupling a similar analysis with the neighbourhood plots on the experimental data I collected could help tackle the unanswered question of whether the morphology and the amount of surface contact shared between losers and winner have a role in determining the outcome of cell competition. Indeed, if winner-loser interface morphology plays a role, one would expect to see different outcomes when comparing results from experiments where relative seeding density and topology arrangement of competing lines are changed, as illustrated in paragraph 7.1.

8.3 Importance of determining the temporal sequence in which loser cells' apoptosis and winner cells' proliferation events occur

Investigating the causality relationship between death of $scribble^{kd}$ cells and proliferation of MDCK wt cells during competition is of great importance to define the nature of winner-loser interactions. As illustrated in section 6.6, different alternative hypotheses can justify the increased proliferation of MDCK wt cells in the presence of $scribble^{kd}$ cells: (i) a compensatory mechanism triggered by apoptosis of losers, either active or passive or (ii) winner-loser recognition signals and induction of division by contact with loser cells. In addition, recent work demonstrated a third possible mechanism to explain the winner cells' proliferation in Minute-induced competition in the *Drosophila melanogaster* wing disc model Kucinski et al. (2017). Particularly, Kucinski and co-workers found that JAK/STAT signalling, a conserved cytokine signalling pathway that can promote growth Zeidler et al. (2000), was involved in such non cell-autonomous proliferation. They showed that this happened via secretion of a specific ligand, a soluble pro-mitotic signal produced by loser cells prior to their apoptosis. Such signal

is, indeed, responsible for promoting growth of loser cell type but, at the same time, it stimulates the proliferation of winner cells. Notably, winner cells have higher responses than losers to such signals. Therefore, in this case, proliferation of winner cells is independent from both winner-loser interactions or losers cell death Kucinski et al. (2017). This possibility could be tested by culturing cells under constant flow conditions in micro-fluidic devices (Figure 7.2).
A first, straightforward approach to address this question is to block the apoptosis of $scribble^{kd}$ cells, to see if this affects the proliferation of MDCK wt cells. Norman and collaborators showed that the pan-caspase inhibitor Z-VAD-FMK does not prevent apoptosis of $scribble^{kd}$ during competition Norman et al. (2011). Indeed, later work of Wagstaff et al showed that the apoptosis of $scribble^{kd}$ is mediated by p53 activation. The involvement of p53 in triggering apoptosis of $scribble^{kd}$ cells is consistent with previous reports displaying Bac and Bax activation in dying $scribble^{kd}$ cells Norman et al. (2011). Such pro-apoptotic proteins, together with the p53 protein, were demonstrated to be transported into the mitochondria, where they cause an increase in the permeability of mitochondrial membranes. This, in turn, induces the release of cytochrome c, which is responsible for the assembly of the "apoptosome" complex Wawryk-Gawda et al. (2014). Once this complex is formed, it activates the group of effector caspases. Altogether, these considerations explained the inefficacy of pan-caspase to block apoptosis in $scribble^{kd}$ loser cells. Furthermore, Z-VAD-FMK does not efficiently inhibit the activity of some caspases (i.e. capsase 2 and 4) Chauvier et al. (2007), which are activated downstream of p53 signalling. Wagstaff and colleagues demonstrated that it was possible to block the apoptosis of $scribble^{kd}$ cells by addition of a chemical inhibitor of p53, pifithrin-α Wagstaff et al. (2016). Hence, by performing competition assay between induced $scribble^{kd}$ cells and MDCK wt in the presence of such drug, one would expect to rescue the loser phenotype and prevent their elimination from the monolayer. Therefore, the analysis of division neighbourhood plots of such experiments should reveal if the increased proliferation of winner cells still occurs. If the MDCK wt cells continue proliferating faster in the presence of viable $scribble^{kd}$ cells, the existence of winner-loser recognition signals will need to be explored, as hypothesised in (ii). Conversely, a symmetric division neighbourhood plot would suggest that the behaviour of MDCK wt was due to a compensatory mechanism triggered by apoptosis of loser cells (i).

In addition to this preliminary experiment, a better understanding of the process would be gained by investigating the temporal sequence in which both losers and winners commit to their fate (either cell death or division). For instance, the commitment of MDCK wt cells to division could be monitored by using a

stable cell line expressing the Fucci sensor Sakaue-Sawano et al. (2008), which enables live monitoring of cell cycle transitions from G1 to S phase. The decision of *scribble*^{kd} cells to commit to apoptosis could be detected by monitoring the oscillations of expression of p53 and its negative regulator Mdm2 Lahav et al. (2004). Indeed, previous reports demonstrated the existence of a feedback loop system for DNA damage repair, where p53 oscillations are observed in a series of discrete pulses, with the mean number of pulses increasing according to the DNA damage. Hence, by performing competition experiments between MDCK wt Fucci and MDCK *scribble*^{kd} cells stably expressing fluorescent p53, I envisage it will be possible to gain more insight into the characterisation of winner-loser interactions.

8.4 Computational model for cellular interactions

To aid interpretation and design of the experimental assays, I collaborated with Daniel Gradeci, a PhD student in the Charras lab, in developing a computational model of cellular interactions. The quantitative model described in section 5.8 was of great help for disentangling the non-autonomous behaviour of competing MDCK wt cells. Nevertheless, such a model ignores several aspects of the experiments, for instance any physical and chemical information relative to cellular interactions. Therefore, a long term objective is to develop a cellularised model that will consist of several computational layers for simulating: i) physical interactions between cells, ii) reaction-diffusion in the medium, and iii) cell decision making. Physical interactions between cells will be simulated using a cellular Potts model, which determines how the shape of each cell in the epithelium evolves based on its intercellular adhesion energy, contractility, and cell elasticity. Such parameters could be experimentally calibrated via E-Cadherin (as a proxy for adhesion energy) and phospho-MLC (as a proxy for contractility) Western blotting. In a separate layer, reaction-diffusion within the model area will be simulated to investigate potential roles for competition for capture of growth factors, nutrients, or drugs (Figure 8.1). Finally, in the decision making layer, a game theory approach will be implemented to model local decision-making (Figure 8.1); these properties make it ideal to model the evolution of the population.

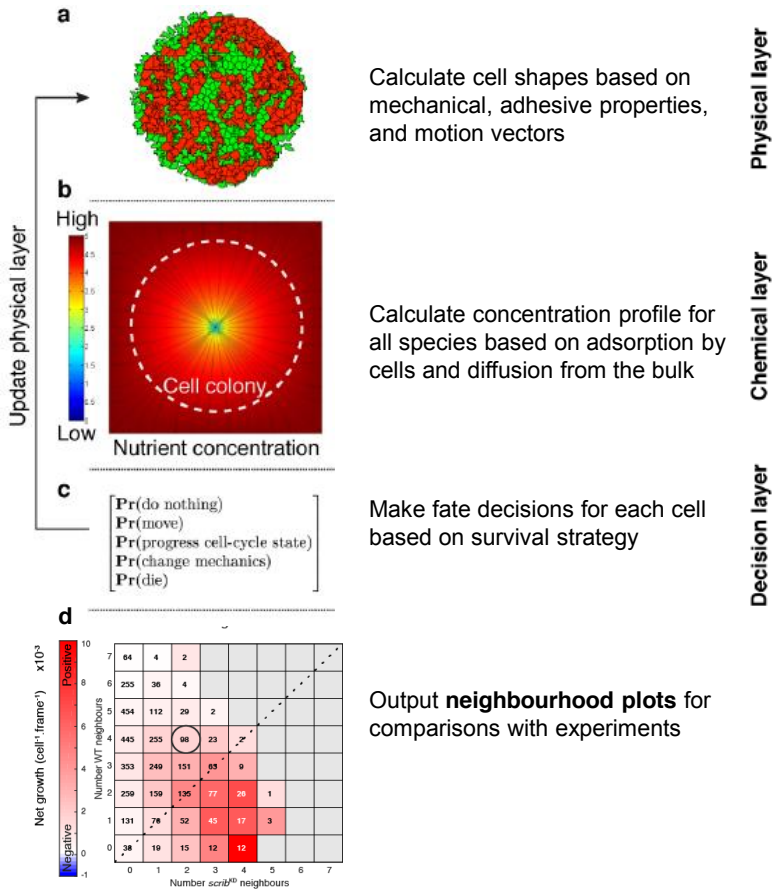

Figure 8.1: Computational model for cellular interactions The model will consist of several computational layers that will simulate: i) physical interactions between cells, ii) reaction-diffusion in the medium, and iii) cell decision making. The model will be calibrated layer-wise. Parameters determining the physical layer will initially be inferred from homogenous populations but, in the case of non-autonomous behaviours, they may change at the interface between two cell lineages. The reaction-diffusion layer will be parametrized using published diffusion constants for growth factors/nutrients/drugs.

8.5 Importance of the elimination of scribble-depleted cells for early stages of tumourigenesis

In this thesis, I have discussed the role of scribble as a tumour suppressor protein. The involvement of scribble in the phenomenon of cell competition supports the theory of competition as a defence mechanism against the spreading of dangerous, pre-cancerous cells. It appears, indeed, that the loss of scribble protein

in one cell within a normal epithelium cannot trigger, by itself, the first stage of tumourigenesis. The induction of apoptosis in the scribble-depleted cell would prevent any further tumourigenesis. This observation is consistent with the notion that scribble depletion causes an increase in the levels of p53, a well known tumour suppressor gene and a general sensor of cell stress. Therefore, it appears that the loss of expression of one important tumour-suppressor (scribble) is compensated by increased expression of another tumour-suppressor protein (p53), which has an important role in initiating apoptosis in damaged cells. For the cancer to develop, the acquisition of resistance to cell death is an essential pre-requisite for transformed cells to have Hanahan and Weinberg (2011), which is not met by the $scribble^{kd}$ cells. In section 1.6.2, I also mentioned the emergence of experimental evidence showing the cooperation of scribble with other oncogenes. In such circumstances, loss of scribble was demonstrated to enhance the tumourigenic ability of the transformed cells Zhan et al. (2011). When loss of scribble is induced in cells already transformed and over-expressing Myc, such cells acquire the ability to escape apoptosis, allowing for the proliferation and spreading of the myc phenotype. The block of apoptosis and enhancement of tumourigenesis produced by cooperation of scribble down-regulation and Myc over expression was demonstrated both in 3D cultures of human epithelial cells and in murine cancer models. The study of the interactions between similar double mutants with wild type cells by means of the single-cell approach described in this thesis would be of great interest for understanding the role of competing interactions in a more physiologically relevant setting.

Bibliography

Al-Kofahi, O., Radke, R. J., Goderie, S. K., Shen, Q., Temple, S., and Roysam, B. (2006). Automated cell lineage construction: A rapid method to analyze clonal development established with murine neural progenitor cells. *Cell Cycle*, 5(3):327–335.

Amoyel, M. and Bach, E. a. (2014). Cell competition: how to eliminate your neighbours. *Development*, 141(5):988–1000.

Atala, A. (2012). Re: Collective and single cell behavior in epithelial contact inhibition. *J. Urol.*, 188(4):1396–1397.

Avgustinova, A., Iravani, M., Robertson, D., Fearns, A., Gao, Q., Klingbeil, P., Hanby, A. M., Speirs, V., Sahai, E., Calvo, F., and Isacke, C. M. (2016). Tumour cell-derived Wnt7a recruits and activates fibroblasts to promote tumour aggressiveness. *Nat. Commun.*, 7:1–14.

Barber, C. B., Dobkin, D. P., and Huhdanpaa, H. (1996). The quickhull algorithm for convex hulls. *ACM Trans. Math. Softw.*, 22(4):469–483.

Bilder, D. (2004). Epithelial polarity and proliferation control: Links from the Drosophila neoplastictumor suppressors. *Genes Dev.*, 18(16):1909–1925.

Bilder, D. and Perrimon, N. (2000). Localization of apical epithelial determinants by the basolateral PDZ protein Scribble. *Nature*, 403(6770):676–680.

Bishop, C. M. (2013). *Pattern Recognition and Machine Learning*, volume 53.

Bondar, Tanya, R. M. (2010). P53-Mediated Hematopoietic Stem and Progenitor Cell Competition. *October*, 6(4):309–322.

Bove, A., Gradeci, D., Fujita, Y., Banerjee, S., Charras, G., and Lowe, A. R. (2017). Local cellular neighbourhood controls proliferation in cell competition. *Mol. Biol. Cell*, 28:mbc.E17–06–0368.

Brumby, A. M. and Richardson, H. E. (2003). scribble mutants cooperate with oncogenic Ras or Notch to cause neoplastic overgrowth in Drosophila. *EMBO J.*, 22(21):5769–5779.

Burke, R. and Basler, K. (1996). Dpp receptors are autonomously required for cell proliferation in the entire developing Drosophila wing. *Development*, 122:000–000.

Campbell, L. L. and Polyak, K. (2007). Breast tumor heterogeneity: Cancer stem cells or clonal evolution? *Cell Cycle*, 6(19):2332–2338.

Charles, N., Ozawa, T., Squatrito, M., Bleau, A. M., Brennan, C. W., Hambardzumyan, D., and Holland, E. C. (2010). Perivascular Nitric Oxide Activates Notch Signaling and Promotes Stem-like Character in PDGF-Induced Glioma Cells. *Cell Stem Cell*, 6(2):141–152.

Chauvier, D., Ankri, S., Charriaut-Marlangue, C., Casimir, R., and Jacotot, E. (2007). Broad-spectrum caspase inhibitors: From myth to reality? [5]. *Cell Death Differ.*, 14(2):387–391.

Chen, C.-L., Schroeder, M. C., Kango-Singh, M., Tao, C., and Halder, G. (2012). Tumor suppression by cell competition through regulation of the Hippo pathway. *Proc. Natl. Acad. Sci.*, 109(2):484–489.

Conrad, C. and Gerlich, D. W. (2010). Automated microscopy for high-content RNAi screening. *J. Cell Biol.*, 188(4):453–461.

Cova, C. D., Abril, M., Bellosta, P., Gallant, P., Johnston, L. A., and Street, W. (2004). Size by Inducing Cell Competition. 117:107–116.

de la Cova, Claire and Johnston, L. A. (2010). Myc in model organisms : A view from the flyroom. 16(4):303–312.

Dow, L. E., Brumby, A. M., Muratore, R., Coombe, M. L., Sedelies, K. A., Trapani, J. A., Russell, S. M., Richardson, H. E., and Humbert, P. O. (2003). hScrib is a functional homologue of the Drosophila tumour suppressor Scribble. *Oncogene*, 22(58):9225–9230.

Fang, D., Nguyen, T. K., Leishear, K., Finko, R., Kulp, A. N., Hotz, S., Van Belle, P. A., Xu, X., Elder, D. E., and Herlyn, M. (2005). A tumorigenic subpopulation with stem cell properties in melanomas. *Cancer Res.*, 65(20):9328–9337.

Fidler, I. J. (2016). Tumor Heterogeneity and the Biology of Cancer Invasion and Metastasis. *Cancer Res.*, 38(September):2651–2660.

Fridman, J. S. and Lowe, S. W. (2003). Control of apoptosis by p53. *Oncogene*, 22(56 REV. ISS. 8):9030–9040.

Garvey, C. M., Spiller, E., Lindsay, D., Chiang, C.-T., Choi, N. C., Agus, D. B., Mallick, P., Foo, J., and Mumenthaler, S. M. (2016). A high-content image-based method for quantitatively studying context-dependent cell population dynamics. *Sci. Rep.*, 6(February):29752.

Gudipaty, S. A., Lindblom, J., Loftus, P. D., Redd, M. J., Edes, K., Davey, C. F., Krishnegowda, V., and Rosenblatt, J. (2017). Mechanical stretch triggers rapid epithelial cell division through Piezo1. *Nature*, 543(7643):118–121.

Hanahan, D. and Weinberg, R. A. (2011). Hallmarks of cancer: The next generation.

Hastie, T., Tibshirani, R., and Friedman, J. (2001). The Elements of Statistical Learning. *Math. Intell.*, 27(2):83–85.

Held, M., Schmitz, M. H. a., Fischer, B., Walter, T., Neumann, B., Olma, M. H., Peter, M., Ellenberg, J., and Gerlich, D. W. (2010). CellCognition: time-resolved phenotype annotation in high-throughput live cell imaging. *Nat. Methods*, 7(9):747–54.

Heppner, G.-a. (1984). Tumor Heterogeneity. (June):2259–2265.

Hill, R. P. (2006). Identifying cancer stem cells in solid tumors: Case not proven. *Cancer Res.*, 66(4):1891–1896.

Hillen, W. and Berens, C. (1994). EXPRESSION OF TNIO Wolfgang Hillen and Christian Berens. *Annu. Rev. Microbiol.*, 48:345–69.

Hogan, C., Dupré-Crochet, S., Norman, M., Kajita, M., Zimmermann, C., Pelling, A. E., Piddini, E., Baena-López, L. A., Vincent, J. P., Itoh, Y., Hosoya, H., Pichaud, F., and Fujita, Y. (2009). Characterization of the interface between normal and transformed epithelial cells. *Nat. Cell Biol.*, 11(4):460–467.

Hogan, C., Kajita, M., Lawrenson, K., and Fujita, Y. (2011). Interactions between normal and transformed epithelial cells: Their contributions to tumourigenesis. *Int. J. Biochem. Cell Biol.*, 43(4):496–503.

Humbert, P. O., Grzeschik, N. a., Brumby, a. M., Galea, R., Elsum, I., and Richardson, H. E. (2008). Control of tumourigenesis by the Scribble/Dlg/Lgl polarity module. *Oncogene*, 27(55):6888–6907.

Hung, P. J., Lee, P. J., Sabounchi, P., Lin, R., and Lee, L. P. (2005). Continuous perfusion microfluidic cell culture array for high-throughput cell-based assays. *Biotechnol. Bioeng.*, 89(1):1–8.

Hunter, T. and Sefton, B. M. (1980). Transforming gene product of Rous sarcoma virus phosphorylates tyrosine. *Proc. Natl. Acad. Sci. U. S. A.*, 77(3):1311–1315.

Igaki, T., Kanda, H., Yamamoto-Goto, Y., Kanuka, H., Kuranaga, E., Aigaki, T., and Miura, M. (2002). Eiger, a TNF superfamily ligand that triggers the Drosophila JNK pathway. *EMBO J.*, 21(12):3009–3018.

Joyce, J. a. and Pollard, J. W. (2009). Microenvironmental regulation of metastasis. *Nat. Rev. Cancer*, 9(4):239–52.

Kajita, M., Hogan, C., Harris, A. R., Dupre-Crochet, S., Itasaki, N., Kawakami, K., Charras, G., Tada, M., and Fujita, Y. (2010). Interaction with surrounding normal epithelial cells influences signalling pathways and behaviour of Src-transformed cells. *J. Cell Sci.*, 123(2):171–180.

Karnoub, A. E. and Weinberg, R. A. (2008). Ras oncogenes: Split personalities. *Nat. Rev. Mol. Cell Biol.*, 9(7):517–531.

Klezovitch, O., Fernandez, T. E., Tapscott, S. J., and Vasioukhin, V. (2004). Loss of cell polarity causes severe brain dysplasia in. *Genes Dev.*, pages 559–571.

Klímek, M. (1962). Effect of lethally irradiated cells on the development of new-born rats. *Nature*, 193(4819):996–997.

Kourou, K., Exarchos, T. P., Exarchos, K. P., Karamouzis, M. V., and Fotiadis, D. I. (2015). Machine learning applications in cancer prognosis and prediction. *Comput. Struct. Biotechnol. J.*, 13:8–17.

Kucinski, I., Dinan, M., Kolahgar, G., and Piddini, E. (2017). Chronic activation of JNK JAK/STAT and oxidative stress signalling causes the loser cell status. *Nat. Commun.*, 8(1).

Kurada, P. and White, K. (1998). Ras promotes cell survival in Drosophila by downregulating hid expression. *Cell*, 95(3):319–329.

Lahav, G., Rosenfeld, N., Sigal, A., Geva-Zatorsky, N., Levine, A. J., Elowitz, M. B., and Alon, U. (2004). Dynamics of the p53-Mdm2 feedback loop in individual cells. *Nat. Genet.*, 36(2):147–150.

Lapidot, T., Sirard, C., Vormoor, J., Murdoch, B., Hoang, T., Caceres-Cortes, J., Minden, M., Paterson, B., Caligiuri, M. A., and Dick, J. E. (1994). A cell initiating human acute myeloid leukaemia after transplantation into SCID mice. *Nature*, 367(6464):645–648.

Levayer, R., Dupont, C., Levayer, R., Dupont, C., and Moreno, E. (2016). Tissue Crowding Induces Caspase-Dependent Competition for Space. *Curr. Biol.*, 26(5):1–8.

Levayer, R., Hauert, B., and Moreno, E. (2015). Cell mixing induced by myc is required for competitive tissue invasion and destruction. *Nature*, 524(7566):476–480.

Levayer, R. and Moreno, E. (2013). Mechanisms of cell competition: themes and variations. *J. Cell Biol.*, 200(6):689–98.

M., W. (2009). NIH Public Access. 39(11):1582–1589.

Martin-Belmonte, F. and Perez-Moreno, M. (2012). Epithelial cell polarity, stem cells and cancer. *Nat. Rev. Cancer*, 12(1):23–38.

Mcallister, S. S. and Weinberg, R. A. (2014). The tumour-induced systemic environment as a critical regulator of cancer progression and metastasis. 16(8):717–727.

Mcmahon, T., Zijl, P. C. M. V., and Gilad, A. A. (2015). NIH Public Access. 27(3):320–331.

Merino, M. M., Rhiner, C., Lopez-Gay, J. M., Buechel, D., Hauert, B., and Moreno, E. (2015). Elimination of unfit cells maintains tissue health and prolongs lifespan. *Cell*, 160(3).

Michor, F. and Polyak, K. (2010). The origins and implications of intratumor heterogeneity. *Cancer Prev. Res.*, 3(11):1361–1364.

Morata, G. and Ripoll, P. (1975). Minutes: Mutants of Drosophila autonomously affecting cell division rate. *Dev. Biol.*, 42(2):211–221.

Moreno, E. (2008). Is cell competition relevant to cancer? *Nat. Rev. Cancer*, 8(2):141–7.

Moreno, E., Basler, K., and Morata, G. (2002). Cells compete for decapentaplegic survival factor to prevent apoptosis in Drosophila wing development. *Nature*, 416(6882):755–759.

Moreno, E., Basler, K., and Zu, C. (2004). dMyc Transforms Cells into Super-Competitors. 117:117–129.

Nagasaka, K., Nakagawa, S., Yano, T., Takizawa, S., Matsumoto, Y., Tsuruga, T., Nakagawa, K., Minaguchi, T., Oda, K., Hiraike-Wada, O., Ooishi, H., Yasugi, T., and Taketani, Y. (2006). Human homolog of Drosophila tumor suppressor Scribble negatively regulates cell-cycle progression from G1 to S phase by localizing at the basolateral membrane in epithelial cells. *Cancer Sci.*, 97(11):1217–1225.

Nagasaka, K., Pim, D., Massimi, P., Thomas, M., Tomaić, V., Subbaiah, V. K., Kranjec, C., Nakagawa, S., Yano, T., Taketani, Y., Myers, M., and Banks, L. (2010). The cell polarity regulator hScrib controls ERK activation through a KIM site-dependent interaction. *Oncogene*, 29(38):5311–5321.

Nakagawa, S. and Huibregtse, J. M. (2000). Human scribble (Vartul) is targeted for ubiquitin-mediated degradation by the high-risk papillomavirus E6 proteins and the E6AP ubiquitin-protein ligase. *Mol. Cell. Biol.*, 20(21):8244–8253.

Navarro, C., Nola, S., Audebert, S., Santoni, M.-J., Arsanto, J.-P., Ginestier, C., Marchetto, S., Jacquemier, J., Isnardon, D., Le Bivic, A., Birnbaum, D., and Borg, J.-P. (2005). Junctional recruitment of mammalian Scribble relies on E-cadherin engagement. *Oncogene*, 24(27):4330–9.

Navin, N., Kendall, J., Troge, J., Andrews, P., Rodgers, L., McIndoo, J., Cook, K., Stepansky, A., Levy, D., Esposito, D., Muthuswamy, L., Krasnitz, A., McCombie, W. R., Hicks, J., and Wigler, M. (2011). Tumour evolution inferred by single-cell sequencing. *Nature*, 472(7341):90–95.

Naylor, T. L., Greshock, J., Wang, Y., Colligon, T., Yu, Q., Clemmer, V., Zaks, T. Z., and Weber, B. L. (2005). High resolution genomic analysis of sporadic breast cancer using array-based comparative genomic hybridization. *Breast Cancer Res.*, 7(6):R1186.

Norman, M., Wisniewska, K. A., Lawrenson, K., Garcia-miranda, P., Tada, M., Kajita, M., Mano, H., Ishikawa, S., Ikegawa, M., and Shimada, T. (2011). Loss of Scribble causes cell competition in mammalian cells.

Oliver, E. R., Saunders, T. L., Tarlé, S. a., and Glaser, T. (2004). Ribosomal protein L24 defect in belly spot and tail (Bst), a mouse Minute. *Development*, 131(16):3907–3920.

Portela, M., Casas-Tinto, S., Rhiner, C., López-Gay, J. M., Domínguez, O., Soldini, D., and Moreno, E. (2010). Drosophila SPARC is a self-protective signal expressed by loser cells during cell competition. *Dev. Cell*, 19(4):562–573.

Prince, D. S. J. D. (2013). *January 2013*, volume 12.

Qin, Y., Capaldo, C., Gumbiner, B. M., and Macara, I. G. (2005). The mammalian Scribble polarity protein regulates epithelial cell adhesion and migration through E-cadherin. *J. Cell Biol.*, 171(6):1061–1071.

Rhiner, C., López-Gay, J. M., Soldini, D., Casas-Tinto, S., Martín, F. A., Lombardía, L., and Moreno, E. (2010). Flower forms an extracellular code that reveals the fitness of a cell to its neighbors in Drosophila. *Dev. Cell*, 18(6):985–998.

Rodrigues, A. B., Zoranovic, T., Ayala-Camargo, A., Grewal, S., Reyes-Robles, T., Krasny, M., Wu, D. C., Johnston, L. A., and Bach, E. A. (2012). Activated STAT regulates growth and induces competitive interactions independently of Myc, Yorkie, Wingless and ribosome biogenesis. *Development*, 139(21):4051–4061.

Rosenblatt, J., Raff, M. C., and Cramer, L. P. (2001). An epithelial cell destined for apoptosis signals its neighbors to extrude it by an actin- and myosin-dependent mechanism. *Curr. Biol.*, 11(23):1847–1857.

Rubin, H. (2011). Fields and field cancerization: The preneoplastic origins of cancer: Asymptomatic hyperplastic fields are precursors of neoplasia, and their progression to tumors can be tracked by saturation density in culture. *BioEssays*, 33(3):224–231.

Ryoo, H. D., Gorenc, T., and Steller, H. (2004). Apoptotic cells can induce compensatory cell proliferation through the JNK and the wingless signaling pathways. *Dev. Cell*, 7(4):491–501.

Sakaue-Sawano, A., Kurokawa, H., Morimura, T., Hanyu, A., Hama, H., Osawa, H., Kashiwagi, S., Fukami, K., Miyata, T., Miyoshi, H., Imamura, T., Ogawa, M., Masai, H., and Miyawaki, A. (2008). Visualizing Spatiotemporal Dynamics of Multicellular Cell-Cycle Progression. *Cell*, 132(3):487–498.

SangWun Kim, JaeWook Kim, Young Tae Kim,* Jae Hoon Kim, Sunghoon Kim, Bo Sung Yoon, E. J. N. and Kim, H. Y. (2007). Analysis of Chromosomal Changes in Serous Ovarian Carcinoma Using High-Resolution Array Comparative Genomic Hybridization: Potential Predictive Markers of Chemoresistant Disease. *Genes. Chromosomes Cancer*, 46(April):1–9.

Simpson, P. and Morata, G. (1981). Differential mitotic rates and patterns of growth in compartments in the Drosophila wing. *Dev. Biol.*, 85(2):299–308.

Singh, S. K., Clarke, I. D., Terasaki, M., Bonn, V. E., Hawkins, C., Squire, J., and Dirks, P. B. (2003). Identification of a cancer stem cell in human brain tumors. *Cancer Res.*, 63(18):5821–5828.

Sommer, C. and Gerlich, D. W. (2013). Machine learning in cell biology âĂŞ teaching computers to recognize phenotypes. *J. Cell Sci.*, 126(24):5529–5539.

Sottoriva, A., Kang, H., Ma, Z., Graham, T. A., Salomon, M. P., Zhao, J., Marjoram, P., Siegmund, K., Press, M. F., Shibata, D., and Curtis, C. (2015). A big bang model of human colorectal tumor growth. *Nat. Genet.*, 47(3):209–216.

Sottoriva, A., Spiteri, I., Piccirillo, S. G. M., Touloumis, A., Collins, V. P., Marioni, J. C., Curtis, C., Watts, C., and Tavare, S. (2013). Intratumor heterogeneity in human glioblastoma reflects cancer evolutionary dynamics. *Proc. Natl. Acad. Sci.*, 110(10):4009–4014.

Takizawa, S., Nagasaka, K., Nakagawa, S., Yano, T., Nakagawa, K., Yasugi, T., Takeuchi, T., Kanda, T., Huibregtse, J. M., Akiyama, T., and Taketani, Y. (2006). Human scribble, a novel tumor suppressor identified as a target of high-risk HPV E6 for ubiquitin-mediated degradation, interacts with adenomatous polyposis coli. *Genes to Cells*, 11(4):453–464.

Tamori, Y. and Deng, W. M. (2011). Cell competition and its implications for development and cancer. *J. Genet. Genomics*, 38(10):483–495.

Tamori, Y., Uli, C., Tian, A.-g., Kajita, M., Huang, Y.-c., Norman, M., Harrison, N., Poulton, J., Ivanovitch, K., Disch, L., Liu, T., Deng, W.-m., and Fujita, Y. (2010). Involvement of Lgl and Mahjong / VprBP in Cell Competition. 8(7).

Thomas, M., Massimi, P., Navarro, C., Borg, J. P., and Banks, L. (2005). The hScrib/Dlg apico-basal control complex is differentially targeted by HPV-16 and HPV-18 E6 proteins. *Oncogene*, 24(41):6222–6230.

Tyler, D. M., Li, W., Zhuo, N., Pellock, B., and Baker, N. E. (2007). Genes affecting cell competition in drosophila. *Genetics*, 175(2):643–657.

Vaira, V., Faversani, A., Dohi, T., Maggioni, M., Nosotti, M., Tosi, D., Altieri, D. C., and Bosari, S. (2011). Aberrant overexpression of the cell polarity module Scribble in human cancer. *Am. J. Pathol.*, 178(6):2478–2483.

Vigil Dominico, Cherfils Jacqueline, Rossman Kent L., D. C. J. (2010). Ras superfamily GEFs and GAPs: validated and tractable targets for cancer therapy? *Nat Rev Cancer*, 10(12):842–857.

Vincent, J.-P., Fletcher, A. G., and Baena-Lopez, L. A. (2013). Mechanisms and mechanics of cell competition in epithelia. *Nat. Rev. Mol. Cell Biol.*, 14(9):581–91.

Vincent, J. P., Kolahgar, G., Gagliardi, M., and Piddini, E. (2011). Steep Differences in Wingless Signaling Trigger Myc-Independent Competitive Cell Interactions. *Dev. Cell*, 21(2):366–374.

Vogelstein, B., Papadopoulos, N., Velculescu, V. E., Zhou, S., Diaz, L. a., and Kinzler, K. W. (2013). Cancer Genome Lanscapes. *Science (80-.).*, 339(6127):1546–1558.

Waclaw, B., Bozic, I., Pittman, M. E., Hruban, R. H., Vogelstein, B., and Nowak, M. A. (2015). A spatial model predicts that dispersal and cell turnover limit intratumour heterogeneity. *Nature*, 525(7568):261–264.

Wagstaff, L., Goschorska, M., Kozyrska, K., Duclos, G., Kucinski, I., Chessel, A., Hampton-O'Neil, L., Bradshaw, C. R., Allen, G. E., Rawlins, E. L., Silberzan, P., Carazo Salas, R. E., and Piddini, E. (2016). Mechanical cell competition kills cells via induction of lethal p53 levels. *Nat. Commun.*, 7:11373.

Wawryk-Gawda, E., Chylińska-Wrzos, P., Lis-Sochocka, M., Chłapek, K., Bulak, K., Jędrych, M., and Jodłowska-Jędrych, B. (2014). P53 protein in proliferation, repair and apoptosis of cells. *Protoplasma*, 251(3):525–533.

Wienert, S., Heim, D., Saeger, K., Stenzinger, A., Beil, M., Hufnagl, P., Dietel, M., Denkert, C., and Klauschen, F. (2012). Detection and segmentation of cell nuclei in virtual microscopy images: A minimum-model approach. *Sci. Rep.*, 2:1–7.

Wolff, T. and Ready, D. F. (1991). Cell death in normal and rough eye mutants of Drosophila. *Development*, 113(3):825–839.

Xu, L. and Jordan, M. I. (1996). On Convergence Properties of the EM Algorithm for Gaussian Mixtures. *Neural Comput.*, 8(1):129–151.

Zarubin, T. and Han, J. (2005). Activation and signaling of the p38 MAP kinase pathway. *Cell Res.*, 15(1):11–18.

Zeidler, M. P., Bach, E. a., and Perrimon, N. (2000). The roles of the Drosophila JAK/STAT pathway. *Oncogene*, 19(21):2598–2606.

Zhan, L., Rosenberg, A., Bergami, K. C., Yu, M., Xuan, Z., Aron, B., Allred, C., and Muthuswamy, S. K. (2011). NIH Public Access. 135(5):865–878.

Zhao, B., Tumaneng, K., and Guan, K.-L. (2011). The Hippo pathway in organ size control, tissue regeneration and stem cell self-renewal. *Nat. Cell Biol.*, 13(8):877–883.

Zhao, M., Szafranski, P., Hall, C. A., and Goode, S. (2008). Basolateral junctions utilize warts signaling to control epithelial-mesenchymal transition and proliferation crucial for migration and invasion of drosophila ovarian epithelial cells. *Genetics*, 178(4):1947–1971.

Ziosi, M., Baena-López, L. A., Grifoni, D., Froldi, F., Pession, A., Garoia, F., Trotta, V., Bellosta, P., Cavicchi, S., and Pession, A. (2010). dMyc functions downstream of yorkie to promote the supercompetitive behavior of hippo pathway mutant Cells. *PLoS Genet.*, 6(9).